공학박사학위논문

불꽃점화엔진에서의 노킹을 억제하기 위한 리서치옥탄가 100 가솔린-에탄올 혼합연료 내 에탄올 함량 최적화

Optimization of Ethanol Content in Gasoline-Ethanol Blend Fuel with RON100 for Knock Suppression in Spark Ignition Engine

2020 년 2 월

서울대학교 대학원

기계항공공학부

조 재 영

Abstract

Optimization of Ethanol Content in Gasoline-Ethanol Blend Fuel with RON100 for Knock Suppression in Spark Ignition Engine

Jaeyoung Cho

Department of Mechanical and Aerospace Engineering

The Graduate School

Seoul National University

This dissertation is devoted to optimize the ethanol content in gasoline-ethanol blend fuel with a fixed RON of 100, for maximizing antiknock characteristics in spark-ignition (SI) engines of light duty fleet in South Korea. To this end, the ethanol reference fuels (ERFs), which is a blend of ethanol and primary reference fuel, with varying ethanol content were chosen as surrogate fuels, then their auto-ignition characteristics were measured on rapid compression machine (RCM). The measurement was manipulated to quantitatively analyze the dependency of knocking characteristics of each ERF on engine operating

condition from the aspect of chemical kinetics, whose results will eventually derive the optimal ethanol content with varying engine operating condition.

The first objective of this study was to analyze the dependency of knocking characteristic of various ERFs on temperature–pressure profile of engine operating condition. To this end, an empirical correlation of the ignition delay with varying temperature, pressure, and ethanol content was derived based on a regression analysis using ignition delay measurement. Then, the deviation in the temperature–pressure profile owing to changes in various engine operating parameters was calculated using a 0-D two zone SI engine simulation. Based on these results, it was quantified how the individual effects of temperature deviation and pressure deviation affect the ignition delay of each tested fuel. Consequently, it was found that the ignition delay of the tested fuels exhibits different dependencies on the temperature and pressure despite a fixed RON. In particular, the ignition delay of the fuel with the higher ethanol content is more sensitive to the temperature deviation, $\Delta T/T$, owing to its higher activation energy, whereas it is less sensitive to the pressure deviation, $\Delta P/P$. Moreover, it was revealed that the effect of temperature–pressure deviation on the ignition delay is independent of the ethanol content, if and only if $\Delta T/T$ is equal to $(\gamma-1)/\gamma*\Delta P/P$, where γ is the specific heat ratio of the end gas. The results of this study were verified to be consistent with those predicted from Kalghatgi's K value principle. Consequently, both approaches exhibited the same result on the knocking characteristics of various ERFs under varying engine operating conditions.

The above results were expanded to cover the engine operating condition with external-exhaust-gas-recirculation (EGR), where the thermodynamic state of end gas is significantly varied with the rate of dilution. Similar as the analysis on the effect of temperature-pressure effect, the total effect of external-EGR on the ignition delay of the simulated end gas was divided into two effects affecting the

auto-ignition behavior: dilution effect and temperature–pressure profile effect, then each effect was evaluated separately. As a result, the dilution effect by adding external-EGR was maximized when the fuel is ERF10. With a regression analysis, it was found that there is the correlation between the amount of dilution effect and the amount of pre-heat release in the end gas during a flame propagation; therefore, it is understood that ERF10 is the most sensitive to dilution effect due to its pre-heat release characteristic. On the other hand, ERF with lower ethanol content was more sensitive to temperature–pressure effect by external-EGR on the ignition delay. It is found out that the deviation of temperature–pressure profile by external-EGR always satisfies the condition of $\Delta T/T>(\gamma-1)/\gamma*\Delta P/P$; therefore, the temperature–pressure effect of the fuel with lower ethanol content is higher than the other fuels, due to its lower sensitivity of ignition delay on temperature. Consequently, ERF10 has the highest external-EGR sensitivity in anti-knock behavior at RON test condition, and it is further discussed that the optimum ethanol content for external-EGR strategy could vary from ERF0 to ERF10 according to engine speed.

Based on the understanding of the effect of engine operating condition on the knocking characteristics of various ERFs, the ethanol content was optimized for maximizing knock suppression of light duty fleet in South Korea. In this regard, the sales volumes of each SI engine models was achieved from the statistics for model year 2018 in South Korea, which can be found from the database of KAMA. Then, the thermodynamic state of each SI engine design at detonation borderline (DBL) condition with varying engine speed were calculated using 0-D two-zone SI engine model. As a result, it was found that 72 % of SI engines sold for model year 2018 operates on the thermodynamic state where ERF30 is optimal for knock suppression. Moreover, as engine speed get faster, in-cylinder pressure at DBL condition increases, and more SI engines becomes operated on the thermodynamic state where ERF30 is optimal. The analysis was expanded to how the optimal

ethanol content changes on the scenario that external-EGR is widely used in the future. Consequently, it was found that the introduction of external-EGR will makes the optimal ethanol content to be ERF10, which is the most sensitive to dilution effect of external-EGR. However, as the engine speed gets faster, the priority of ERF10 on dilution effect was surpassed by the priority of ERF30 on pressure effect, thus ERF30 still be optimal at the faster engine speed regardless of external-EGR.

This is the first experimental study to analyze the effect of engine operating condition on the ignition delay of various ERFs and develop quantitative correlations between ignition delay and knocking phenomena, reflecting operating conditions of modern engines. Moreover, this study suggested the useful diagram determining the optimal ethanol content at an arbitrary engine operating condition, which can be manipulated for government to determine the optimal ethanol content in gasoline-ethanol blend fuel suitable for the countries.

Keywords: Ethanol, Knocking, Octane number, Rapid compression machine, Ignition delay, Spark-ignition engine

Student Number: 2014-21867

Table of Content

List of Figures

List of Tables

Chapter 1. Introduction

1.1 Research background

1.1.1 Regulations on carbon dioxide emissions and petroleum consumption from light duty vehicles

In the past few decades, the automobile industry has faced the challenge of reducing greenhouse gas emissions and fossil fuel consumption. **Figure 1.1** shows the historical evolution of CO_2 emission from energy consumption for each end-use sector in U.S. [1]. In 1973, the transportation sector emitted 28 % of total carbon dioxide emission in U.S., but it has gradually increased to 36 % in 2017. Meanwhile, the historical change of petroleum consumption in U.S., as depicted in **Figure 1.2**, shows that the petroleum consumption in the transportation sector has reached the 69 % of total consumption in U.S.

In this regard, strict regulations are being imposed on the CO_2 emissions from automobile. **Table 1.1** and **Figure 1.3** show the brief summary on the regulation in various countries [2]. U.S. government has enacted the Corporate Average Fuel Economy (CAFE) standard to regulate CO_2 emission from vehicles according to its footprint, which is defined as a multiplication of wheelbase length and track width. For example, Hyundai Motors Sonata has a footage area of 5.23 m^2, and its target CO_2 emission for CAFE standard is 163.2 gCO_2/km for in 2017 and will be tightened to 111.5 gCO_2/km by 2025 [3].

European Commission also has set the CO_2 reduction target since 2009. The first target was 130 gCO_2/km of average CO_2 emission from new passenger cars by 2015. In 2021, the target will be stricter to 95 gCO_2/km with phased-in period from 2020, which is corresponds to 21 % lower emission of the average CO_2 emission from new passenger cars for 2018. Similar as U.S., the target emission varies with the weight of automobile; the 1 kg heavier car is subject to 0.0457 gCO_2/km higher target [4].

Meanwhile, South Korea government regulates the CO_2 emission from new passenger cars to 140 gCO_2/km in 2015, which was relatively higher than that of U.S. and E.U., but it is planned to be rapidly reinforced to 97 gCO_2/km in 2020. South Korea also defines the different regulation according to the weight of automobile, 0.0533 gCO_2/km higher target per 1 kg of automobile weight.

Beside the regulations on CO2 emissions, there are other regulations on the automobile with high emission such as low emission zone (LEZ) for restricting the available area of high emission vehicles, and bonus-malus system where the owner of vehicle is taxed or credited according to its CO_2 emission; all the regulation get ever stricter.

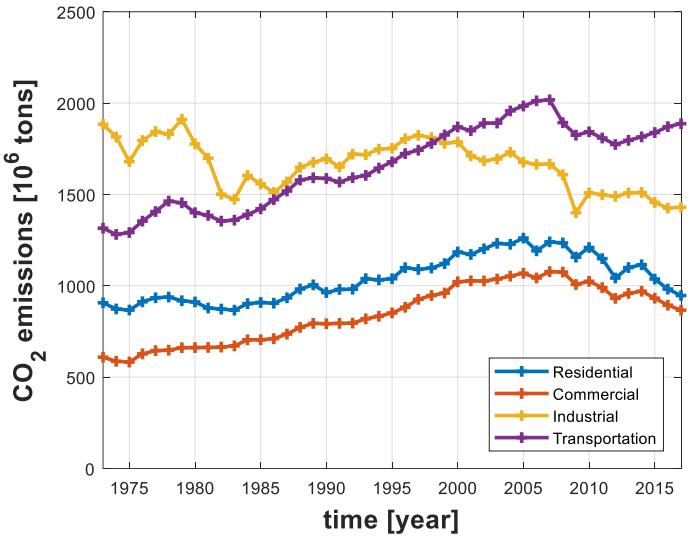

Figure 1.1 Carbon dioxide emissions from each end-use sector in U.S. [1]

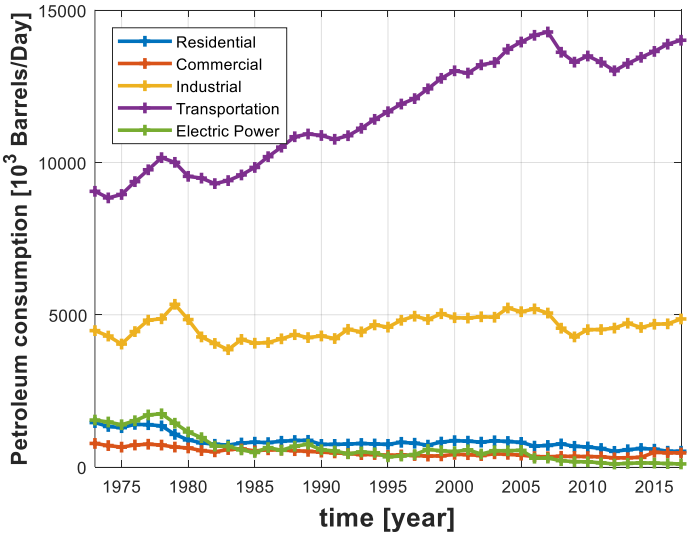

Figure 1.2 Petroleum consumption from each end-use sector in U.S. [1]

Table 1.1 Regulations for passenger car in various countries [2]

Country	Regulated metric	Target year	Unadjusted Fleet target	Form of target curve	Test cycle
Brazil	Energy consumption	2017	1.82 MJ/km	Weight-based corporate average	U.S. combined
Canada	GHG	2016	217 gCO_2/mile	Footprint-based corporate average	U.S. combined
		2025	N/A		
China	Fuel consumption	2015	6.9 L/100km	Weight-class based corporate average	NEDC
		2020	5 L/100km		
EU	CO_2	2015	130 gCO_2/km	Weight-based corporate average	NEDC
		2021	95 gCO_2/km		
India	CO_2	2017	130 g/km	Weight-based corporate average	NEDC for low-powered vehicle
		2022	113 g/km		
Japan	Fuel economy	2015	16.8 km/L	Weight-class based corporate average	JC084
		2020	20.3 km/L		
Mexico	Fuel economy/GHG	2016	39.3 mpg or 140 g/km	Footprint-based corporate average	U.S. combined
Saudi Arabia	Fuel economy	2020	17 km/L	Footprint-based corporate average	U.S. combined
South Korea	Fuel economy/GHG	2015	17 km/L or 140 gCO_2/km	Weight-based corporate average	U.S. combined
		2020	24 km/L or 97 gCO_2/km		
U.S.	Fuel economy/GHG	2016	36.2 mpg or 225 gCO_2/mile	Footprint-based corporate average	U.S. combined
		2025	55.2 mpg or 147 gCO_2/mile		

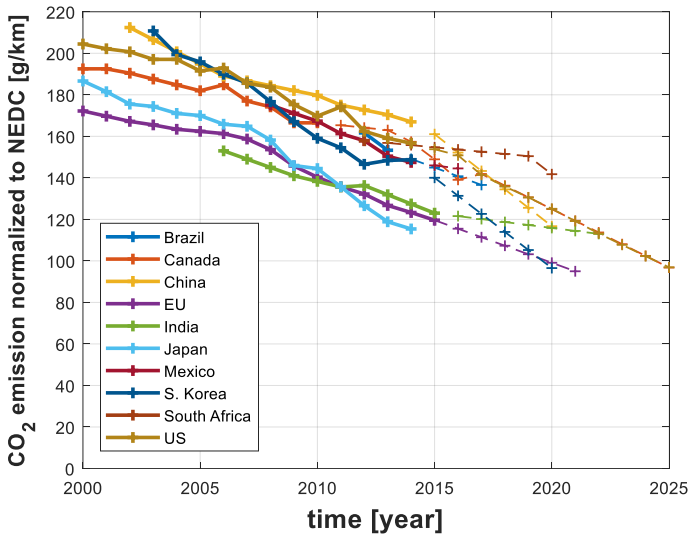

Figure 1.3 Historical and target CO_2 emission of various countries [2]

1.1.2 Advance in engine design for high thermal efficiency

In order to achieve the target CO_2 emission of aforementioned regulations, numerous technologies have been suggested and applied to the internal combustion engines. Especially for spark-ignition (SI) engine, where the premixed fuel-air mixture is supplied to cylinder and ignited by electrical spark, the fuel supply system has been replaced from carburetor to port fuel injection (PFI) or gasoline direct injection (GDI) for accurate control of fuel supply. Replacing the carburetor to PFI was studied mainly in late 1960s; Freeman and Stahman reported that injecting fuel rather than carburetion is more beneficial for combustion efficiency [5]. Meanwhile, GDI system was considered as an alternative to PFI since early 2000s. According to Stein et al., using GDI leads to more charge cooling effect than PFI, which is beneficial for enhancing volumetric efficiency of engine [6].

Turbocharging is another promising technology for enhancing thermal efficiency of SI engine by downsizing the displacement volume of engine and reducing pumping loss [7]. It uses the remained enthalpy of exhaust gas for rotating a turbine, whose work is used to pumping the intake air over the atmosphere pressure by using a compressor. The study of Han et al. reported that the turbocharged engine with the displacement of 2.0L has up to 17 % lower fuel consumption in FTP city mode than the larger natural aspired engine with the similar performance, owing to reduced pumping loss and friction [8].

Figure 1.4 shows the adoption rate of each technologies for SI engines in U.S. [9]. As shown, the most of carburetor was replaced to PFI system during 1980s owing to digitalization of engine control system, and the adoption rate of GDI and turbocharging system is rapidly increasing since 2007, when the U.S. government signed the Energy Independence and Security Act (EISA) and doubled the national fuel standard target of fuel economy [10].

Meanwhile, geometry of engine cylinder has been also optimized for lower fuel economy. **Figure 1.5** depicts the historical change of average compression ratio (CR) and displacement volume in U.S. [9, 10]. As shown, CR is gradually increasing from 8.4 in 1975 to 10.5 in 2015, which results in enhanced thermal efficiency [11]. Displacement volume decreased rapidly until early 1980s, which is thought to be related with shortening combustion duration, and keeps around 550 cc for past three decades.

Besides the configuration and geometrical optimization of engine cylinder, there have been other approaches to enhance the thermal efficiency of engine; the heat loss is reduced with ceramic coating on piston, head, valve, and liner [12], whereas intake temperature (IT) is decreased using more effective intercooler to achieve higher volumetric efficiency [13].

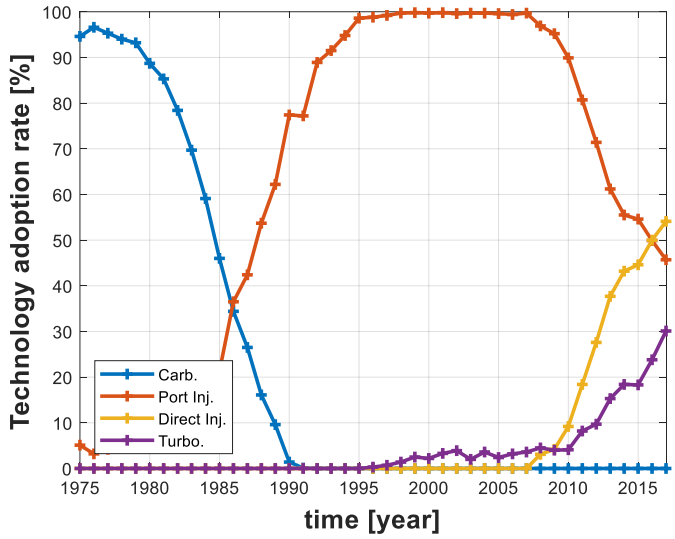

Figure 1.4 Technology adoption rate of light duty vehicles in U.S. [9]

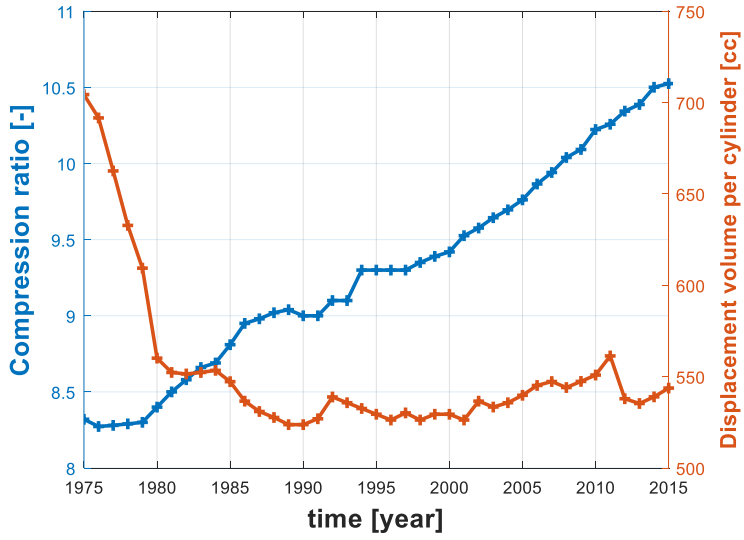

Figure 1.5 The average compression ratio and displacement volume per cylinder of light duty vehicles in U.S. [9, 10]

1.1.3 Knocking

Most of advance in SI engine, however, are limited by an abnormal combustion phenomenon: knocking. As shown in **Figure 1.6**, the knocking is characterized by a pressure oscillation in the cylinder with audible sound, which is caused by the auto-ignition of the end gas before flame arrival. Most approaches for enhancing thermal efficiency of SI engines elevate the in-cylinder pressure and temperature and promote auto-ignition of the end gas. The heat release rate from auto-ignition is about thousands of deflagration. Thus, it generates the local instability of pressure, which leads to shock wave developing to detonation. Shock wave from knocking disturbs the temperature gradient in thermal boundary layer between burned gas and piston, and it leads to drastic heating of piston. Thermal expansion of piston results reduces the clearance between the piston and liner, eventually, damages the piston and liner [14].

Figure 1.7 shows the example of damage on a piston by knocking reported by Ceschini et al. [15]. In their study, the knocking intensity was varied with the cylinder, the most weak with the piston 1 and the most severe with the piston 4. They found the obvious trend between the knocking intensity and piston damage. As shown, knocking results in seizure of piston and its severity increases with knocking intensity. Moreover, it was found that carbon was deposited on the piston top land, whose surface was eroded because high pressure and temperature from knocking induce the thermal stress on the piston.

Under a knock-prone condition, retarding the ignition timing and compromising the thermal efficiency of the engine is unavoidable for reducing in-cylinder pressure and temperature. According to Ayala [16], retarding ignition timing from maximum brake toque (MBT) timing results in lower brake thermal efficiency by approximately 0.6 % per 1 crank angle degree (CAD) of retardation.

Knocking characteristics of SI engine is determined not only by engine design but also by fuel characteristics; that is, more reactive fuel is prone to cause auto-ignition and knocking. Conventionally, the knocking characteristics of fuel has been represented by the research octane number (RON) and motor octane number (MON), which are measured using the cooperative fuel research (CFR) engine under the standardized conditions of ASTM D2699 [17] and ASTM D2700 [18], as described on **Table 1.2**. These two different octane numbers characterize the knocking propensity of fuel at two different condition; RON is for the moderate engine operating condition, while MON is for more harsh condition with faster engine speed and higher intake temperature. In these days, it is well-known that RON is more proper for predicting the knocking characteristics of fuel rather than MON [19] since the thermodynamic condition in modern SI engine is more closer to RON condition.

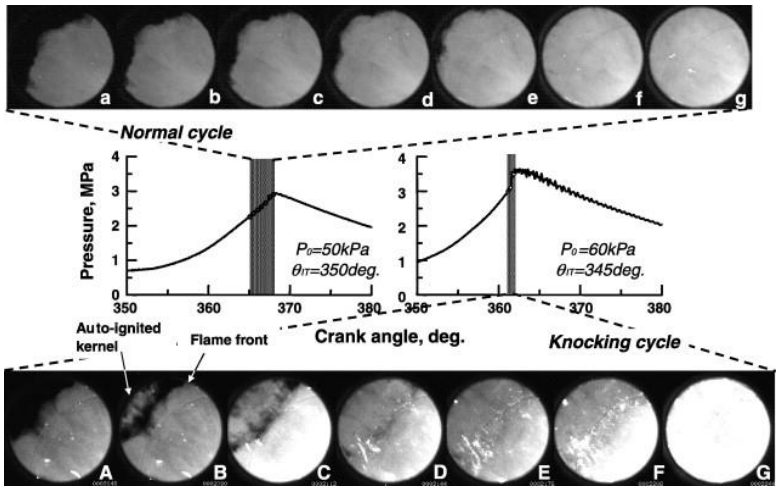

Figure 1.6 Characteristic behavior of in-cylinder pressure in knocking cycle and its corresponding image of flame[1] [20]

[1] Reprinted from Proceedings of the Combustion Institute, Vol 31, N. Kawahara, E. Tomita, Y. Sakata, Auto-Ignited Kernels during Knocking Combustion in a Spark-Ignition Engine, 2999-3006, Copyright (2007), with permission from Elsevier.

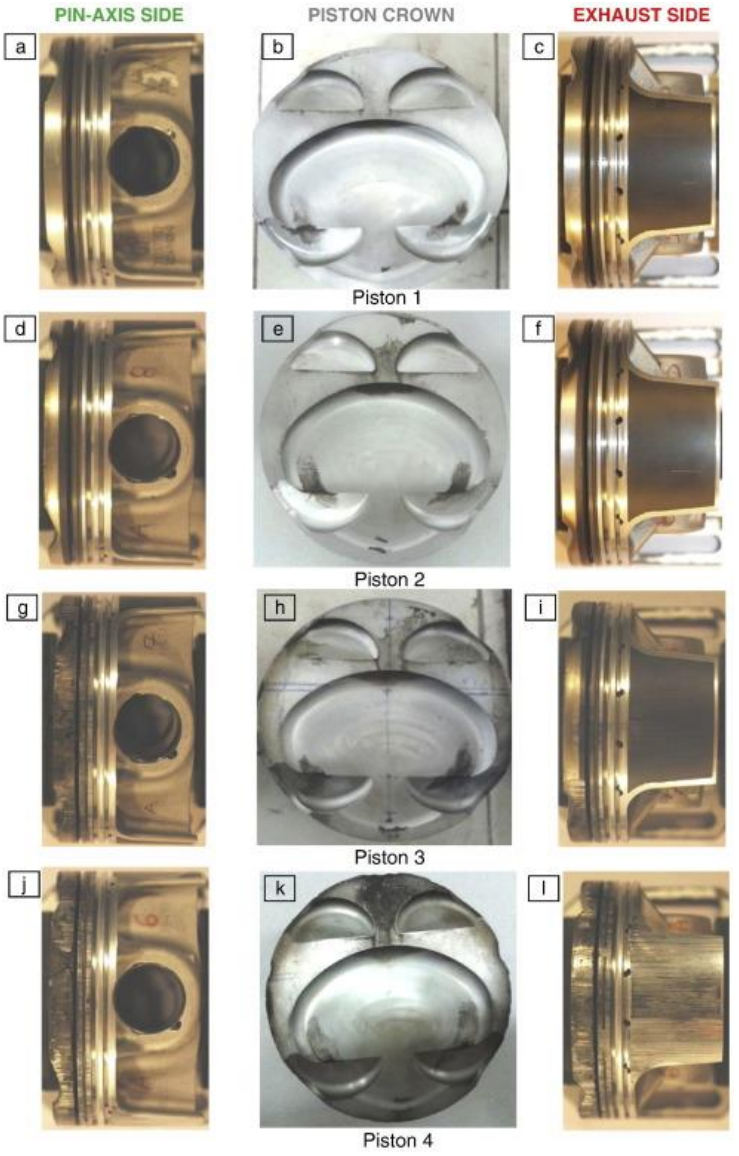

Figure 1.7 Damage on piston from knocking with varying intensity[2] [15]

[2] Reprinted from Materials & Design, Vol 114, L. Ceschini, A. Morri, E. Balducci, N. Cavina, N. Rojo, L. Calogero, L. Poggio, Experimental Observations of Engine Piston Damage Induced by Knocking Combustion, 312-325, Copyright (2017), with permission from Elsevier.

Table 1.2 Operating parameters for RON [17] and MON [18] test condition

Parameter	RON condition	MON condition
Cylinder bore [mm]	82.6	82.6
Stroke [mm]	114.3	114.3
Connecting rod length [mm]	265.2	265.2
IVC [aBDC]	34	34
Spark timing [bTDC]	13	14-26 [a]
Engine speed [rpm]	600	900
Compression ratio [-]	4-18 [b]	4-18 [b]
Intake pressure [bar]	1	1
Intake air temperature [K]	325.15	422.15

[a] Spark timing for MON test condition is varied with compression ratio; higher compression ratio, more retarded spark timing.
[b] Compression ratio is adjusted for the test fuel to have standard knocking intensity.

1.1.4 Ethanol as an antiknock additive

To suppress knocking, several studies have investigated using alternative fuels with high octane number, such as hydrogen [21], methanol [22], butanol [23], and dimethylfuran [24]. Among them, using alcohol fuel as a fuel additive is one of the prominent solution with several advantages. **Table 1.3** describes the fuel characteristics of gasoline and alcohol fuels with low carbon less than four. As shown, RON of low carbon alcohol fuel is generally higher than gasoline due to its longer ignition delay and higher latent heat of vaporization [6]. Moreover, alcohol fuel has lower vapor pressure than gasoline, suppressing evaporative emission during fuel delivery [25], and most of alcohol including methanol, ethanol and butanol can be produced from renewable resources like corn, cassava, and wheat [26].

Among the various alcohol fuel, ethanol is the most widely used species across the world due to its high productivity in most countries. In U.S., one of the countries that use the most of ethanol fuel, renewable fuel standard (RFS) program has been set for promoting the usage of ethanol as an alternative to conventional gasoline. RFS program regulates the refiners or importers of gasoline or diesel to blend renewable fuels to petroleum-based fuel at least the certain percentage to meet the volume standard of biofuel per year, which is rapid increasing as shown on **Figure 1.8**. In this regard, the transportation section of U.S in 2017 consumed 1,115 trillion Btu of the ethanol, which is successfully replacing about 6.5 % of motor gasoline consumption in U.S [1].

Brazil also has produced and consumed the abundant amount of ethanol as an alternative fuel since 1975. Ethanol is replacing 27 % of gasoline consumption in transportation section [27], most of which is made from sugarcane. Moreover, Brazil government has launched RenovaBio Program in December 2016, in order to meet the commitments under Paris Agreement and encourage the ethanol production. RenovaBio Program sets a target of decarbonization for each fuel distributors, which can be met by purchasing biofuels from biofuel producers or decarbonization credits from the stock market [28].

Meanwhile, South Korea has not legalized the usage of ethanol for gasoline-motored vehicles yet, but several research has been done to prove applicability of biofuel in South Korea under the support from government [29]. For example, Kim et al. measured the fuel characteristics and emission characteristics of gasoline-ethanol blend fuel with varying ethanol content, including RON, RVP, and distillation temperature [30, 31]. Meanwhile, Jeon et al. [32] studied the method for enhancing the productivity of ethanol from the limited resources in South Korea. Based on these results, it is thought that South Korea government would introduce the biofuel for gasoline-motored vehicles in near future.

Table 1.3 Fuel characteristics of low carbon alcohols [33]

Parameter	Gasoline	Methanol	Ethanol	nPropanol	nButanol
RON [-]	88-98	109	109	104	98
MON [-]	80-88	89	90	89	85
LHV [MJ/L]	30-33	15.8	21.4	24.7	26.9
HoV [kJ/L]	~351	1168	919.6	792.1	707.9
RVP [kPa][a]	54-103	32	16	6.2	2.2
Specific gravity [-]	0.72-0.78	0.792	0.794	0.804	0.81

[a] RVP for alcohol fuel is from the study of Andersen et al. [25].

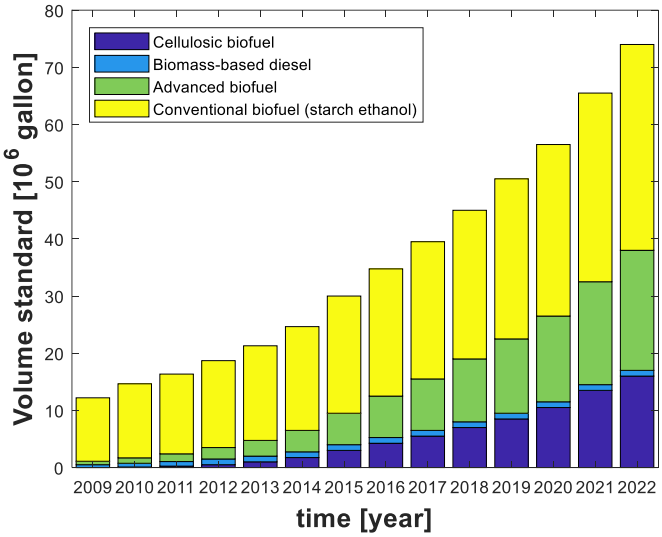

Figure 1.8 Volume standard for each type of biofuels in RFS program

1.1.5 Optimal ethanol content for a fixed RON

When the ethanol is blended to gasoline for enhancing the octane number of fuel, various compositions can be suggested. According to Anderson et al. [34], the RON of blend fuel can be estimated from the linear combination of molar

concentration of gasoline and ethanol as **Eq. (1.1)**, which can be depicted as **Figure 1.9**. For example, in case of producing the gasoline-ethanol blend fuel with RON 100, it can be made by blending RON 93 gasoline with 20 % ethanol or blending RON 88 gasoline with 30 % ethanol.

$$RON_{Blend} = (1 - x_E)RON_G + x_E RON_E \qquad \textbf{Eq. (1.1)}$$

$$\text{where } x_E = \frac{z_E}{z_E + (1 - z_E)\dfrac{MW_E \rho_{L_G}}{MW_G \rho_{L_E}}}$$

The fuels with the same RON is expected to have the identical knocking characteristics regardless of its detailed composition, however, they do not. This is because modern engines utilize various devices to enhance fuel economy, thus the thermodynamic state of the engine is different from that obtained under the RON test conditions. For example, Stein et al. studied how the knocking characteristics of gasoline-ethanol content depends on the ethanol content with fixed RON of blend fuel, especially on the modern SI engine with direct injection. They found that higher ethanol content is beneficial for knock suppression at the given engine design because the charge cooling effect of ethanol is amplified with direct injection [6].

In this regard, it can be inferred that there is the optimal ethanol content of gasoline-ethanol blend fuel with a fixed RON which maximizes the anti-knock characteristics in modern SI engine. To find the optimal ethanol content for a fixed RON, the new knock metric is required for representing the knocking characteristics of fuel in varying engine operating condition and engine design. Moreover, given the knock metric, a careful inspection on the fleet-wide optimization of ethanol content is essential considering the dependency of the

optimal ethanol content on the design of SI engines in light duty fleet in the country.

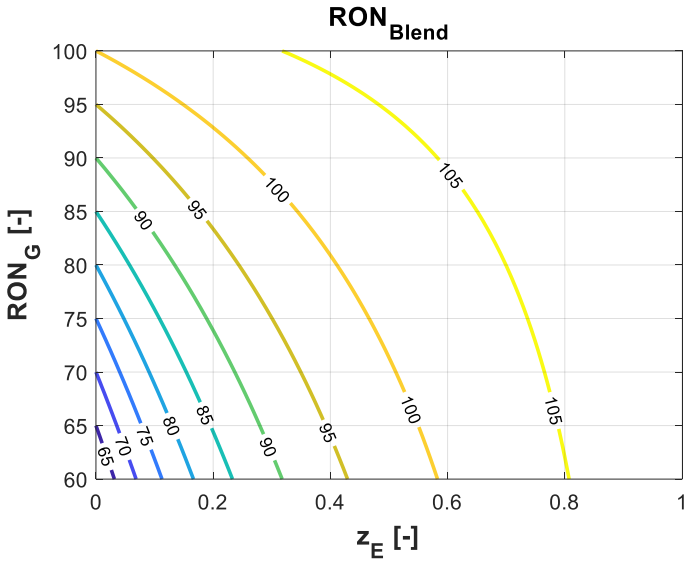

Figure 1.9 RON of gasoline-ethanol blend fuel according to liquid volume fraction of ethanol and RON of base gasoline

1.2 Literature review

1.2.1 New knock metrics

In order to predict knocking characteristics of fuel in SI engine with varying type of fuel supply system, Foong et al. [35] suggested the modified RON, where the charge cooling effect of fuel on knock suppression is eliminated by controlling the intake air temperature according to the latent heat of vaporization of fuel. This modified knock metric is useful for separating the charge cooling effect and fuel chemistry effect by comparing it with the original RON value, and better for predicting knock characteristics of fuel in varying fuel supply system. However,

this method cannot be applied generally to knock prediction in arbitrary engine design such as turbocharged, variable CR, or lean burn engine.

Meanwhile, Mittal and Heywood [36] suggested the modified RON and MON test condition as described on **Table 1.5**, where the CFR engine is operated with a lower intake temperature, higher intake pressure, and faster engine speed so as to be similar to the modern SI engine. Similarly, Mehl et al. [37] employed the bench octane number (BON), which represents the octane number of the fuel for the given engine condition; thus, the BON depends not only on the fuel but also on the target engine operating condition. These studies successfully correlated the modified octane number with the knocking characteristics of the fuel in modern engines; however, they have a limitation in that the standardized test conditions must be adjusted as engine design progresses in the future.

In contrast, Kalghatgi et al. investigated the effect of engine design modification on the knocking characteristics of fuel including knock onset [19, 38], knock intensity [39], and its stochastic behavior [40]. Among them, the K value principle [19, 38] describes the effect of engine design and operating condition on the knocking characteristics with a single parameter, K. In this study, he suggested the octane index (OI) of the fuel for representing the knocking characteristics of fuel at the given engine operating condition, then assumed that OI is expressed as linear combination of RON and MON as described in **Eq. (1.2)**. In order to achieve K value for the given engine operating condition, he measured knocking limited spark advance (KLSA) of fuel matrix with varying RON and MON, then executed the regression analysis of calculate K value with which the correlation between OI and KLSA of fuel matrix is maximized. Then, he found K value depends on the engine operating parameters such as intake pressure and temperature, thus can represent the effect of engine operating

condition on the knocking characteristics as RON and MON characterize the effect of fuel.

$$OI = (1 - K) * RON + K * MON \qquad \textbf{Eq. (1.2)}$$

K value principle has been widely used in other research in the past decade [36, 41, 42] and has shown a high reliability. However, the reason why OI and K value vary with the operating condition has not been adequately investigated from the aspect of chemical kinetics.

Table 1.4 Operating parameters for modified RON suggested by Foong et al. [35]

Parameter	Modified RON condition
IVC pressure [bar]	1
IVC temperature [K]	400.15

Table 1.5 Operating parameters for modified RON and MON test condition suggested by Mittal and Heywood [36]

Parameter	Modified RON condition	Modified MON condition
Engine speed [rpm]	900	1500
Intake pressure [bar]	1.4	1
Intake air temperature [K]	303.15	343.15

1.2.2 Optimization of fuel composition

There have been several studies on optimizing the composition of fuel for SI engine. Yitao et al. studied the effect of gasoline hydrocarbon compositions on the emission characteristics, by varying olefin and aromatic composition, to find optimal fuel composition with the minimal emission [43]. On the other hand,

Masum et al. optimized the concentration of each alcohol components such as ethanol, iso-butanol, iso-pentanol, and hexanol, for maximizing RON [44]. Their extensive study gives an intuition for proper composition of alcohol components in gasoline-alcohol blend fuel, but have limitation on that the knocking characteristics of blend fuel was represented solely with RON, which is not consistent in some cases as reported by Kalghatgi et al. [45].

Co-optima initiative is one of the biggest project on optimization of fuel and engine [46]. In this project, the merit function of fuel was defined as a function of RON, MON, heat of vaporization, air-fuel ratio, particulate matter index, and laminar flame speed, then suggested the optimal oxygenated component of blend fuel with a fixed RON of 97 for maximizing the merit function. As a result, Sluder et al. reported that n-propanol is more beneficial for fuel efficiency than the other candidates such as ethanol, iso-propanol, iso-butanol, or di-iso-butylene [47]. Their strategy for maximizing anti-knock characteristics is remarkable in that they used the K value for representing the effect of engine operating condition on the merit function of fuel. However, it was not considered that K value can be widely varied according to the design and operating condition of SI engine in light duty fleet.

The most of studies on the optimizing fuel composition have focused on the specific design or operating condition of engine, and there is no discussion on fleet-wide optimization of fuel composition. Since it is efficient to fixed fuel composition to all of light duty fleet in a country, it is essential to find the optimal fuel composition, which maximizes the overall performance of light duty fleet with varying engine operating condition.

1.3 Research objective and implication

The objective of this dissertation is listed below:

1. To develop a new framework to understand and predict the effect of engine operating condition on the knocking characteristics of fuel, based on ignition delay measurement.

2. To evaluate the optimal ethanol content for light duty fleet in South Korea by using the developed framework for knocking analysis.

This dissertation is the first to present experimental results demonstrating the effect of thermodynamic state of the end gas on the ignition delay of various ethanol reference fuels (ERFs) and the quantitative correlation between ignition delay and knocking phenomena with the operating condition of modern engines. Thus, this study is expected to provide guidelines for a quantitative understanding on the effect of fuel and engine operating conditions on knocking characteristics from the aspect of chemical kinetics. Moreover, this study has an additional novelty that the optimal ethanol content with a fixed RON was found not only for the arbitrary design of SI engine, but also for the entire light duty fleet in South Korea.

1.4 Summary

This study explored the novel framework for evaluating the knocking characteristics of fuel in varying engine operating condition, then suggested the optimal ethanol content for light duty fleet in South Korea. The main body of this dissertation consists of four chapters. **Chapter 2** deals with methodology of this study for analyzing knocking characteristics of gasoline-ethanol blend fuel, including the selection of the fuel matrix, evaluation of thermodynamics state in SI engine, and measurement of auto-ignition characteristics of tested fuel. Then,

Chapter 3 suggests and validates the novel framework for analyzing the knocking characteristics of fuel on varying engine operating condition, especially on the cases where the temperature–pressure of the end is deviated from that of RON test condition. Based on the results from the chapter, **Chapter 4** expands the framework for covering the dependency of knocking characteristics on the rate of dilution in SI engine. Finally, **Chapter 5** evaluates the optimal ethanol content for light duty fleet in South Korea by calculating the temperature, pressure, and dilution rate of end gas in light duty fleet and applying the framework developed in previous chapters.

Chapter 2. Methodology

This chapter describes how the effect of engine operating condition on the knocking characteristics of fuel was analyzed; it is divided into four sub-chapters. **Chapter 2.1** provides details on the selected fuel matrix, and **Chapter 2.2** covers the SI engine simulation, which was performed to evaluate the thermodynamic state of the end gas in various engine operating conditions. Lastly, **Chapter 2.3** describes how the ignition delay was measured to characterize the auto-ignition characteristics of fuel with a given thermodynamic state.

2.1 Fuel matrix

Various ERFs, which are a blend of primary reference fuel and ethanol, with a fixed RON of 100 were selected as the fuel matrix for this study. To this end, the experimental results of Foong et al. [48], who measured the RON and MON for various ERFs, were interpolated. **Table 2.1** shows the composition of base primary reference fuel (PRF) which would have 100 of RON after blended with varying ethanol content. As shown, the n-heptane content increases with higher ethanol content to compensate the octane-enhancing effect of ethanol. Additionally, octane sensitivity (OS), which is defined in **Eq. (2.1)**, also increases owing to the higher OS of ethanol.

$$OS = RON - MON \qquad \textbf{Eq. (2.1)}$$

The ethanol content was restricted from 0 % to 30 %. It is because ERFs with the ethanol content higher than 40 % requires the base PRF with RON lower than 63; however, the gasoline with RON lower than 63 is hard to be achieved from

the conventional refinery process since the RON of the straight-run gasoline, which is the raw gasoline right after fractional distillation, is around 60-70.

Table 2.1 Composition of tested fuels

	ERF0	ERF10	ERF20	ERF30
ON of base PRF [-]	100.0	93.0	85.0	75.0
C_2H_5OH [%]	0.0	10.0	20.0	30.0
RON [-]	100.0	100.5	100.3	99.9
MON [-]	100.0	95.6	92.7	91.5

2.2 0-D two-zone SI engine model

2.2.1 Determination of representative engine operating condition

To analyze the effect of engine operating conditions, the RON test condition [17] was defined as the baseline engine condition. The RON test condition is well established and plenty of experimental and computational data are available, making it suitable for simulation and validation. Moreover, the effect of the engine operating condition on the knocking characteristics of various ERFs can be accurately compared as all the fuels would show the same knocking characteristics under the RON test condition.

Details of the parameters for the RON test condition are listed in the 2nd column of **Table 1.2**. Compression ratio was set for the fuel with RON 100 to have standard knocking intensity, which is 7.9 [17]. Although equivalence ratio is slightly rich in the RON test condition [46, 47], the stoichiometric condition was

chosen as a representative condition since it is closer to that of commercial SI engines.

2.2.2 Governing equation for the model

To calculate the thermodynamic state of the end gas in an arbitrary engine operating condition, an in-house SI engine model [49, 50] was used, which is built on MATLAB and Cantera. The model is based on a 0-D two-zone scheme, and the volume inside the cylinder was divided into two zones as shown on **Figure 2.1**: burned zone for the product gas and unburned zone for the end gas.

Governing equations of 0-D two-zone SI engine model was derived from mass balance, energy balance, ideal gas law, and volume constraint as described in **Eq. (2.2)-Eq. (2.5)**. These equations are a system of linear equations for $(2N_{species} + 5)$ unknown variables, $\frac{dm_{i,j}}{dt}; \frac{dT_i}{dt}; \frac{dP}{dt}; \frac{dV_i}{dt}$; thus, they could be solved using linear algebra. All the thermodynamic properties for the equations were obtained from the reduced mechanism of Mehl et al. with 679 species and 5627 reactions [51]. It should be noted that the composition of the burned zone was assumed the same as that of complete combustion, and reaction progression in the unburned zone was neglected as it is considered in the ignition delay correlation, which will be discussed in **Chapter 2.3**.

$$\frac{dm_{i,j}}{dt} = \begin{cases} i = \text{burned zone} \\ \dot{m}_b y_{i,j} \\ \\ i = \text{unburned zone} \\ -\dot{m}_b y_{i,j} \end{cases} \qquad \textbf{Eq. (2.2)}$$

$$\frac{dT_i}{dt} = \begin{cases} i = \text{burned zone} \\ \dfrac{-\dot{Q}_{loss_i} - P\dfrac{dV_i}{dt} + \dot{m}_b \sum_j y_{i,j} h_{i,j} - \sum_j \dfrac{dm_{i,j}}{dt} u_{i,j}}{\sum_j c_{v_{i,j}} m_{i,j}} \\ i = \text{unburned zone} \\ \dfrac{-\dot{Q}_{loss_i} - P\dfrac{dV_i}{dt} - \dot{m}_b \sum_j y_{i,j} h_{i,j} - \sum_j \dfrac{dm_{i,j}}{dt} u_{i,j}}{\sum_j c_{v_{i,j}} m_{i,j}} \end{cases} \quad \textbf{Eq. (2.3)}$$

$$V_i \frac{dP}{dt} + P\frac{dV_i}{dt} = \frac{R_u T_i}{\overline{MW_i}} \sum_j \frac{dm_{i,j}}{dt} + \frac{R_u m_i}{\overline{MW_i}} \frac{dT_i}{dt} \quad \textbf{Eq. (2.4)}$$

$$\sum_i \frac{dV_i}{dt} = \frac{dV_{cyl.}}{dt} \quad \textbf{Eq. (2.5)}$$

The in-cylinder temperature at intake valve closure (IVC) is one of the most important variable affecting the knocking characteristics and having a high uncertainty. It is calculated considering charge cooling, residual temperature, and residual mass. First, the effect of charge cooling was evaluated by using the model suggested by Foong et al. [35]. In the model, the temperature of the fuel–air mixture at the downstream of the fuel supplying system, T_m, was assumed as an arbitrary value, then the surface temperature of the intake manifold, T_s, was calculated by solving the heat transfer balance equation, **Eq. (2.6)**. Subsequently, T_m was updated using energy balance equation, **Eq. (2.7)**. This process was iterated until T_m converges. The parameters required for the calculation, $T_{amb.}; h_{c.im,i(e)}; A_{im,i(e)}; \dot{Q}_{im,in}$, are listed on the paper of Foong et al. [35]. Meanwhile, the residual temperature was achieved by assuming the state of residual gas is equals to the adiabatically expanded state from the state right before the exhaust valve opening (EVO) timing on the previous cycle [52]. Finally, residual mass was determined based on the assumption that the trapped volume of residual gas is equals to the clearance volume, V_c, as **Eq. (2.8)**. Here, the

calibration variable, C_r, was multiplied to consider the effect of valve overlap, which was set to be 1.5.

$$h_{c_{im,i}} A_{im,i} \left(\frac{(T_a + T_m)}{2} - T_s \right) = h_{c_{im,e}} A_{im,e} (T_s - T_{amb.}) + \sigma A_{im,e} \left(T_s^4 - T_{amb.}^4 \right) \quad \textbf{Eq. (2.6)}$$

$$\dot{m}_m c_{p,m} T_m = \dot{m}_a c_{p,a} T_a + \dot{m}_f \left(c_{p,f} T_f - \Delta h_{v,f} \right) + \dot{Q}_{im,out} - \dot{Q}_{im,in} \quad \textbf{Eq. (2.7)}$$

where $\dot{Q}_{im,out} = h_{c,im,e} A_{im,e} (T_s - T_{amb.}) + \sigma A_{im,e} \left(T_s^4 - T_{amb.}^4 \right)$

$$m_r = C_r \rho_r V_c = C_r \frac{P_{em} \overline{MW_r}}{R_u T_r} V_c \quad \textbf{Eq. (2.8)}$$

The burning rate of mass, $\dot{m}_b$, is modeled by Wiebe function and Hires's correlation [53], which are expressed as **Eq. (2.9)**. The dependency of burning rate on alcohol content was assumed to be negligible based on the observation of Kar et al. [54], Cooney et al. [55], and de Melo et al. [56], where the variation of $\Delta\theta_{90}$ with the ethanol content was measured less than 0.13 CAD per 1 % of ethanol content. Here, it should be noted that C_θ in **Eq. (2.9)** is a calibration variable determined to reproduce burn angle at the validation condition, and were determined to be suitable for the experimental combustion phase measured by Foong [57]. Meanwhile, the laminar flame speed, S_L, of ERF0 was calculated based on the Middleton's correlation, which expresses the dependency of S_L as an analytic function of temperature, pressure, equivalence ratio, and dilution rate [58].

$$y_b(\theta) = 1 - \exp\left(-a_W \left(\frac{\theta - \theta_{ST}}{\Delta\theta} \right)^{m_W + 1} \right) \quad \textbf{Eq. (2.9)}$$

$$\text{where } \Delta\theta = C_\theta \left(\frac{D_B}{H_{CA50}}\right)\left(\frac{\rho_{ST}}{\rho_{u,CA50}}\right)^{\frac{10}{9}} (\overline{S_P}\nu_{CA50})^{\frac{1}{3}}\left(\frac{H_{ST}}{S_{L,CA50}}\right)^{\frac{2}{3}},$$

$$S_{L,CA50} = f_{Middleton}(T_{u,CA50}, P_{CA50}, x_D)$$

Heat loss to the wall was determined based on Woschni's heat transfer model as **Eq. (2.10)** [59]. The portion of heat loss from burned zone or unburned zone was assumed to be proportional to the portion of volume of each zone, $\frac{V_i}{V_{cyl.}}$. The characteristic flow speed, w, was expressed differently in compression stroke and combustion-expansion stroke, in order to consider the enhanced gas velocity due to the density change from combustion, which is proportional to the difference between the in-cylinder pressure from fired cycle and motored cycle, $(P - P_{mtr})$.

$$\dot{Q}_{loss_i} = h_{c_i}\left(\frac{\pi D_B^2}{2} + \pi D_B H\right)\frac{V_i}{V_{cyl.}}(T_i - T_{wall}) \qquad \textbf{Eq. (2.10)}$$

$$\text{where } h_{c_i} = 3.26{D_B}^{-0.2}P^{0.8}T_i^{-0.55}w^{0.8},$$

$$w = \begin{cases} \theta < \theta_{ST} \\ 2.28\,\overline{S_P} \\ \\ \theta \geq \theta_{ST} \\ 2.28\,\overline{S_P} + 0.00324\dfrac{V_D T_{IVC}}{P_{IVC}V_{IVC}}(P - P_{mtr})^{0.8} \end{cases}$$

From the modeling results, the temperature of the adiabatic core in the end gas, $T_{u,core}$, was separately evaluated and used as a representative temperature of the end gas since auto-ignition occurs first in the adiabatic core due to its higher temperature. In calculating the adiabatic core temperature in the end gas, in-cylinder pressure was used as in **Eq. (2.11)** below.

$$\frac{dP}{P} = \frac{\gamma(T_{u,core})}{\gamma(T_{u,core}) - 1} \frac{dT_{u,core}}{T_{u,core}} \qquad \textbf{Eq. (2.11)}$$

The resultant temperature and pressure of the end gas of various ERFs are shown as **Figure 2.2**. All the variable is plotted on the burned mass fraction (BMF) axis, which is defined as the mass fraction burned by flame propagation in cylinder. As shown, the temperature of the end gas decreases and pressure increases slightly as the ethanol content increases since a higher latent heat of vaporization of ethanol leads to more charge cooling effect.

Figure 2.3 shows the validation of the in-cylinder pressure from the developed model with the experimental result of Foong et al. [57] under the RON tested condition with isooctane. As shown, calculated pressure-CAD profile was well-matched with the measurement.

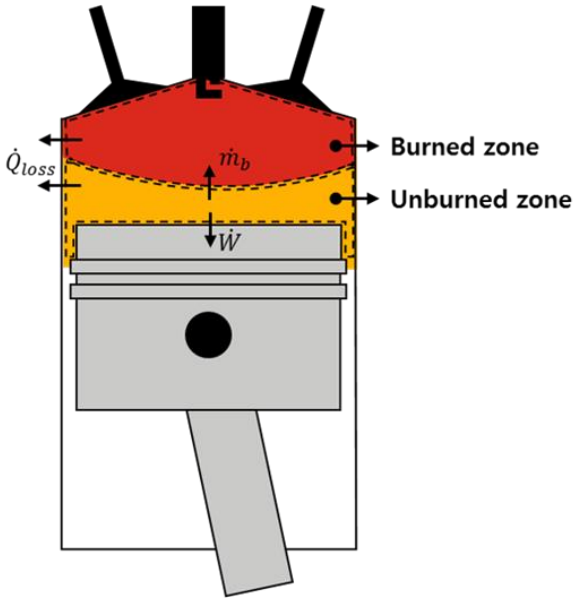

Figure 2.1 Schematic of 0-D two-zone SI engine model[50]

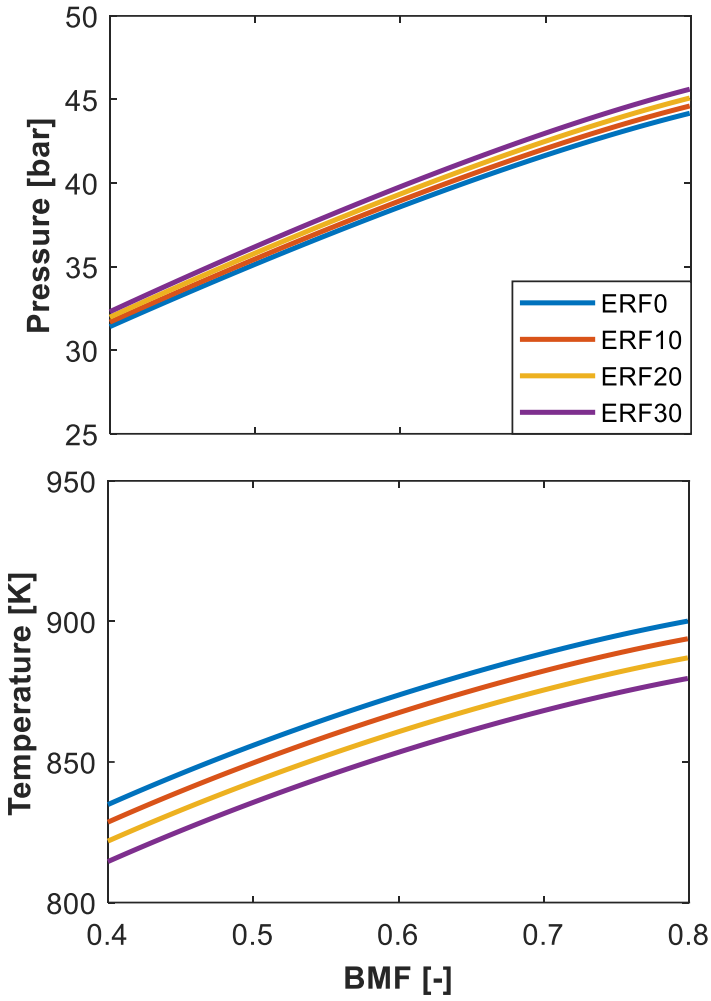

Figure 2.2 Dependency of (a) pressure and (b) temperature profile on ethanol content under RON test condition.

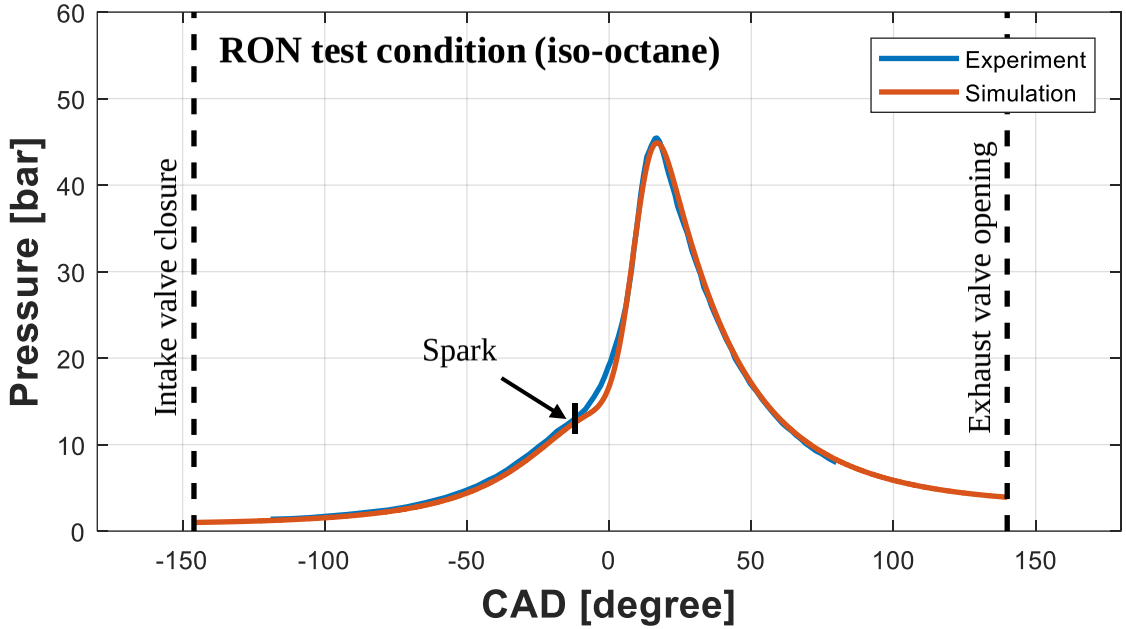

Figure 2.3 Validation of in-cylinder pressure from 0-D two-zone SI engine model with the measurement from Foong's Ph.D. dissertation [50, 57]

2.3 Rapid compression machine experiment

2.3.1 Measurement procedure and data processing

The auto-ignition characteristics of the end gas for the given thermodynamic state and ethanol content were measured using the RCM in Seoul National University (SNU). Schematic and specification of RCM are described on **Figure 2.4** and **Table 2.2**. The details of measurement procedure is as follow:

1. Mixing chamber, which is depicted on **Figure 2.5**, was heated to 373.15 K by electric heater to prevent the condensation of liquid fuel. After two hour, the temperature of gas inside chamber was stabilized around 340 K, then, the chamber was vacuumed to 0.001 bar.

2. Liquid fuel was injected into the vacuumed mixing chamber first using syringe, in order to induce the flash boiling of fuel. Then the gas component such as O_2, N_2, CO_2, and Ar was supplied with monitoring its quantity based on pressure inside the chamber. Fuel and gas component in the mixing chamber were stirred with electric fan for 30 minutes. It should be noted that the purity of gas component was over 99.999 % and that of liquid fuel was over 99.9 %.

3. Combustion chamber, which is shown on **Figure 2.6**, was heated to the desired temperature. The gas temperature inside the chamber was calculated based on the wall temperature, by using the correlation equation between them determined by calibration measurement as **Figure 2.7**.

4. Main accumulator in the hydraulic circuit, which is shown in **Figure 2.8**, was charged with hydraulic oil to 80 kgf/cm^2 using oil pump; it acts a constant force pushing the driving piston to top dead center (TDC). Then, driving piston were moved back to bottom dead center (BDC) by pressurizing the opposite side of piston to 130 kgf/cm^2.

5. The combustion chamber was vacuumed to 0.001 bar. Then, the mixture from the mixing chamber was supplied to the combustion chamber to the desired pressure, and rested for 1 minute for stabilizing the temperature of the mixture.

6. By flushing the high pressure oil in the opposite side of piston, the driving piston was shoot and the mixture inside the combustion chamber was rapidly compressed with the compression time less than 30 ms. The driving piston stopped at TDC, and the auto-ignition process was observed using the pressure transducer mounted on the head of the cylinder. It should be noted that the flushing valve was actuated by spool piston, which is driven by the secondary accumulator, since it is superior to conventional solenoid valve system with short response time less than 10 ms.

7. The product gas was exhaust, then the procedure 4 to 7 were repeated by 3-5 times.

The measurement from pressure transducer was processed to achieve the ignition delay through following procedure.

1. Low-pass filter was applied to the raw data to remove the noise. Cutoff frequency was set to be 2.5 kHz.

2. Since the pressure transducer measures the relative change of pressure from the start of measurement, the absolute pressure sensor mounted on the feeding line was used to measure the initial pressure and compensate the measurement from the pressure transducer.

3. The temperature inside the combustion chamber was calculated based on adiabatic core assumption as **Eq. (2.12)**.

$$\frac{dP_{RCM}}{P_{RCM}} = \frac{\gamma(T_{RCM})}{\gamma(T_{RCM}) - 1}\frac{dT_{RCM}}{T_{RCM}} \qquad \textbf{Eq. (2.12)}$$

4. The end of compression was determined by finding the first instant where the pressure rise rate becomes negative from the instant of pressure reaching 15 bar. The ignition delay was defined as the time interval from the end of compression to the instant of maximum pressure rise rate.

Typical result of measurement is shown in **Figure 2.9**. There were a fluctuation of pressure right after the compression led by the vibration of piston, but its amplitude was less than 5 % of the compressed pressure. In order to validate the reliability of measurement, the ignition delay of stoichiometric ERF0–air mixture at 20 bar was measured and compared with the measurement from other research groups. As shown on **Figure 2.10**, the measurement from RCM in SNU was consistent with the others.

Table 2.2 Specifications of the RCM at SNU

Parameter	Value
Cylinder bore [mm]	60
Stroke [mm]	90
Compression ratio [-]	8–19[a]
Compression time for full stroke [ms]	~30[b]
Compression time for 50 % of compression [ms]	~3[b]
Sampling frequency of pressure transducer [kHz][c]	10

[a] Adjustable by varying the clearance at TDC.
[b] Dependent on the compression ratio.
[c] Kistler 6052C31 piezoelectric sensor

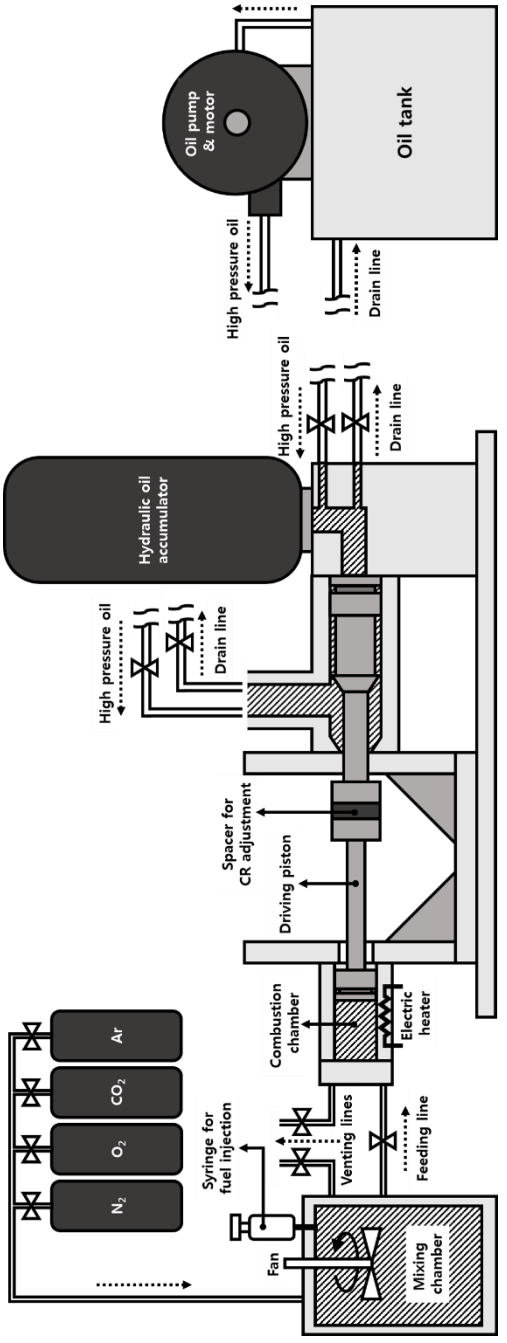

Figure 2.4 Schematic of RCM in SNU[50]

Figure 2.5 Mixing chamber of RCM

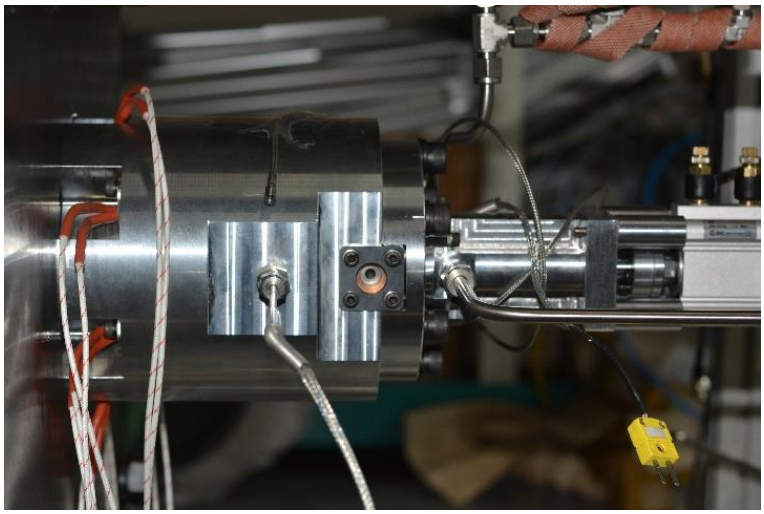

Figure 2.6 Combustion chamber of RCM

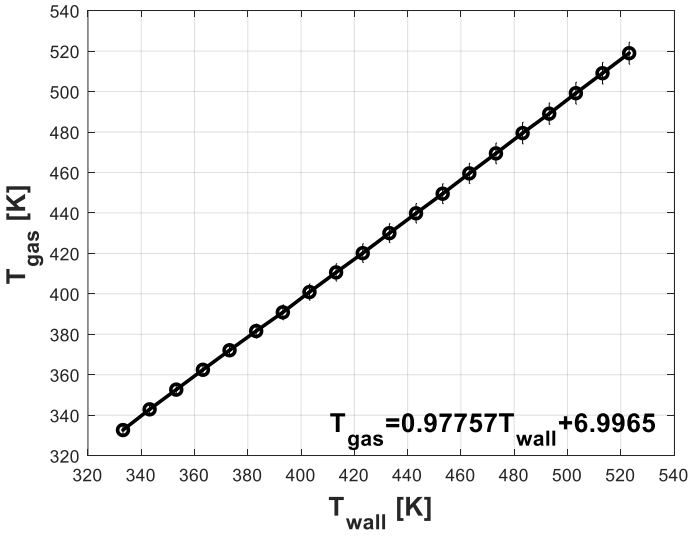

Figure 2.7 Correlation between the temperature of wall and gas in the combustion chamber

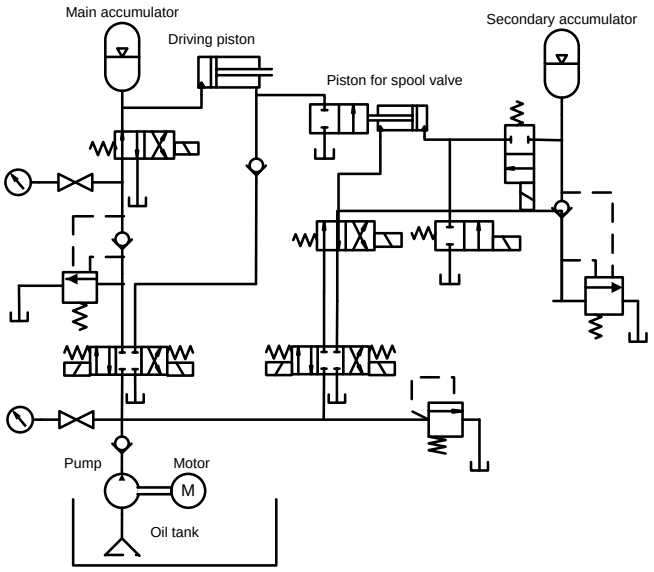

Figure 2.8 Hydraulic circuit for driving piston of RCM [60]

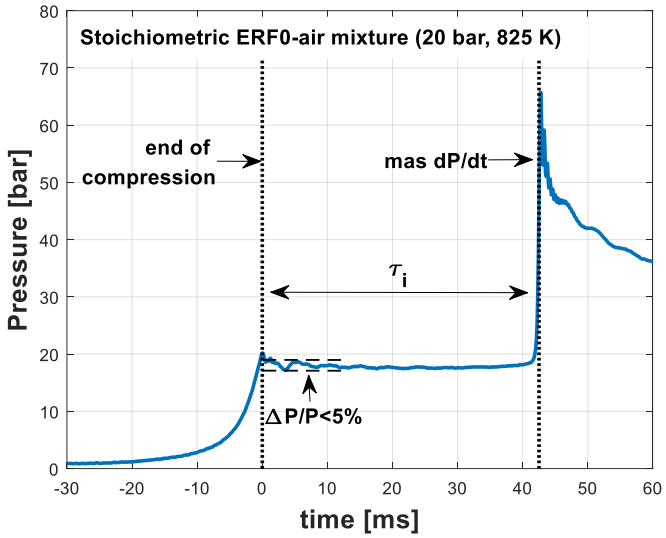

Figure 2.9 Typical pressure-time profile inside the combustion chamber of RCM and the definition of ignition delay

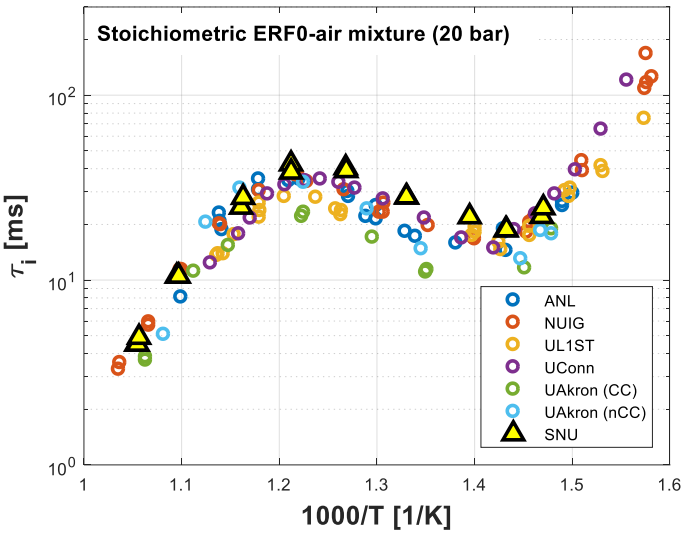

Figure 2.10 Comparison of ignition delay of ERF0 (iso-octane) from different RCMs [61] including that of SNU

2.3.2 Active manipulation of compression process for simulating the flame propagation process in SI engine

In conventional RCM experiments, the piston is driven as fast as possible to suppress the reaction during the compression stroke [62]. The facility in SNU, however, actively manipulates the compression process in the RCM to simulate the thermodynamic state of the end gas during the flame propagation process in the SI engine. The end gas in the SI engine undergoes an almost adiabatic compression during flame propagation owing to the expanding volume of burned gas, and the process can be simulated with adiabatic compression by piston movement with the RCM. Consequently, as shown in **Figure 2.11**, the pressure–time history during the compression process in the RCM is similar to that of the engine during the flame propagation process in RON test condition. Moreover, the temperature–pressure profile inside the RCM cylinder, where the temperature was calculated with adiabatic core assumption, follows that of the end gas during the flame propagation process, as shown in **Figure 2.12**.

This method allows us to measure the ignition delay with considering the effect of the reaction integration during the flame propagation process in the SI engine. Thus, the measured ignition delay is generally shorter than the conventional meaning of ignition delay, which assumes no reaction progression during the compression process in the RCM. This modified ignition delay definition, although confusing, is suitable for this study because the measurement inherently contains the effect of reaction integration along the given temperature–pressure profile, which has been considered by using Livengood–Wu integration in previous studies, thus able to quantify the effect of the temperature–pressure profile from the measurements.

This idea can be expressed mathematically as follow. **Figure 2.13** shows difference between the measured ignition delay from RCM, $\tau_{i_{RCM}}$ and the original ignition delay, $\tau_{i_{orignal}}$, which are calculated from 0-D reactor simulation using the reduced mechanism of Mehl et al. with 679 species and 5627 reactions [51]. According to Livengood-Wu integration method, $\tau_{i_{RCM}}$ is related with $\tau_{i_{orignal}}$ as **Eq. (2.13)**; SOC (or EOC) is the subscript for the start (or end) of compression. Here, **Eq. (2.13)** can be transformed with respect to $\tau_{i_{RCM}}$ as **Eq. (2.14)**. As shown, $\tau_{i_{RCM}}$ is proportional to both $\tau_{i,orignal}$ and $(1 - LW_{EOC})$. It should be noted that LW_{EOC}, the integration of reaction during compression process in RCM, has a physical meaning of that during flame propagation process in SI engine. Therefore, $\tau_{i_{RCM}}$ can be used for a representative quantity of the auto-ignition characteristics in SI engine, with considering both the integration of reaction at the given instant, LW_{EOC}, and the original ignition delay at the given instant, $\tau_{i_{orignal}}$.

$$1 = \int_{t_{SOC}}^{t_{EOC}} \frac{dt}{\tau_{i_{original}}\big(T(t), P(t)\big)} + \frac{\tau_{i,RCM}}{\tau_{i_{orignal}}(T_{EOC}, P_{EOC})} \quad \textbf{Eq. (2.13)}$$

$$\tau_{i_{RCM}} = (1 - LW_{EOC})\tau_{i_{orignal}}(T_{EOC}, P_{EOC}) \quad \textbf{Eq. (2.14)}$$

$$\text{where } LW_{EOC} \equiv \int_{t_{SOC}}^{t_{EOC}} \frac{dt}{\tau_{i_{orignal}}\big(T(t), P(t)\big)}$$

Because the reaction progresses exothermically during the compression process, the pressure at the end of compression is slightly higher than that of the inert gas compression case, as shown in **Figure 2.14.** Based on this observation, the pre-heat release, Q_{PHR}, was defined as the heat released during compression process, which can be calculated as **Eq. (2.15)**. From my previous researches, it was found that Q_{PHR} has a significant effect on the overall ignition delay [49]. This is why the ignition delay should be measured experimentally, not calculated from detailed

mechanism, since the most of detailed mechanism shows less accuracy for predicting cool flame chemistry determining Q_{PHR} [63].

$$Q_{PHR} = \frac{\overline{MW}}{\gamma(T_{EOC}) - 1} \frac{\left(P_{EOC(react.)} - P_{EOC(inert)}\right)}{\rho_{EOC}} \qquad \textbf{Eq. (2.15)}$$

Here, it is noteworthy that the temperature and pressure at the end of compression are based on those of the inert case, which can be considered the thermodynamic state of the end gas under a condition without pre-heat release. This allows for a fair comparison of the reactivity of various fuels, which show the different pre-heat release characteristics.

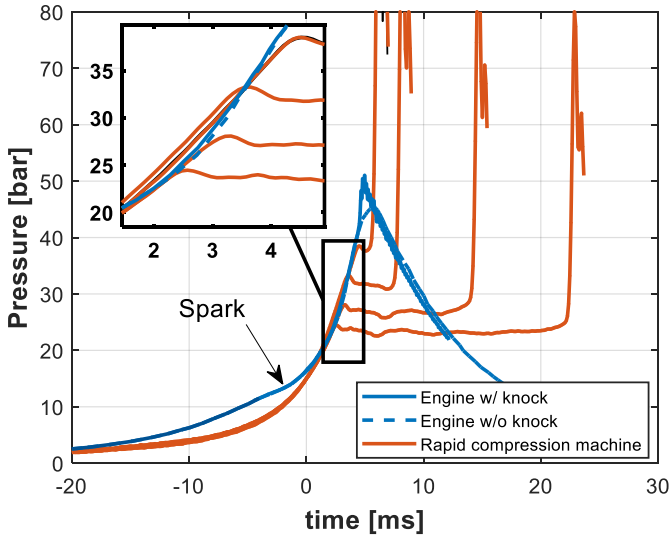

Figure 2.11 Comparison between representative pressure-time profiles from the RON test condition [57] and from the RCM experiment[49]

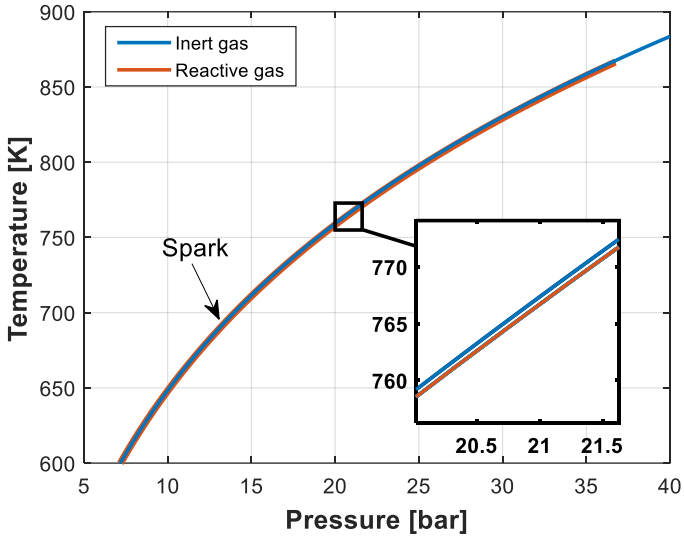

Figure 2.12 Comparison between the temperature-pressure profiles from the SI engine model and from the RCM experiment[49]

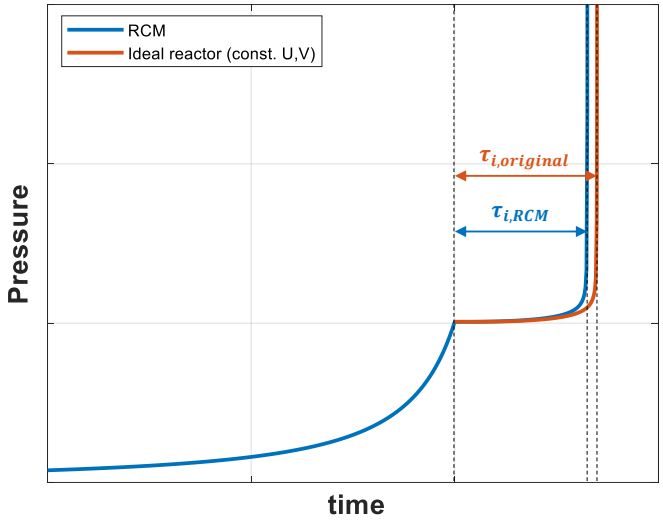

Figure 2.13 The difference of the measured ignition delay from RCM and the original ignition delay from ideal reactor (adiabatic and constant volume)

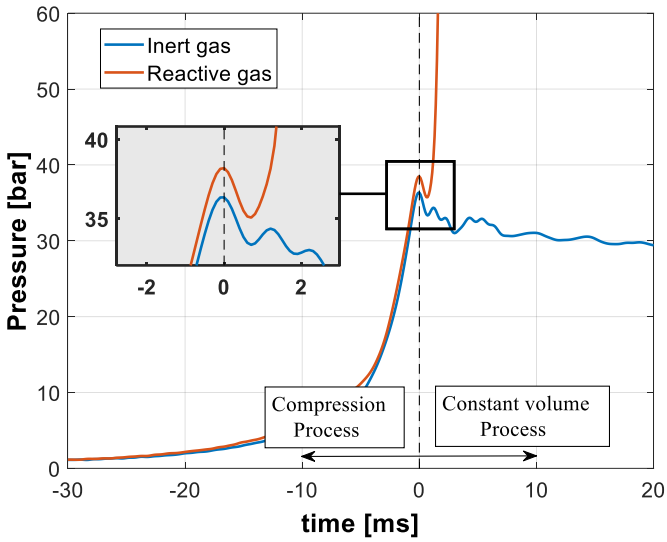

Figure 2.14 Pre-heat release during the compression process of RCM[49]

Chapter 3. Effect of temperature–pressure profile of the end gas on optimal ethanol content

As engine operating conditions or engine design are varied, the thermodynamic state of end gas is deviated, which results in different knocking characteristics. Among all the state thermodynamic variables, the temperature and pressure of the end gas are the most sensitive to engine operating condition, and the most influential to knocking characteristics.

In this regard, there have been numerous studies on the effect of temperature and pressure of the end gas on knocking characteristics of SI engine. Szybist and Splitter executed the experimental study on the effect of pressure and temperature in knocking characteristics of fuels with varying octane sensitivity [64]. As a result, they found that the fuel with low OS is more sensitive to the change of in-cylinder pressure. Meanwhile, the study from Yi et al. also gives a similar result [65] using homogeneous charge compression ignition (HCCI) engine; the combustion phase of ethanol, which has high OS, shows lower sensitivity to pressure and higher sensitivity to temperature than gasoline. However, both study are based on the engine experiment, thus give a practical information on the effect of temperature and pressure on auto-ignition characteristics of certain type of engines. However, they have a limitation on applying the results to the arbitrary design or operating condition of SI engine since the thermodynamic state of tested design or operating condition is hard to be characterized precisely.

This chapter discusses how the ignition delay of the end gas is varied according to engine operating condition and ethanol content in the fuel, in order to understand how knocking characteristics is related with the ignition delay characteristics. All the discussion was restricted to the engine operating condition

where equivalence ratio is stoichiometric and no significant rate of dilution is used; thus the only temperature and pressure are varied according to engine operating condition.

In this regard, ignition delay of various ERFs, was measured in varying temperature and pressure using the rapid compression machine (RCM) and regressed to realize an empirical correlation of ignition delay. Then, the effect of engine operating condition on the knocking characteristics of each fuel was quantified by evaluating the dependency of ignition delay on the temperature–pressure profile of the end gas in the given engine operating condition.

The main body of this paper consists of seven sub-chapters. **Chapter 3.1** covers the SI engine simulation for four different design or operating conditions of engine, turbocharging, higher CR, lower heat loss, and higher IT, which mainly deviate the temperature-pressure profile of end gas in SI engine. Then, **Chapter 3.2** describes the result of ignition delay measurement and the regression analysis on them. Based on the achieved empirical correlation, **Chapter 3.3** and **Chapter 3.4** handles the quantitation of the effect of engine design modification on knocking, and its uncertainty. Then, **Chapter 3.5** and **Chapter 3.6** describes the quantitative comparison between the effects of different types of engine operating conditions on knocking phenomena. Finally, the results on knocking characteristics from ignition delay measurement is validated by analyzing the analogy with Kalghatgi's K value principle, which is dealt with on **Chapter 3.7**.

3.1 Engine simulation for varying engine operating conditions

Based on the RON test condition, four different operating conditions were considered, which are relevant to the modern SI engine: turbocharging, higher CR, lower heat loss, and higher IT. Although the IT has been successfully decreased in recent years, owing to the high efficiency of the intercooler and enhanced charge-cooling effect using direct injection [66], the simulation was performed with a higher IT value to consider a knocking-promoting case as the other candidate. Operating parameters for each condition are described on **Table 3.1**.

The turbocharger was simply modeled by considering the isentropic efficiencies of the compressor and the turbine [52], which were assumed to be 80 %, and its effect on the exhaust manifold pressure was considered by increasing the density of the residual gas. The effect of lower heat loss, which can be achieved with a ceramic coating [12], was considered by reducing the heat convection coefficient from that of Woschni's heat transfer model to zero. The effects of higher CR and higher IT were evaluated by varying the boundary conditions of the model.

The deviation of the temperature–pressure profile according to engine operating condition is plotted along BMF axis, which is evaluated from the Wiebe function, as shown in **Figure 3.1**. It can be seen that turbocharging leads to higher pressure and slightly lower temperature because the mole fraction of the residual gas decreases as the intake pressure increases. Meanwhile, a higher CR and lower heat loss lead to higher pressure and temperature of the end gas. The case with higher IT shows higher temperature and lower pressure owing to decreased volumetric efficiency of the engine.

Table 3.1 Operating parameters for test engine conditions

Parameter	RON condition	Turbocharging	Higher CR	Lower heat loss	Higher IT
Cylinder bore [mm]	82.6	-	-	-	-
Stroke [mm]	114.3	-	-	-	-
Connecting rod length [mm]	265.2	-	-	-	-
IVC [aBDC]	34	-	-	-	-
Spark timing [bTDC]	13	-	-	-	-
Engine speed [rpm]	600	-	-	-	-
Compression ratio [-]	7.9	-	8.2	-	-
Intake pressure [bar]	7.9	1.05	-	-	-
Intake air temperature [K]	325.15	-	-	-	356.15
Equivalence ratio [-]	1	-	-	-	-
Convection heat coefficient [W m^{-2} s^{-1}]	Woschini's model [59]	-	-	0	-

[c] The lower heat loss condition was assumed to be that of an adiabatic engine
[d] The change in the engine operating condition was chosen to have the same effect on ignition delay (at BMF0.7) of ERF0 with that of the lower heat loss condition

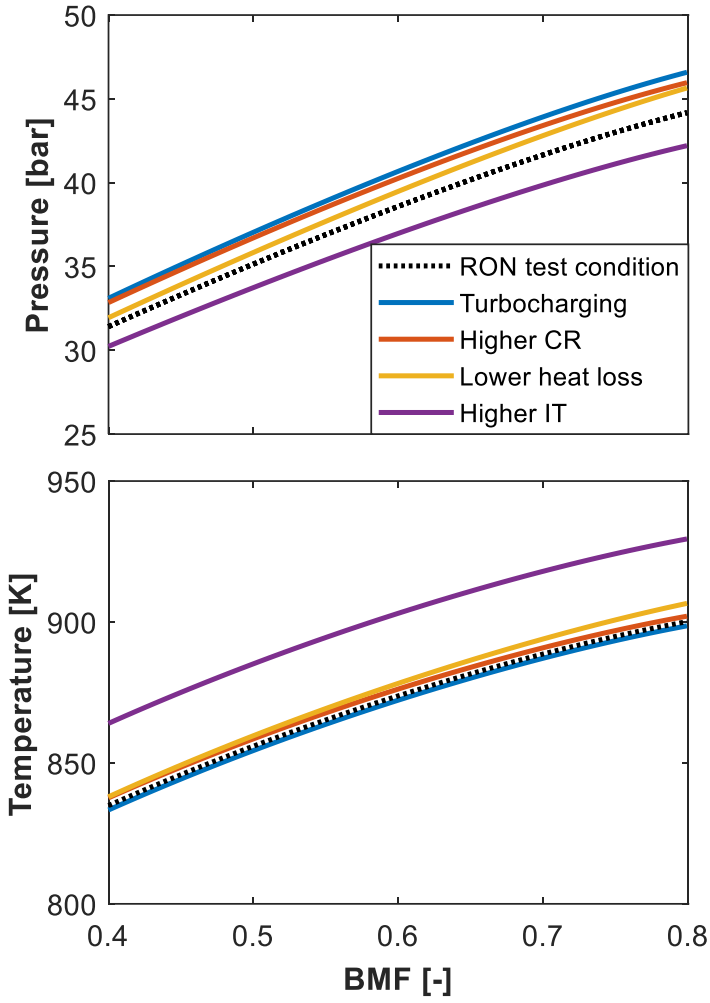

Figure 3.1 (a) Pressure and (b) temperature deviation induced from various type of engine design modification for ERF0.

3.2 Regression analysis on the ignition delay data

The ignition delay was measured around the thermodynamic condition of the end gas in the RON test condition; thus, the tested temperature decreases as ethanol content increases. In addition, to account for the effect of residual gas on the specific heat ratio and heat capacity, pseudo-residual gas, which consists of N_2 by 82 % and CO_2 by 18 % and has the same specific heat ratio as that of the residual gas, was mixed with the fuel-air mixture for all the conditions by 6.1 % (in mole fraction), as calculated in an SI engine model.

Table 3.2 shows the result of ignition delay measurement for various ERFs. The experiment was reiterated for the same condition about 3–5 times. The coefficient of variation for the compression time was under 2 %, and for the ignition delay it was lower than 14 % for all of the results.

In order to make the discrete information of the measured ignition delay to be continuous function, which is essential for differentiation of the ignition delay with respect to temperature or pressure in **Chapter 3.4** and **Chapter 3.5**, an analytical form of the ignition delay was required. There have been several approaches to derive the empirical correlation of the ignition delay with NTC behavior with various form of regression. AlAbbad et al. [67] used the combination of three Arrehnius equations as **Eq. (3.1)**. Meanwhile, Goldsborough [68] and DelVescovo et al. [69] assumes one Arrehnius equation, then express the coefficients of equation as complicate function of 1/T as **Eq. (3.2)**.

$$\frac{1}{\tau_i} = \frac{1}{\tau_{i_1} + \tau_{i_2}} + \frac{1}{\tau_{i_3}} \qquad \textbf{Eq. (3.1)}$$

$$\text{where } \tau_{i_k} = C_{1,k}\left(\frac{P}{P_{ref}}\right)^{C_{2,k}} \phi^{C_{3,k}} \exp\left(\frac{C_{4,k}}{T}\right), k = 1,2, \text{or } 3$$

$$\tau_i = C_1 x_{O_2}^{C_1} P^{C_2} \phi^{C_3} \exp(C_4) \qquad \textbf{Eq. (3.2)}$$

$$\text{where } C_k = C_k\left(\frac{1}{T}\right), k = 1,2,3, \text{or } 4$$

In this study, the ignition delay data was regressed with a mathematical function described by **Eq. (3.3)**, which assumes the power rule dependency on pressure and exponential cubic dependency on the reciprocal of the temperature to cover a wide range of thermodynamic states, including the negative temperature coefficient (NTC) region. It should be noted that **Eq. (3.3)** is equivalent to **Eq. (3.4)**, which is the conventional form of the Arrhenius equation employed by a number of previous works [70, 71], with a quadratic expression of the activation energy for consideration of the NTC region.

$$\tau_i = P^n \exp\left(\sum_{i=0}^{3} a_i \left(\frac{1000}{T}\right)^i\right) \qquad \textbf{Eq. (3.3)}$$

$$\tau_i = A_r P^n \exp\left(\frac{E_a}{R_u T}\right) \qquad \textbf{Eq. (3.4)}$$

$$\text{where } E_a = \sum_{i=0}^{2} E_{a,i} \left(\frac{1000}{T}\right)^i$$

It might be confusing that the empirical correlation of $\tau_{i,RCM}$, **Eq. (3.3)**, is solely based on T_{EOC} and P_{EOC}, even though $\tau_{i,RCM}$ also depends on LW_{EOC} as discussed in **Eq. (2.14)**. To understand this, it should be noted that $T(t)$ and $P(t)$ during compression process in RCM, which determine the magnitude of LW_{EOC}, are uniquely determined by T_{EOC} and P_{EOC}. This is because the $P(t)$

during compression process is fixed to be similar with RON test condition, and $T(t)$ during compression process is determined by $P(t)$ and T_{EOC} using the adiabatic core assumption. Consequently, LW_{EOC} can be expressed as a function of T_{EOC} and P_{EOC}, thus $\tau_{i,RCM}$ is only dependent on T_{EOC} and P_{EOC}, as described on **Eq. (3.5)**.

$$\tau_{i,RCM}(T_{EOC}, P_{EOC}) = \left(1 - LW_{EOC}(T_{EOC}, P_{EOC})\right)\tau_{i,orignal}(T_{EOC}, P_{EOC}) \quad \textbf{Eq. (3.5)}$$

Figure 3.2 shows the fitting coefficients of empirical correlation, $n; a_0; a_1; a_2; a_3$, for each tested fuel. It was found that all the parameters vary with z_E monotonically; thus, they can be expressed as a quadratic function of z_E, as described in **Eq. (3.6)**. Consequently, the integrated correlation covers the dependency of ignition delay on the ethanol content as well as temperature and pressure, via 15 independent coefficients, as described in **Table 3.3**.

$$X(z) = X_0 + X_1 z_E + X_2 z_E^2 \quad \textbf{Eq. (3.6)}$$

$$\text{where } X = n, a_0, a_1, a_2, \text{and } a_3$$

The exponent on pressure, n, is much lower than that obtained in previous studies, where it was reported to be higher than -2 [70]. This is because the measurement of this study includes the effect of reaction integrated during the flame propagation process in an SI engine; therefore, the ignition delay at higher pressure is subject to more integration effect, which results in a sharp decrease of ignition delay with increase in pressure, than that when the integration effect is not considered.

The reliability of the empirical correlation was validated by comparing the predicted ignition delay with the measured one. As shown in **Figure 3.3 (a) and (b),** the correlation represents the behavior of the ignition delay with a determination factor of 0.98242. It should be noted that this empirical correlation is based on the ignition delay measurement around RON test condition, thus should be carefully used for the condition far from it.

Table 3.2 Ignition delay of ERFs for various temperature and pressure

No.	Fuel	P [bar]	T [K] [a]	τ_i [ms] [b]	No.	Fuel	P [bar]	T [K] [a]	τ_i [ms] [b]
1			787-30	19.8 (±0.4)	25			772-30	16.9 (±0.3)
2		23.7	787	20.9 (±0.9)	26		23.7	772	18.5 (±0.8)
3			787+30	20.8 (±0.6)	27			772+30	20.7 (±0.3)
4			812-30	11.8 (±0.5)	28			795-30	11.9 (±0.3)
5		27.2	812	11.3 (±0.4)	29		27.2	795	12.6 (±0.2)
6	**ERF0**		812+30	9.6 (±0.6)	30	**ERF20**		795+30	10.7 (±0.7)
7			842-30	5.4 (±0.3)	31			826-30	7.6 (±0.3)
8		32.4	842	4.5 (±0.1)	32		32.4	826	5.9 (±0.1)
9			842+30	4.2 (±0.1)	33			826+30	4.3 (±0.1)
10			866-30	1.9 (±0.1)	34			849-30	3.7 (±0.2)
11		36.7	866	1.4 (±0.1)	35		36.7	849	2.2 (±0.2)
12			866+30	1.0 (±0.1)	36			849+30	1.3 (±0.2)
13			779-30	19.3 (±0.2)	37			760-30	17.0 (±0.6)
14		23.7	779	23.6 (±0.2)	38		23.7	760	15.2 (±0.3)
15			779+30	25.1 (±0.3)	39			760+30	17.6 (±0.4)
16			803-30	13.6 (±0.2)	40			783-30	10.3 (±0.1)
17		27.2	803	13.1 (±0.4)	41		27.2	783	11.0 (±0.1)
18	**ERF10**		803+30	10.5 (±0.3)	42	**ERF30**		783+30	10.6 (±0.4)
19			833-30	7.0 (±0.1)	43			814-30	7.3 (±0.1)
20		32.4	833	5.8 (±0.2)	44		32.4	814	6.6 (±0.3)
21			833+30	4.4 (±0.1)	45			814+30	4.8 (±0.1)
22			857-30	3.2 (±0.2)	46			836-30	4.1 (±0.3)
23		36.7	857	2.0 (±0.2)	47		36.7	836	2.5 (±0.2)
24			857+30	1.3 (±0.0)	48			836+30	1.3 (±0.0)

[a] The temperature at the end of compression was controlled by varying initial temperature.
[b] The values inside brackets represent 95 % confidence interval of ignition delay.

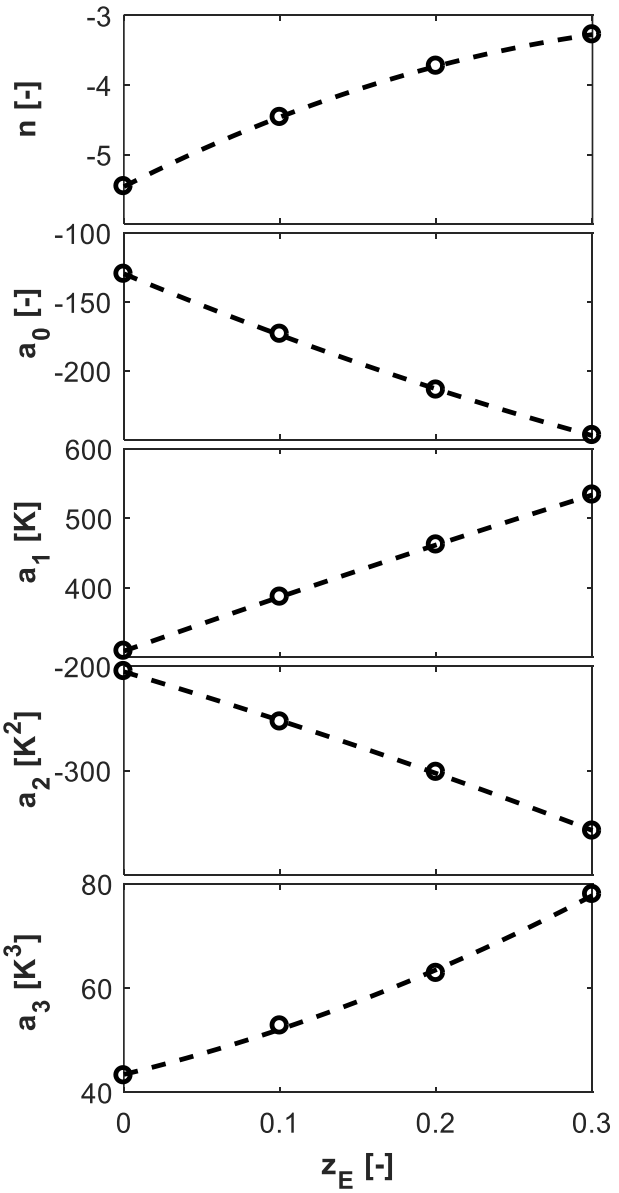

Figure 3.2 Coefficient of the empirical correlation for ignition delay

Table 3.3 Coefficients of the empirical correlation for ignition delay

X	X_0	X_1	X_2
n	-5.4587	11.4628	-13.9702
a_0	-126.9790	-519.6181	403.9925
a_1	302.0360	916.3686	-495.3292
a_2	-199.4397	-549.4583	86.4812
a_3	41.7599	100.8337	60.7577

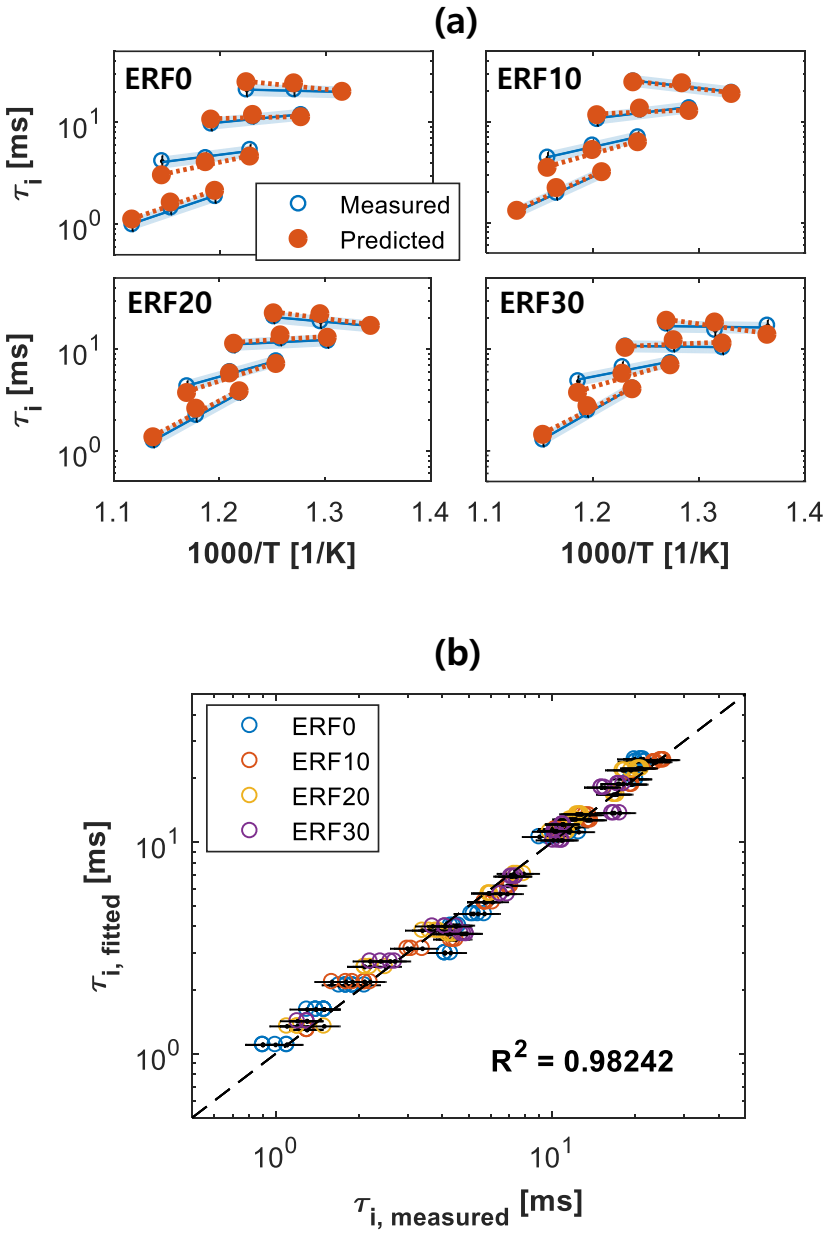

Figure 3.3 Validation of empirical correlation on the ignition delay

3.3 Quantitative analysis on the effect of engine operating condition on knocking characteristics

Based on the calculated temperature–pressure profile and the empirical correlation for ignition delay, the effect of engine operating condition on knocking characteristics was quantitatively assessed. For this, there is an issue which variable should be used as an axis for comparing the ignition delay from different engine operating conditions. The possible candidates are pressure axis or CAD axis. However, it is thought that the comparing the ignition delay on pressure axis or CAD axis does not give the fair evaluation of knocking intensity, since the occurrence of auto-ignition at the same pressure or CAD from two different engine condition does not guarantee the identical intensity of knocking for both condition.

Therefore, BMF axis was chosen for comparing the ignition delay from different engine operating conditions. This is based on the idea that a lower BMF at auto-ignition generally leads to more intensive knocking [72]; thus, a longer ignition delay at a given BMF can be considered more resistive to knocking or auto-ignition, and vice versa.

In this regards, the effect of temperature deviation, E_T, which is the logarithmic change of the ignition delay on the BMF axis from the RON test condition to the modified engine condition with no pressure deviation, is defined by **Eq. (3.7)**. Similarly, E_P, the effect of pressure deviation, which is the logarithmic change of the ignition delay on the BMF axis from the condition used for E_T to the modified engine condition, is defined by **Eq. (3.8)**. Consequently, the total effect of the temperature–pressure deviation, E_{TP}, can be simply defined as the arithmetic sum of E_T and E_P, as described by **Eq. (3.9)**.

$$E_T = \log\left(\frac{\tau_i(T_{mod.}, P_{RON})}{\tau_i(T_{RON}, P_{RON})}\right)\Bigg|_{BMF} \qquad \textbf{Eq. (3.7)}$$

$$E_P = \log\left(\frac{\tau_i(T_{mod.}, P_{mod.})}{\tau_i(T_{mod.}, P_{RON})}\right)\Bigg|_{BMF} \qquad \textbf{Eq. (3.8)}$$

$$E_{TP} = \log\left(\frac{\tau_i(T_{mod.}, P_{mod.})}{\tau_i(T_{RON}, P_{RON})}\right)\Bigg|_{BMF} = E_T + E_P \qquad \textbf{Eq. (3.9)}$$

3.4 Uncertainty Quantification of E_T, E_P, and E_{TP}

E_T, E_P, and E_{TP} are determined based on the empirical correlation, **Eq. (3.3)**, which are derived from the regression analysis on the 48 set of data described on **Table 3.2**. Thus, there can be uncertainty of E_T, E_P, and E_{TP}, from the measurement error, $e(E_T)$; $e(E_P)$; and $e(E_{TP})$, and they were calculated based on independent parameter method as described on **Eq. (3.10)**–**Eq. (3.11)**; $\tau_{i,k}$ is the measured ignition delay, $T_{EOC,k}$ is the temperature at the end of compression in RCM experiment, and $P_{EOC,k}$ is the pressure at the end of compression.

$$e(E_{T(or\ P)}) = \sqrt{\sum_{k=1}^{48}\left\{\left(\frac{\partial E_{T(or\ P)}}{\partial \tau_{i,k}} e(\tau_{i,k})\right)^2 + \left(\frac{\partial E_{T(or\ P)}}{\partial T_{EOC,k}} e(T_{EOC,k})\right)^2 + \left(\frac{\partial E_{T(or\ P)}}{\partial P_{EOC,k}} e(P_{EOC,k})\right)^2\right\}} \qquad \textbf{Eq. (3.10)}$$

where $E_{T(or\ P)} = E_{T(or\ P)}(T_{mod}, P_{mod}, T_{RON}, P_{RON}, \tau_{i,1}, T_{EOC,1}, P_{EOC,1}, \dots, \tau_{i,48}, T_{EOC,48}, P_{EOC,48})$

$$e(E_{TP}) = \sqrt{e(E_T)^2 + e(E_P)^2} \qquad \textbf{Eq. (3.11)}$$

The uncertainty of the ignition delay measurement, $e(\tau_{i,k})$, was chosen as 95 % confidence interval of measurement. Meanwhile, those of temperature and pressure at the end of compression, $e(T_{EOC,k})$; $e(P_{EOC,k})$, were determined by

considering the accuracy of the thermocouple and absolute pressure sensor used to measure the initial state before the compression. It should be noted that the uncertainty quantification assumes zero uncertainty on the temperature-pressure profile calculated from 0-D two-zone SI engine model due to the difficulty on reasonable quantification of them. Nevertheless, the effect of uncertainty on temperature-pressure profile was thought to be marginal since E_T, E_P, and E_{TP} are defined with the relative difference of temperature-pressure profile from varying engine design, not with the absolute value of them.

3.5 The effect of engine operating condition on the knocking characteristics

$E_T, E_P,$ and E_{TP} for the four types of engine operating conditions are depicted in the second to fourth rows of **Figure 3.4**, where the uncertainty of result is marked by the shaded areas. It should be noted that the $\frac{\Delta T}{T}$ and $\frac{\Delta P}{P}$ barely vary with the ethanol content in the fuel, thus they were represented with those of ERF0. First, as shown in **Figure 3.4 (a)**, 0.05 bar of turbocharging leads to negative E_T and positive E_P for all types of fuels. Consequently, E_{TP} for the turbocharging condition is negative, which implies that knocking becomes intensive with the introduction of the turbocharger. Meanwhile, E_{TP} increases as the ethanol content increases in the turbocharging condition. It is thus inferred that fuel with higher ethanol content has longer ignition delay in the turbocharging condition and is thus favorable for knocking suppression. Second, **Figure 3.4 (b)** shows that E_T, E_P, and E_{TP} are all negative for higher CR. Similar to the former case, E_{TP} increases as ethanol content increases, but the variation is small. Next, the lower heat loss condition, as shown in **Figure 3.4 (c)**, also leads to negative

E_T, E_P, and E_{TP}. However, there is no variation of the E_{TP} depending on ethanol content; thus, all the tested fuel would show the same knocking characteristics in the lower heat loss condition. Finally, the higher IT condition shows a completely opposite characteristic of E_{TP} from the others, as depicted in **Figure 3.4 (d)**; E_{TP} increases as ethanol content decreases, which implies that the fuel with lower ethanol content is advantageous for knocking suppression**.**

The above results can be understood qualitatively by assessing the dependency of ignition delay on the infinitesimal changes in temperature and pressure, which can be evaluated from the empirical correlation for ignition delay, i.e., **Eq. (3.3)**. As shown in **Figure 3.5**, the dependency of ignition delay on temperature, which is related to E_T, increases as the ethanol content increases, while that on the pressure shows an opposite trend. Thus, fuel with higher ethanol content is beneficial to the design modification that raises the in-cylinder pressure more than the temperature as turbocharging and higher CR, whereas the fuel with lower ethanol content is favorable in the design that increases the in-cylinder temperature more than pressure as higher IT. These results are consistent with the previous study from Yi et al. [65], where the auto-ignition characteristics of ethanol and gasoline was measured in HCCI. They also reported that the ethanol is more sensitive to temperature than the gasoline does, while less sensitive to pressure.

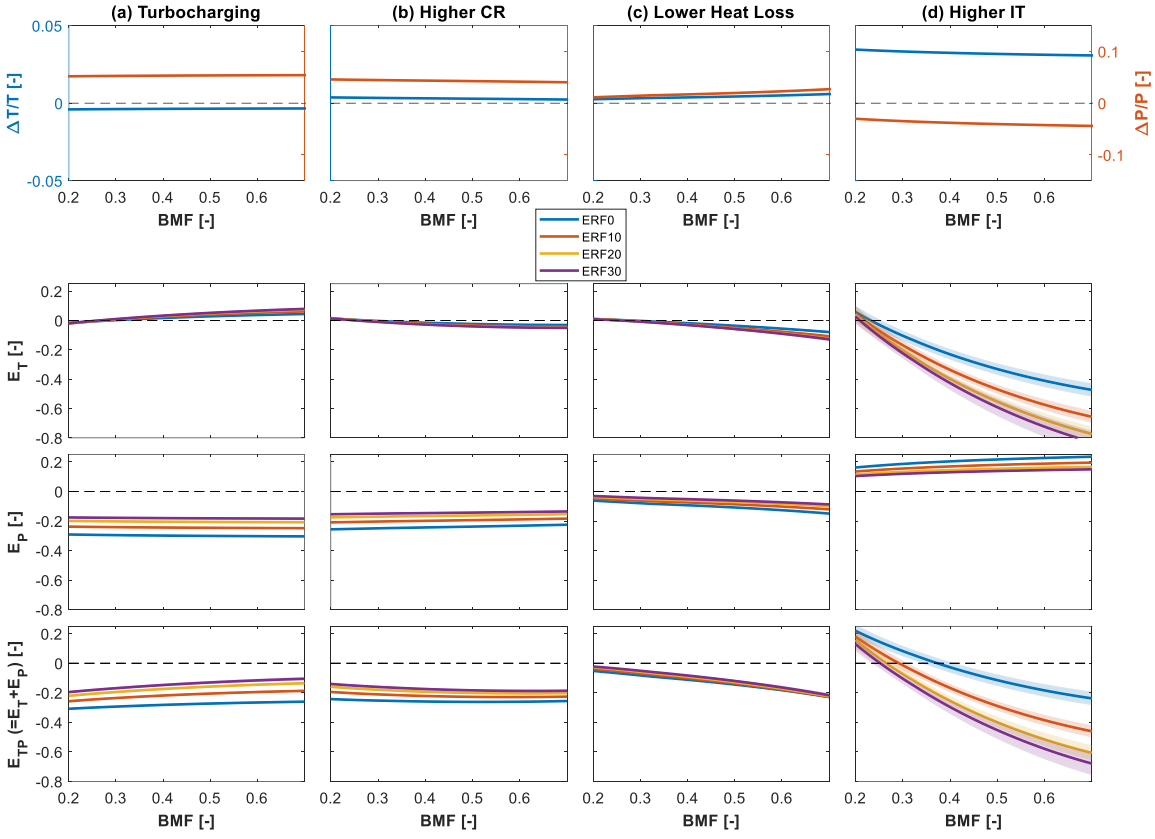

Figure 3.4 Effect of temperature and pressure deviations induced from four different engine operating conditions: (a) turbocharging, (b) higher CR, (c) lower heat loss, and (d) higher IT

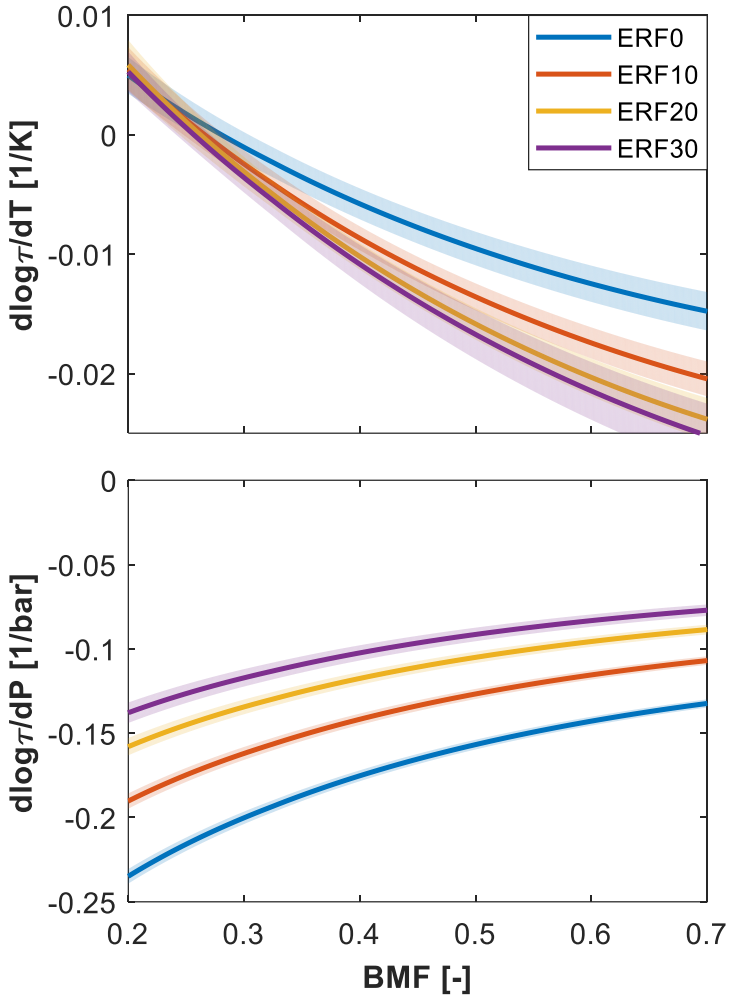

Figure 3.5 Dependency of the ignition delay on the infinisimal changes in temperature and pressure

3.6 Dependency of optimal ethanol content on the engine design

The results from the previous chapter depict that the optimal ethanol content for knock suppression depends on the temperature–pressure profile of the end gas for the given engine operating condition. In order to generalize these results to arbitrary engine operating conditions, **Figure 3.6** describes the difference between E_{TP} for ERF0 and ERF30 for the varying extent of temperature and pressure deviations. Based on this diagram, the temperature–pressure profile of the end gas in the arbitrary engine operating condition can be represented with a specific locus on the x- and y-axes of the diagram, and the optimal ethanol in the given engine operating condition can be inferred by comparing E_{TP} of ERF0 and ERF30. For example, the RON test condition is represented as (0, 0) in the diagram where E_{TP} of ERF0 is equal to that of ERF30, which implies that knocking characteristic is independent of ethanol content in the RON test condition. It should be noted that all the variables in **Figure 3.6**, i.e., E_{TP}, T, and P, are based on the values at BMF 0.7, which is the critical BMF where auto-ignition or knocking is reported to occur for the RON test condition with isooctane [57].

Figure 3.6 shows that there is no difference of E_{TP} for ERF0 and ERF30 if the relative change of temperature, $\frac{\Delta T}{T}$, is equal to 0.22 times of the relative change of pressure, $\frac{\Delta P}{P}$. Here, it is interesting to note that 0.22 is close to $\frac{\gamma-1}{\gamma}$ of the fuel–air mixture at BMF 0.7. In other words, E_{TP} is independent of ethanol content when the deviations of temperature and pressure follow the adiabatic compression line, which can be represented by **Eq. (3.12).** This is because the

adiabatic compression line is the extension of the temperature–pressure profile where the end gas undergoes the RON test condition; therefore, the ignition delay from fuels with the same RON would show the same dependency along the line. Meanwhile, E_{TP} decreases with ethanol content in the region where $\frac{\Delta T}{T}$ is greater than $\frac{\gamma-1}{\gamma}\frac{\Delta P}{P}$. This implies that the fuel with lower ethanol content is favorable for knock suppression in this region. On the other hand, the fuel with higher ethanol content is optimal in the region where $\frac{\Delta T}{T}$ is smaller than $\frac{\gamma-1}{\gamma}\frac{\Delta P}{P}$. This observation provides a clear understanding of the nature of interaction between the fuel characteristics and engine operating condition: fuels with a fixed RON would have the same knocking characteristics, if and only if the temperature–pressure profile at the given engine operating condition follows the adiabatic compression line of the RON test condition.

$$\frac{\Delta T}{T} = \frac{\gamma - 1}{\gamma}\frac{\Delta P}{P} \qquad \textbf{Eq. (3.12)}$$

This discussion helps understand the results shown in **Figure 3.4** in a more general sense. Compared to the RON test condition, the turbocharging condition starts with higher intake pressure, and the higher CR condition has lower IVC temperature owing to decreased residual gas fraction. These conditions cause the end gas to follow the temperature–pressure profile, where $\frac{\Delta T}{T}$ is always smaller than $\frac{\gamma-1}{\gamma}\frac{\Delta P}{P}$, as shown in **Figure 3.6**. Therefore, fuel with less ethanol content is more resistive to knocking for both these engine operating conditions. Meanwhile, the temperature–pressure profile of the end gas from the higher IT condition

always satisfies the condition $\frac{\Delta T}{T} > \frac{\gamma-1}{\gamma}\frac{\Delta P}{P}$. This causes the fuel with more ethanol content to show knock mitigation in the higher IT condition. Finally, the case with lower heat loss confirms that the end gas follows a profile wherein $\frac{\Delta T}{T}$ is equal to $\frac{\gamma-1}{\gamma}\frac{\Delta P}{P}$; thus, all the fuels with the same RON demonstrate the same knocking characteristics.

The former discussion on the difference of the E_{TP} of ERF0 and ERF30 was expanded to the analysis on the dependency of E_{TP} on the infinitesimal change of ethanol content. In this regard, the derivative of E_{TP} on the ethanol content for a BMF of 0.7, $\left.\frac{\partial E_{TP}}{\partial z_E}\right|_{BMF0.7}$, was calculated as shown in **Figure 3.7.** As shown, the sign of $\left.\frac{\partial E_{TP}}{\partial z_E}\right|_{BMF0.7}$ also depends on whether $\frac{\Delta T}{T}$ is larger than $\frac{\gamma-1}{\gamma}\frac{\Delta P}{P}$. In addition, the magnitude of $\left.\frac{\partial E_{TP}}{\partial z_E}\right|_{BMF0.7}$ was found to decrease as ethanol content increases, implying that the dependency of knocking characteristics on ethanol content decreases as ethanol content increases. It is noteworthy that $\left.\frac{\partial E_{TP}}{\partial z_E}\right|_{BMF0.7}$ at ERF30 does not appear to be zero along the adiabatic compression line; however, because the magnitude of $\left.\frac{\partial E_{TP}}{\partial z_E}\right|_{BMF0.7}$ is too small at ERF30, the error of ignition delay measurement has a substantial effect on the contour.

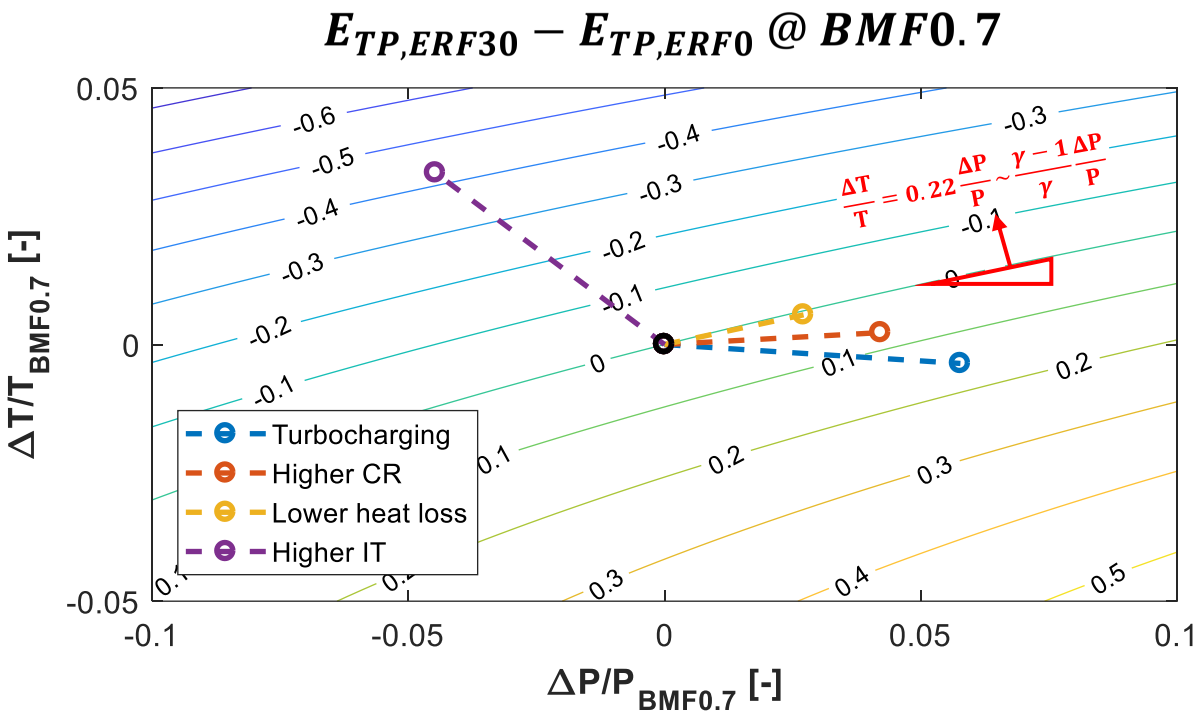

Figure 3.6 Difference between E_{TP} (@ BMF 0.7) for ERF0 and ERF30

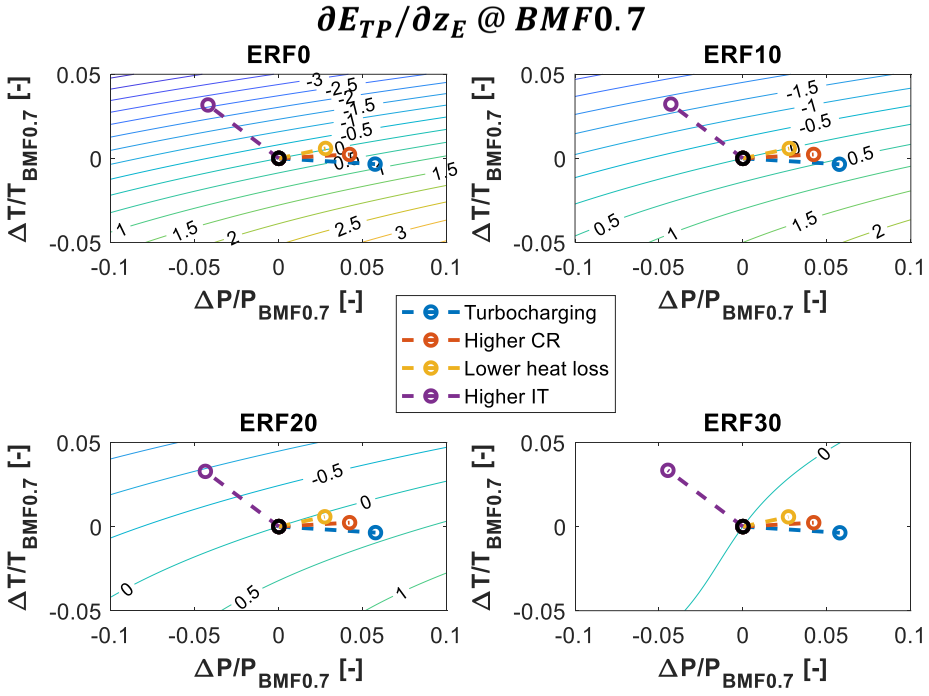

Figure 3.7 Dependency of $\frac{\partial E_{TP}}{\partial z_E}$ ($@$ $BMF0.7$) on ethanol content

3.7 Analogy with K value principle

The results of this study provide new insights into the effect of fuel composition and engine operating condition on the knocking characteristics based on the chemical kinetics or ignition delay of the fuels. To validate the reliability of the results, it was analyzed whether the results are consistent with those obtained from Kalghatgi's K value principle [19, 38]. According to Kalghatgi, the knocking characteristics of the fuel for a given engine operating condition can be expressed using an OI, which can be evaluated as a linear combination of the RON and MON as **Eq. (1.2)**. Here, K is a representative value for the engine operating condition, where the deterministic coefficient of linear regression between OI and knocking limited spark advance (KLSA) of various fuels is maximized. By definition, the K value for the RON test condition is zero and that for the MON test condition is one [19, 38].

In order to find the determining factor of K value, Kalghatgi et al. executed extensive experiment on knock characteristics at varying fuel and engine operating conditions [45, 73-75]. Consequently, Kalghatgi found that the K value is dependent on the temperature–pressure profile of the end gas. A low temperature and high pressure lead to a low K value, sometimes negative for modern engine designs. This idea was clarified by other studies conducted by Kalghatgi et al. [73, 76], where the K value was correlated with the temperature of the end gas at the moment the in-cylinder pressure reaches 15 bar, T_{comp15}, as described in **Eq. (3.13)**.

$$K(T_{comp15}) = 0.0056 * T_{comp15} - 4.68 \qquad \textbf{Eq. (3.13)}$$

However, **Eq. (3.13)** did not predict zero of the K value for the calculated T_{comp15} for the RON test condition; it is thought to be originated from nonzero

root mean squared error (RMSE) of regression analysis for deriving **Eq. (3.13).** Thus, the original equation was modified to **Eq. (3.14)**, where the constant of 4.86 was replaced with $0.0056 * T_{comp15,RON}(z_E)$, in order to predict zero of the K value for all the tested fuels. The modified equation shifts the original equation by approximately 0.7, and it has a zero K value under the RON test condition irrespective of the ethanol content. It should be noted that there can be slight error of K value prediction according to the design or combustion strategy of the given engine, considering nonzero RMSE of **Eq. (3.13)**.

$$K\left(T_{comp15}, z_E\right) = 0.0056 * \left(T_{comp15} - T_{comp15,RON}(z_E)\right) \quad \textbf{Eq. (3.14)}$$

$$\text{where } T_{comp15,RON}(x_E) = 710 - 62z_E - 26z_E^2$$

Figure 3.8 describes the derivative of OI on the ethanol content, $\frac{\partial OI}{\partial z_E}$, along the extent of temperature and pressure deviation. As shown, the K value principle induces a conclusion consistent with the result of this study. In other words, the fuel with higher ethanol content is more resistive to knocking in the engine operating condition with lower temperature and higher pressure than those of the RON test condition, whereas it is vulnerable in higher temperature and lower pressure. The magnitude of $\frac{\partial OI}{\partial z_E}$ is found to decrease as ethanol content increases, as $\left.\frac{\partial E_{TP}}{\partial z_E}\right|_{BMF0.7}$ does. Moreover, the K value principle provides the same results for the condition where all the fuels have the same knocking tendency: If the difference between temperature–pressure profile under the RON test condition and given engine operating condition follows **Eq. (3.12)**, the K value is equal to zero and OI does not depend on the ethanol content.

Figure 3.9 shows the quantitative correlation between $\frac{\partial OI}{\partial z_E}$ and $\frac{\partial E_{TP}}{\partial z_E}\Big|_{BMF0.7}$.

As shown, there is a strong linear correlation between $\frac{\partial OI}{\partial z_E}$ and $\frac{\partial E_{TP}}{\partial z_E}\Big|_{BMF0.7}$, which can be expressed as **Eq. (3.15)**. This result confirms again that both approaches yield the same conclusion for the effect of fuel and engine operating condition on knocking characteristics; however, this is explained from different perspectives: One is through measurement of knocking for varying engine operating conditions, and the other is through ignition delay measurement for varying thermodynamic states of the end gas. Moreover, E_{TP} can be applied to another engine operating condition, e.g., varying RPM, using EGR, or lean burn strategy.

$$\frac{\partial OI}{\partial z_E} = 3.7003 \frac{\partial E_{TP}}{\partial z_E}\Big|_{BMF0.7} + f\left(\frac{\partial E_{RPM}}{\partial z_E}\Big|_{BMF0.7}, \frac{\partial E_{EGR}}{\partial z_E}\Big|_{BMF0.7}, \frac{\partial E_{\phi}}{\partial z_E}\Big|_{BMF0.7}, \dots\right) \quad \textbf{Eq. (3.15)}$$

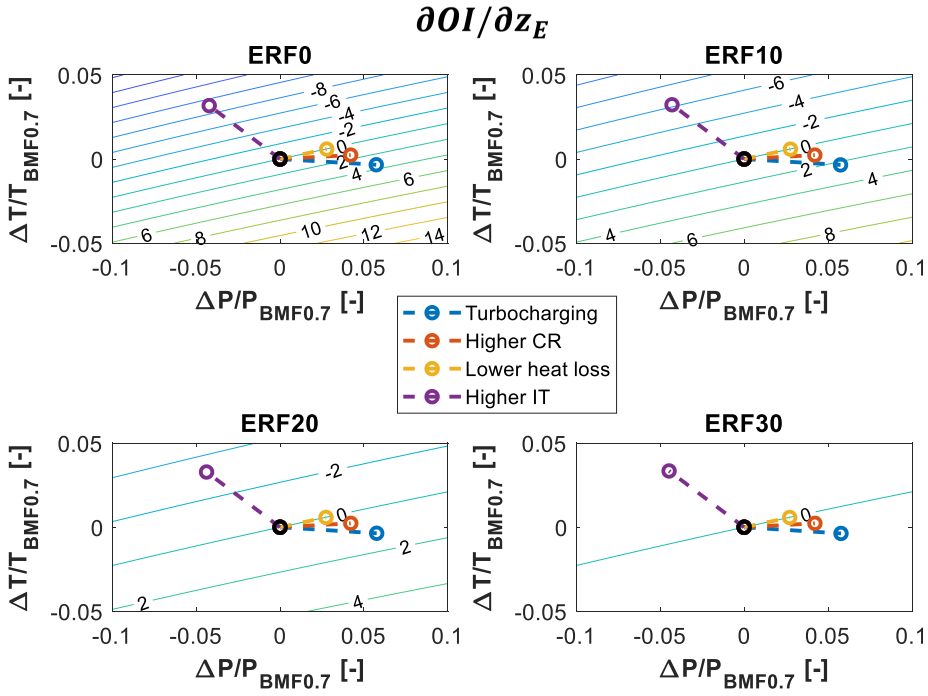

Figure 3.8 Dependency of $\frac{\partial OI}{\partial z_E}$ on ethanol content

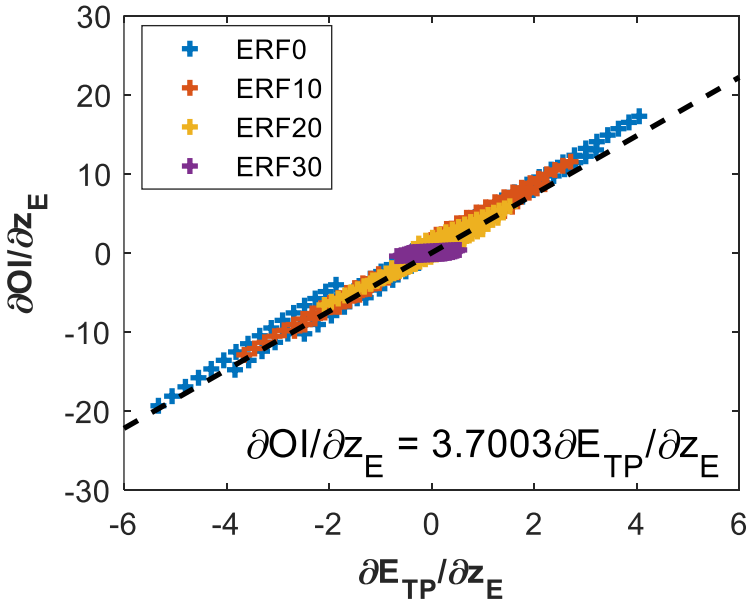

Figure 3.9 Correlation between the dependency of OI and E_{TP} on ethanol content.

3.8 Summary

This study investigated the effect of engine operating condition on knocking characteristics of various ERFs with a fixed RON of 100. To this end, an empirical correlation of the ignition delay for various ERFs was derived by regressing the data previously measured. The effect of engine operating condition on knocking characteristics was then quantified by evaluating the relative variation in ignition delay according to the deviation of temperature–pressure profile of the end gas. The conclusions are as follows:

1. The ignition delay for the fuel with higher ethanol content is more sensitive to temperature, while less sensitive to pressure. This implies that the knocking characteristics of the various ERFs have different

dependencies on the temperature–pressure profile even for a fixed RON; thus, the optimal ethanol content for maximizing knocking suppression could be also dependent on the engine operating condition.

2. The effect of the following variation in the engine operating condition on the ignition delay of the end gas was evaluated:

    a) For the turbocharging case, the overall in-cylinder pressure increased, whereas the temperature slightly decreased owing to the decreased mole fractions of residual gas, which led to a significant reduction in ignition delay for the fuel with less ethanol.

    b) A high CR increased both the in-cylinder pressure and temperature, which led to a significant reduction of ignition delay for the fuel with less ethanol.

    c) Low heat loss also increased the in-cylinder pressure and temperature similar to the higher CR case; however, the ignition delays for all the fuels reduced by the same extent.

    d) Meanwhile, the effect of a high IT on various fuels demonstrated an inverse characteristic: The more is the ethanol content in the fuel, the more is the reduction effect on the ignition delay.

3. The optimal ethanol content for knock suppression depends on the temperature–pressure profile of the end gas under a given engine operating condition. The fuel with less ethanol content is more resistive to auto-ignition for the region of $\frac{\Delta T}{T} > \frac{\gamma-1}{\gamma}\frac{\Delta P}{P}$, whereas the fuel with more ethanol content is more resistive in the region of $\frac{\Delta T}{T} < \frac{\gamma-1}{\gamma}\frac{\Delta P}{P}$.

Further, the knocking characteristics are independent of the ethanol content, if and only if the temperature–pressure profile under the given engine operating condition satisfies the specific condition, $\frac{\Delta T}{T} = \frac{\gamma-1}{\gamma}\frac{\Delta P}{P}$.

This criterion provides a useful guideline to determine the optimal ethanol content for knock suppression under the given engine operating condition, based on the temperature–pressure profile of the end gas.

4. The aforementioned results of this study were compared with those of Kalghatgi's K value principle; both the principles are commutable. In other words, the dependency of OI on ethanol content and engine operating condition was quantitatively explained with the dependency of auto-ignition characteristics, E_{TP}. Thus, the results of this study provide the physical interpretation on Kalghatgi's K value principle from the aspect of chemical kinetics.

Chapter 4. Effect of external exhaust gas recirculation on optimal ethanol content

Most of the combustion devices have an issue of reducing nitric oxide (NOx) emission, which causes ozone layer depletion, photochemical smog and acid rain [77]. European commission regulates the NOx emission from gasoline-motored passenger cars less than 60 mg/km since 2015 [78], which is 40 % of the regulation in 2001; the regulation gets ever stricter.[79]

In this regard, there have been numerous approaches to reduce the NOx emission from combustion process, and the external-EGR is one of the most effective technologies. External-EGR reduces the flame temperature, and it leads to decreased NOx formation from thermal mechanism, which is the most prominent source of NOx emission [80]. Grandin et al. reported that NOx emission is reduced about 50 % by mixing 10 % of external-EGR to the fuel–air mixture in the SI engine [81].

Beside the effect on the NOx emission, external-EGR also affects the knocking characteristics of fuel–air mixture by deviating the thermodynamic state of end gas, and the amount of effect depends on fuel composition. According to Diana et al. [82], the external-EGR sensitivity of the fuels with the same MON, which was defined as the sensitivity of the anti-knock characteristic by changing the amount of external-EGR, increases with adding methyl tert-butyl ether (MTBE) which is an oxygenated fuel additive like ethanol. On the other hand, Splitter and Szybist [83] also studied the external-EGR sensitivity with changing ethanol content in a given gasoline blend stock, and thus varying octane number, and found out that the external-EGR sensitivity decreases with adding ethanol.

However, the effect of external-EGR on knocking characteristics is hard to be predicted from octane number since EGR not only deviates the temperature-pressure profile but also dilutes the end gas. Risberg et al. applied K value principle to the engine operating condition with EGR, but found that auto-ignition characteristics of fuel has low deterministic coefficient with OI, in the cases with high external-EGR or internal-EGR rate [75].

In this regard, this study focused on measuring the dependency of ignition delay of end gas according to external-EGR rate, especially for various ERFs with a fixed RON, then explains the different external-EGR sensitivity of fuels from the chemical kinetic point of view.[84] If the optimal ethanol content with the high external-EGR sensitivity can be verified, it could provide an important information in determining the future gasoline/ethanol blend fuel to effectively deal with the knocking phenomena.

The main body of **Chapter 4** consists of five sub-chapters. In **Chapter 4.1**, evaluation of the thermodynamic state profiles of end gas in an SI engine with external-EGR, which are used in the RCM experiment, is discussed. **Chapter 4.2** is devoted to explain the result of RCM experiments and regression analysis on them, then **Chapter 4.3** describes how the effect of external-EGR on knocking characteristic can be evaluated with the ignition delay measurements, based on the similar quantity as E_{TP} used in **Chapter 3.** The calculated effect of external-EGR for various ERFs is discussed in **Chapter 4.4**, by dividing the effect into the sub-effect of dilution and temperature-pressure profile deviation, and suggests the best ERF with the most sensitivity of the external-EGR on the knock prevention. In **Chapter 4.5**, the discussion will be provided on how the optimal ethanol content would change at faster engine speed.

4.1 Engine simulation for the engine operating condition with external-EGR

ASTM D2699 does not define operating parameters for external-EGR, i.e. temperature of external-EGR and maximum external-EGR rate, and therefore, assumptions as made as follow. Firstly, the temperature of external-EGR is assumed to be 373.15 K, which is slightly higher than the typical engine coolant temperature, since the recirculated exhaust gas is cooled by the engine coolant in the EGR cooler. Secondly, the upper limit of the external-EGR rate, defined as the mole fraction of external-EGR in the intake manifold, is set to be 20 %, which is the typical allowable limit at high load and low speed condition of a contemporary SI engine [85]. The spark timing was advanced for the slower speed of the EGR case to maintain the similar crank angle at 50 % burned (CA50), which would be a reasonable constraint for comparing knocking characteristics of two different engine conditions. The resultant engine operating condition, with or without external-EGR, is described on **Table 4.1**.

Figure 4.1 compares the calculated thermodynamic state of the end gas from the engine operating condition with or without external-EGR, where x_D is defined as the mole fraction of external-EGR in the end gas. As shown, external-EGR results in slightly higher temperature at low BMF due to higher temperature of external-EGR than fuel–air mixture, but is drastically decreases due to reduced amount of fresh mixture and longer flame propagation speed as well as in-cylinder pressure.

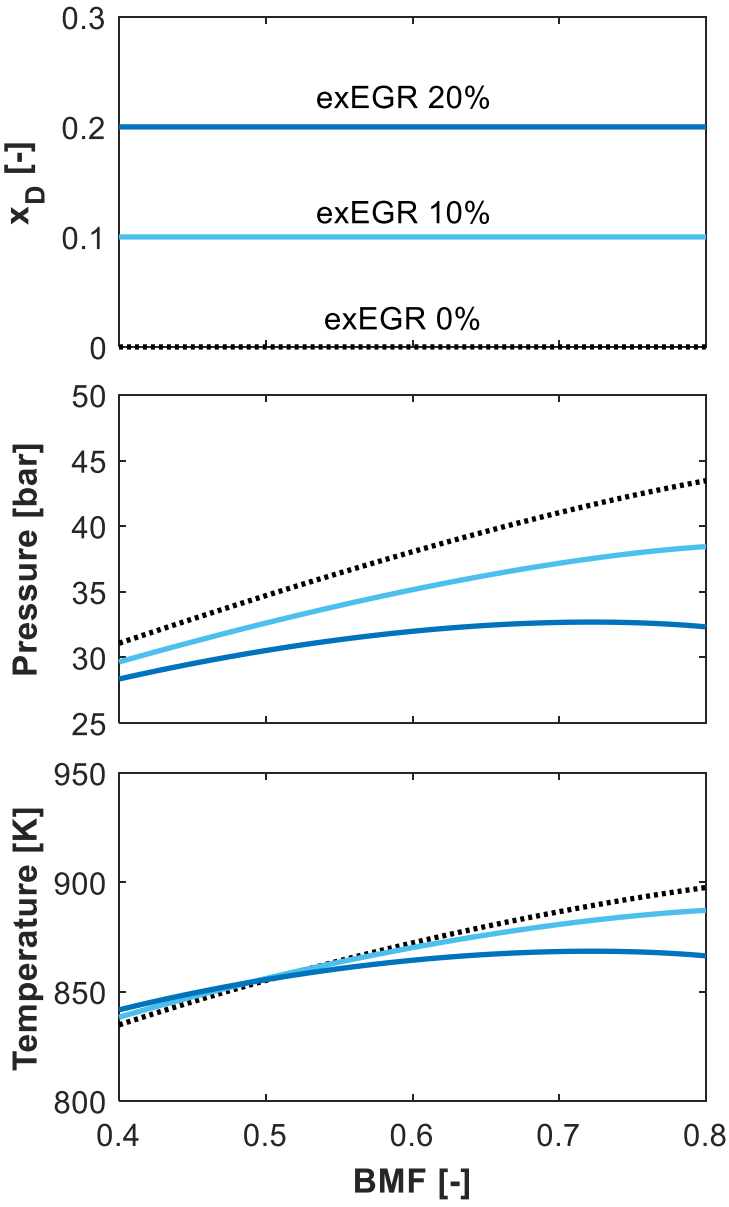

Figure 4.1 (a) Dilution rate, (b) pressure and (b) temperature deviation induced from introducing external-EGR for ERF0

Table 4.1 Operating parameters for RON test condition with or without external-EGR

Parameter	RON condition w/o external-EGR	RON condition w/ external-EGR
Cylinder bore [mm]	82.6	-
Stroke [mm]	114.3	-
Connecting rod length [mm]	265.2	-
IVC [aBDC]	34	-
Spark timing [bTDC]	13	Adjusted according to external-EGR rate [a]
Engine speed [rpm]	600	-
Compression ratio [-]	7.9	-
Intake pressure [bar]	1	-
Intake air temperature [K]	325.15	-
Equivalence ratio [-]	1	-
External-EGR temperature [K]	N/A	373.15
External-EGR rate [%]	N/A	0-20

[a] Spark timing was adjusted to have the same CA50 regardless of external-EGR rate.

4.2 Regression analysis on the ignition delay data

In order to understand the effect of external-EGR on the ignition delay of various ERFs, RCM experiment was conducted on both the diluted and non-diluted condition. Especially for the diluted condition, when executing the experiment with the composition of the engine exhaust gas, there is a possibility of condensation of H_2O; for example, after mixing with ambient air and fuel in the real engine operation. Moreover, exhaust gas has higher specific heat ratio than fuel-air mixture, and it results in the diluted condition following different temperature-pressure profile to that of non-diluted condition. To resolve these issues in the RCM experiment, the pseudo-EGR was devised, which consisted only of CO_2 and N_2. In order to match the temperature-pressure profiles of both

diluted and non-diluted condition, the specific heat ratio of the pseudo-EGR was designed to have nearly the same with the original fuel-air mixture, where the composition was 31 % of CO_2 and 69 % of N_2. It is noted that the difference in the specific heat ratio of the exhaust gas for various ERFs was neglected, since they have small relative error.

The results from RCM experiment are illustrated in **Table 4.2** and **Figure 4.2**. Ignition delay was measured repeatedly with 3-4 times at the same condition, and coefficient of variation was lower than 14 % in all the results. As shown on **Figure 4.2**, the 20 % of external-EGR leads to longer ignition delay of all the test fuels, but the amount of effect differs from ethanol content in the fuel. Moreover, the amount of effect was found to increases as BMF increases for all the test fuels.

Based on the measurement, the empirical correlation of the ignition delay derived on **Chapter 3.2** was expanded to cover the effect of external-EGR. The revised form of empirical correlation is described by **Eq. (4.1)**, which assumes the power rule dependency of ignition delay on $(1 - x_D)$ as several previous study did [71, 86]. Here, it should be noted that the exponent of $(1 - x_D)$ was assumed to be proportional to BMF at the given condition. This is based on the observation that the effect of external-EGR increases as BMF increases.

$$\tau_i = P^n \exp\left(\sum_{i=0}^{3} a_i \left(\frac{1000}{T}\right)^i\right)(1 - x_D)^{b_0 + b_1 BMF} \qquad \textbf{Eq. (4.1)}$$

Figure 4.3 shows how b_0 and b_1 vary with ethanol content in the fuel. Unlike the other parameters, both b_0 and b_1 showed non-monotonic dependency on z_E; they have the maximal (or minimal) value around ERF10. Thus, they were expressed as a cubic function of z_E, as described in **Eq. (4.2)**. Consequently, the integrated correlation covers the dependency of ignition delay

on the external-EGR as well as ethanol content, temperature and pressure, via 23 independent coefficients, as described in **Table 4.3**.

$$X(z_E) = X_0 + X_1 z_E + X_2 z_E^2 + X_2 z_E^3 \qquad \textbf{Eq. (4.2)}$$

where $X = b_0$ and b_1

The reliability of the empirical correlation was validated by comparing the predicted ignition delay with the measured one. As shown in **Figure 4.4**, the correlation represents the behavior of the ignition delay with a determination factor of 0.97185. It is noteworthy that this empirical correlation is based on the ignition delay around 0% and 20% of dilution rate, thus should be carefully used for the highly diluted condition more than 20%.

Table 4.2 Ignition delay of ERFs for various temperature, pressure, and dilution rate

Fuel	P [bar]	T [K]	x_D [-]	τ_i [ms] [a]
ERF0	23.5	794	0.0	23.8 (±3.2)
			0.2	63.9 (±8.7)
	31.3	845	0.0	5.6 (±0.8)
			0.2	18.4 (±2.5)
	36.5	877	0.0	1.8 (±0.2)
			0.2	7.0 (±0.9)
ERF10	23.5	784	0.0	20.1 (±2.7)
			0.2	56.2 (±7.6)
	31.3	836	0.0	5.3 (±0.7)
			0.2	18.2 (±2.5)
	36.5	863	0.0	1.4 (±0.2)
			0.2	7.0 (±0.9)
ERF20	23.5	778	0.0	16.3 (±2.2)
			0.2	44.3 (±6.0)
	31.3	827	0.0	6.2 (±0.8)
			0.2	21.0 (±2.8)
	36.5	856	0.0	2.5 (±0.3)
			0.2	9.0 (±1.2)
ERF30	23.5	770	0.0	14.5 (±2.0)
			0.2	38.7 (±5.2)
	31.3	819	0.0	6.6 (±0.9)
			0.2	19.3 (±2.6)
	36.5	848	0.0	3.4 (±0.5)
			0.2	10.7 (±1.5)

[a] The values inside brackets represent 95 % confidence interval of ignition delay.

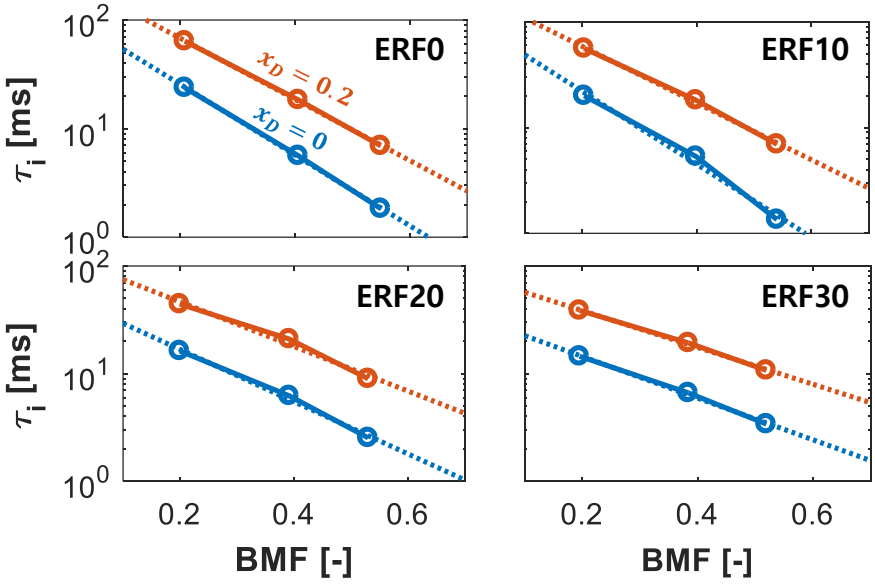

Figure 4.2 Ignition delay of ERFs for diluted and non-diluted condition

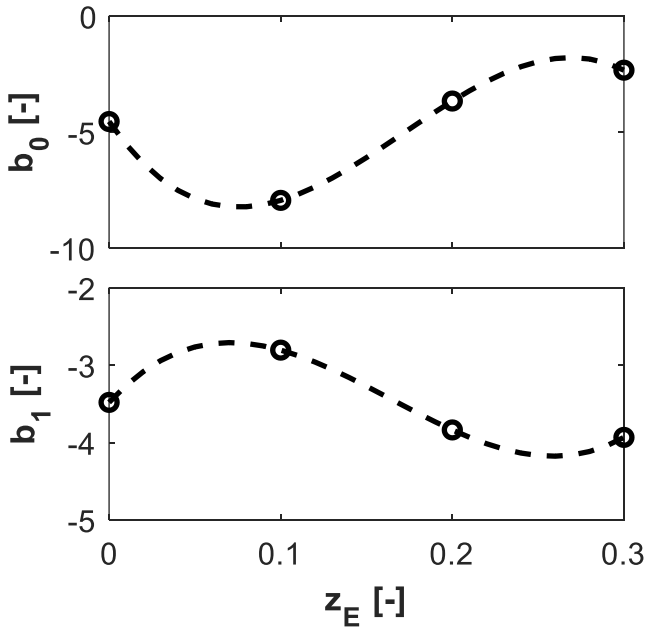

Figure 4.3 Coefficient of the empirical correlation for ignition delay covering the effect of external-EGR

Table 4.3 Coefficients of the empirical correlation for ignition delay

X	X_0	X_1	X_2	X_3
b_0	-3.4785	24.1118	-217.5916	440.6329
b_1	-4.5321	-107.8424	915.7112	1772.1550

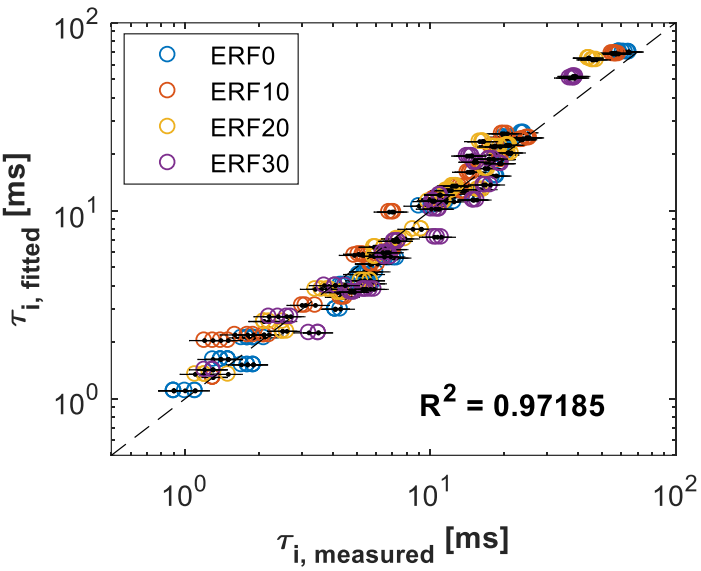

Figure 4.4 Validation of empirical correlation on the ignition delay covering the effect of external-EGR

4.3 Quantitative analysis on the effect of engine operating condition on knocking characteristics

In order to analyze the effect of external-EGR with the similar framework used in **Chapter 3**, the effect of external-EGR was divided into two sub-effect: dilution effect, temperature–pressure profile effect. Then, each effect was defined quantitatively as follows. The amount of dilution effect, E_D, was defined as **Eq. (4.3)**, which means the relative difference between the ignition delay of RON test condition and that of the diluted condition at the fixed temperature and pressure. The amount of temperature–pressure profile effect, E_{TP}, was defined as **Eq. (4.4)**, which is consistent with the definition in **Chapter 3.3**. Accordingly, the amount

of external-EGR effect, E_{DTP}, could be evaluated as the sum of E_D and E_{TP} as **Eq. (4.5)**.

$$E_D = \log\left(\frac{\tau_i\left(x_{D\,mod.}, T_{RON}, P_{RON}\right)}{\tau_i\left(x_{D\,RON}, T_{RON}, P_{RON}\right)}\right)\Bigg|_{BMF} \qquad \textbf{Eq. (4.3)}$$

$$E_{TP} = \log\left(\frac{\tau_i\left(x_{D\,mod.}, T_{mod.} P_{mod.}\right)}{\tau_i\left(x_{D\,mod.}, T_{RON}, P_{RON}\right)}\right)\Bigg|_{BMF} \qquad \textbf{Eq. (4.4)}$$

$$E_{DTP} = \log\left(\frac{\tau_i\left(x_{D\,mod.}, T_{mod.} P_{mod.}\right)}{\tau_i\left(x_{D\,mod.}, T_{RON}, P_{RON}\right)}\right)\Bigg|_{BMF} = E_D + E_{TP} \qquad \textbf{Eq. (4.5)}$$

4.4 The effect of external-EGR on the knocking characteristics

4.4.1 Dilution effect

E_D was evaluated along BMF axis using the empirical correlation of the ignition delay, and its results is depicted in **Figure 4.5**. As shown, E_D was maximized when the fuel was ERF10.

To understand why E_D is maximized at ERF10, the dilution effect can be divided into fuel-oxygen concentration decrease effect and heat release absorption effect. The former effect does not considerably vary with ethanol content because the amount of fuel-oxygen concentration decrease is almost independent of fuel. The latter effect represents the absorption of pre-heat release in the unburned zone, and it depends on ethanol content because the amount of pre-heat release from the chemical reaction of the end gas during flame propagation varies with the fuel

composition. During flame propagation on an SI engine, there can be pre-heat release prior to auto-ignition due to low temperature chemistry [87], and it is dependent on the fuel characteristic.

Here, the pre-heat release during flame propagation can be measured by calculating the amount heat released during compression stroke in RCM as mentioned in **Chapter 2.3.2**. To validate the correlation between E_D and pre-heat release during compression stroke, a regression analysis is executed and plotted in **Figure 4.6.** In this analysis, E_D was evaluated using individual ignition delay data from various BMF point. As a result, there is the positive correlation between E_D and the amounts of pre-heat release, Q_{PHR}, which can be expressed as **Eq. (4.6)**. Moreover, ERF10 demonstrates larger pre-heat release than that of the other ERFs, and this can explain the reason why E_D is maximized on ERF10.

$$E_D \cong 0.151 Q_{PHR}^2 + 1.021 \qquad \textbf{Eq. (4.6)}$$

To understand why the amount of pre-heat release is maximized at ERF10, separate analysis was carried out on cool flame characteristics of ERF's, which is thought to be related with pre-heat release, by using the reduced chemical kinetics mechanism with 679 species and 5627 reactions developed by Mehl et al. [51]. As shown on **Figure 4.7**, it is observed that the cool flame intensity, which is defined as the amount of temperature rise due to cool flame, becomes stronger with higher ethanol content, or at the same time, higher n-heptane concentration to fix the octane number at 100. However, with higher ethanol content, Livengood-Wu integration value of the cool flame delay, $LW_{cf,EOC}$, is smaller along the temperature and pressure history of the end gas, implying that the cool flame is less likely at higher ethanol content. Consequently, there is a trade-off between two aforementioned factors, and ERF10 might have turned out to demonstrate the most dominant cool flame or pre-heat release behavior among the tested fuels.

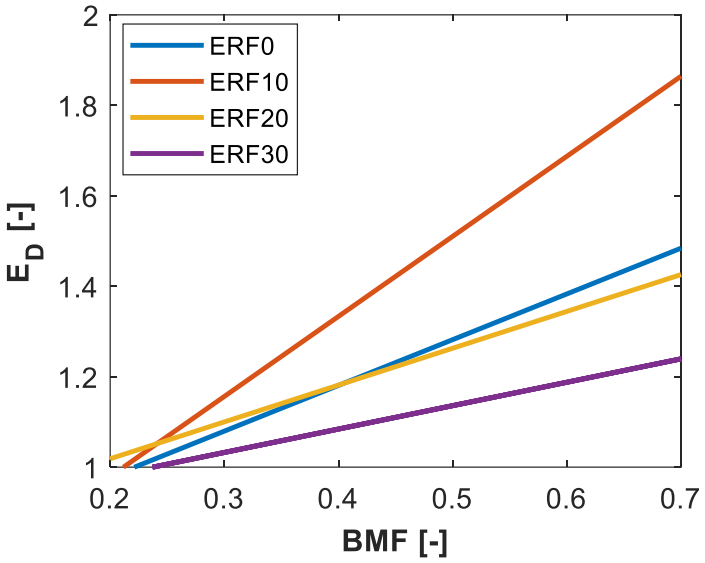

Figure 4.5 E_D along BMF axis for various ERFs

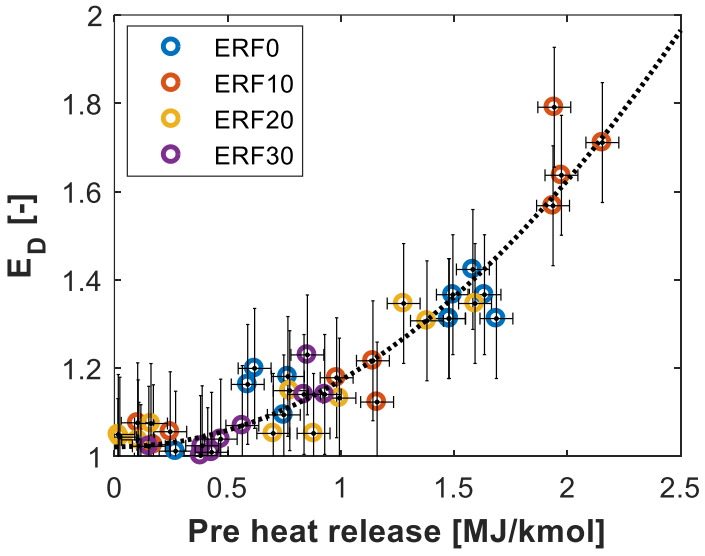

Figure 4.6 Correlation between E_D and the amount of pre-heat release

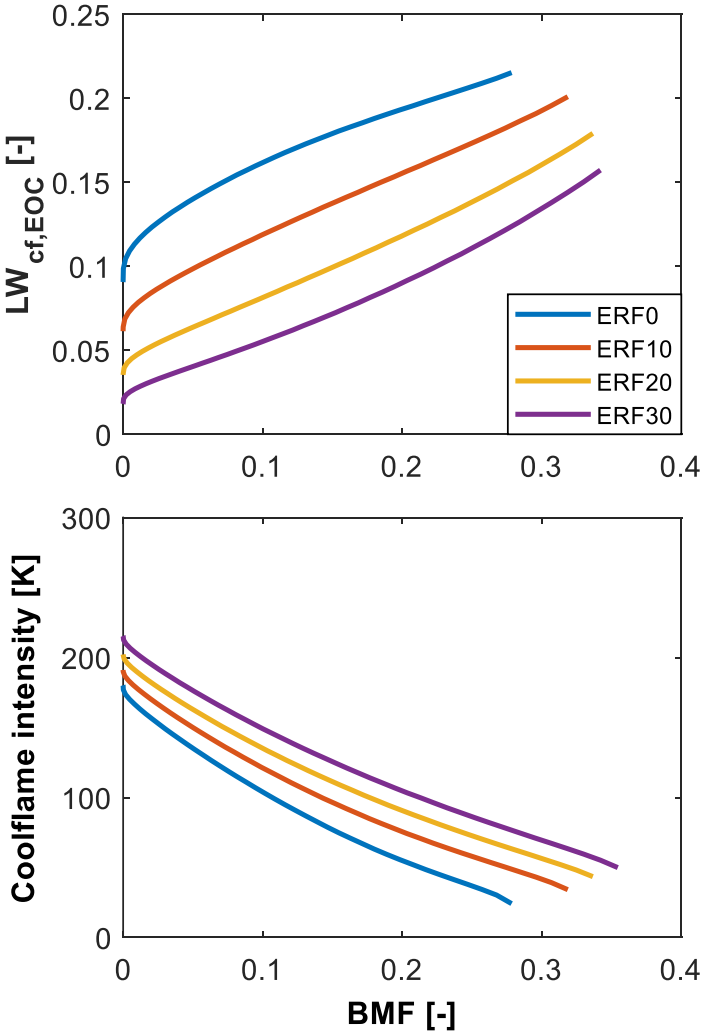

Figure 4.7 Analysis on cool flame characteristics of ERFs

4.4.2 Temperature and pressure profile effect

E_{TP} was also calculated with empirical correlation of ignition delay along BMF axis, and the results is depicted in **Figure 4.8**. As shown, ERF with lower

ethanol content has higher E_{TP}, which implies that lower ethanol content is preferable for temperature–pressure profile effect of external-EGR.

To understand the above result, the magnitude of $\frac{\Delta T}{T}$ and $\frac{\gamma-1}{\gamma}\frac{\Delta P}{P}$ were compared as shown **Figure 4.9**. It was found that the deviation of temperature–pressure profile induced by external-EGR satisfies the condition of $\frac{\Delta T}{T} > \frac{\gamma-1}{\gamma}\frac{\Delta P}{P}$ as higher IT condition did in **Chapter 3.6**, where the lower ethanol content is optimal for knock suppression. This is because higher temperature of external-EGR than fuel-air mixture enhances the IVC temperature while IVC pressure keeps atmospheric pressure, and this explains why the fuel with lower ethanol content is desirable for temperature–pressure profile effect of external-EGR.

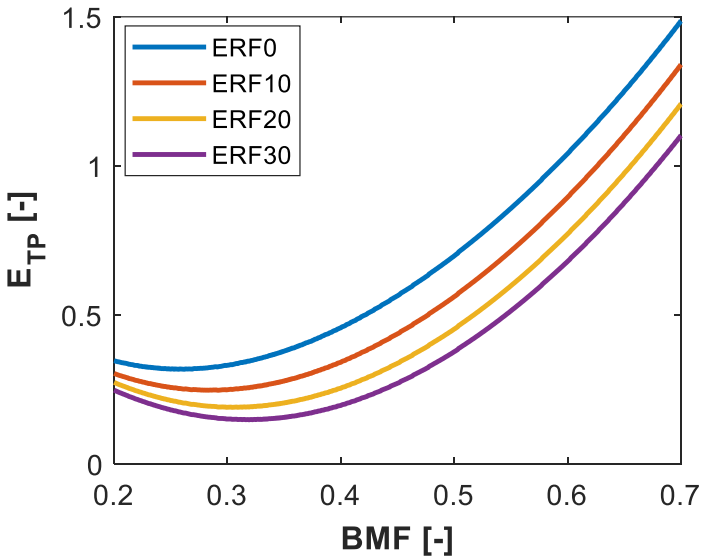

Figure 4.8 E_{TP} along BMF axis for various ERFs

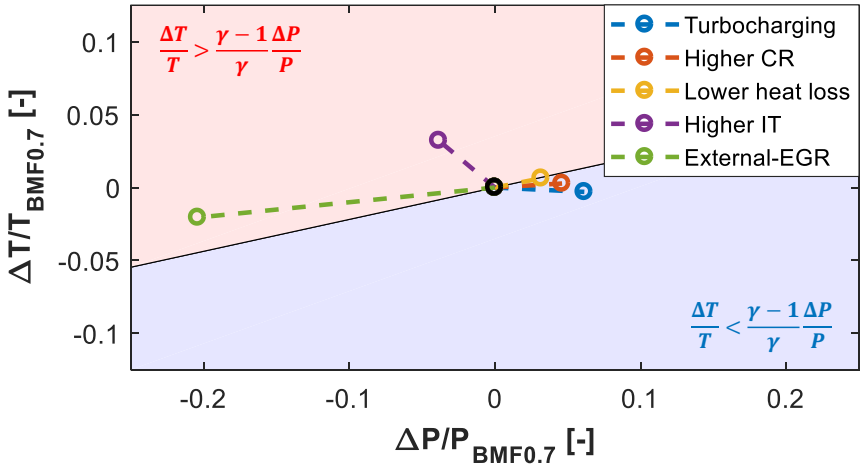

Figure 4.9 Comparison of $\frac{\Delta T}{T}$ and $\frac{\gamma-1}{\gamma}\frac{\Delta P}{P}$ with the external-EGR

4.4.3 The total effect of external-EGR

The amount of external-EGR effect, defined as the sum of E_D and $E_{TP,}$ was also calculated and the result is shown in **Figure 4.10**. The amount of external-EGR effect is maximized, or the ignition delay is the most prolonged, when ethanol content is 10 %. As discussed in earlier chapters, it is because E_D is maximized at ERF10 while E_{TP} on ERF10 is also relatively bigger than those of the other ERFs with higher ethanol content.

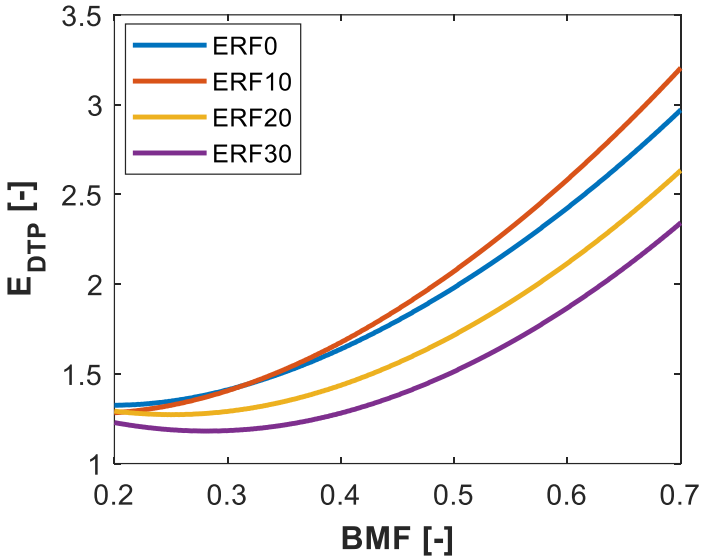

Figure 4.10 E_{DTP} along BMF axis for various ERFs

4.5 Dependency of the effect of external-EGR on engine speed

In this study, the reference engine condition was set to be the RON test condition whose engine speed is 600 rpm, which is slower than that of contemporary engine. If the engine speed is higher, it should be noted that the amount of pre-heat release would be changed. The dependency of pre-heat release on engine speed can be confirmed from the study of Hosseini et al. [88], where the dependency of low temperature heat release characteristics was measured using homogeneous charge combustion ignition in CFR engine. Therefore, at higher engine speed, the effect of decrement of E_D by lower pre-heat release should be considered to find the optimal ethanol content.

The situation could be simulated with separate analysis that was carried out by estimating E_D at faster engine speed. For this, the **Eq. (4.6)** was manipulated to calculated E_D with the reduced amount of pre-heat release, $E_D(Q_{PHR})$, as **Eq. (4.7)**. Then, it was assumed that Q_{PHR} is anti-proportional to engine speed for expressing the dependency of E_D on engine speed, ω_{RPM}, as **Eq. (4.8)**. Consequently, **Figure 4.11** shows the predicted results for engine speed of 1200 rpm, and the optimal ethanol content becomes to ERF0 at faster engine speed, which is because the effect of dilution become less dominant at faster engine speed than that of temperature-pressure profile, for which ERF0 is optimal.

$$E_D(Q_{PHR}) = \left(\frac{Q_{PHR}}{Q_{PHR_0}}\right)^2 \left(E_D\left(Q_{PHR_0}\right) - 1.012\right) + 1.012 \quad \textbf{Eq. (4.7)}$$

$$E_D(\omega_{RPM}) = \left(\frac{\omega_{RPM,0}}{\omega_{RPM}}\right)^2 \left(E_D\left(\omega_{RPM,0}\right) - 1.012\right) + 1.012 \quad \textbf{Eq. (4.8)}$$

$$\text{where } Q_{PHR} \propto \frac{1}{\omega_{RPM}}$$

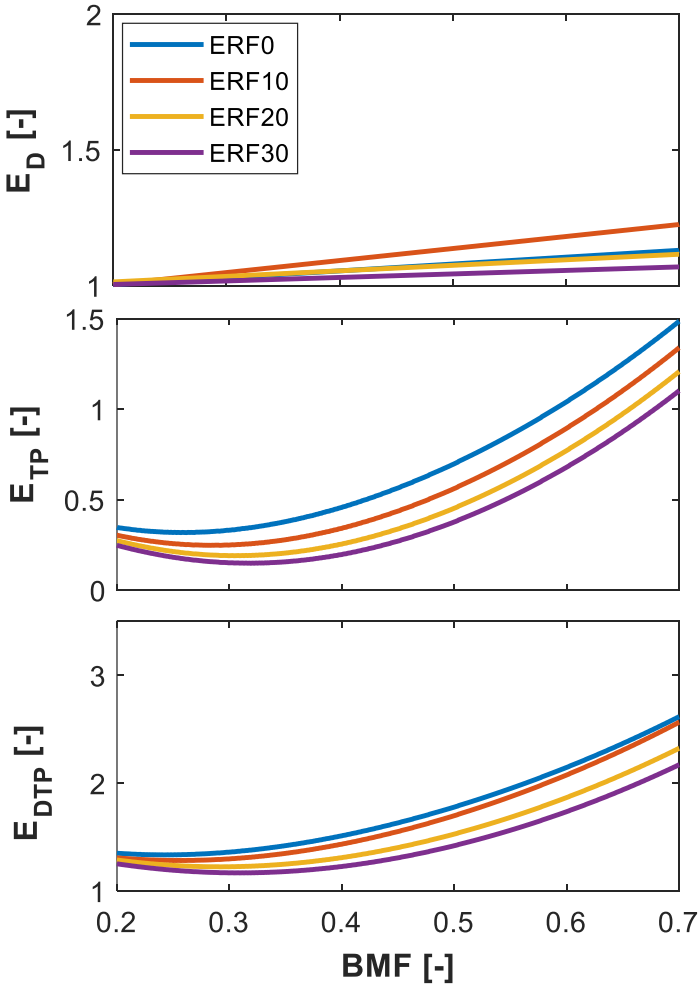

Figure 4.11 the effect of external-EGR along BMF axis for various ERFs at high engine speed (around 1200rpm)

4.6 Summary

In this research, the effect of external-EGR on anti-knock characteristic of various ERFs with RON 100 is analyzed by measuring the change of the ignition delay of the simulated end gas when external-EGR is introduced. Here is the summary of the findings.

1. The dilution effect of external-EGR on the ignition delay, which is dominated by dampening of the pre-heat release from the low-temperature chemistry of the fuel, thus increasing the ignition delay, is maximized on ERF10, which demonstrates the most intensive pre-heat release characteristic during flame propagation without external-EGR.

2. The temperature–pressure profile effect of external-EGR on the ignition delay was also separately assessed, which is mostly affected by decreases of fuel supply rate, slower flame propagation speed, and increase of intake temperature due to hotter EGR gas than fresh fuel and air. It was found that the temperature–pressure profile effect increases as ethanol content in ERF decreases. This is because the deviation of temperature-pressure profile from external-EGR always satisfies the condition of $\frac{\Delta T}{T} > \frac{\gamma-1}{\gamma}\frac{\Delta P}{P}$, where lower ethanol content is optimal for knock suppression as described on **Chapter 3.6**.

3. Consequently, the optimal composition of ERF with RON 100 which maximizes the synergy with external-EGR is ERF10 when the engine is running near the RON test condition. Furthermore, the effect of the engine speed was discussed, which would predict the best fuel being from ERF0 to ERF10, depending on the engine speed.

Chapter 5. Ethanol content optimization for light duty fleet in South Korea

Previous chapters discussed the dependency of optimal ethanol content on engine operating condition, including varying temperature–pressure profile and external-EGR rate. The results can be used to derive the optimal ethanol content for an arbitrary engine operating condition.

However, the ethanol content in the fuel is hard to be adjusted instantaneously to be optimal according the engine operating condition. One of the possible solution is to adopt dual fuel system. For example, two independent fuel supply system, where one is for ERF0 and the other is for ERF30, can supply the optimal ethanol content to the cylinder as the operating condition varies. Nevertheless, little of light duty fleet in South Korea is equipped with the dual fuel system, thus it is difficult to be realized in the near future.

In this regard, the ethanol content in the gasoline-ethanol blend fuel should be fixed to all of the automobile regardless of engine operating condition. Thus, the fleet-wide optimization of ethanol content is important for realistic implication of gasoline-ethanol blend fuel.

This study is devoted to suggest which ethanol content is optimal for light duty fleet in South Korea by using the understanding of the dependency of knocking characteristics of various ERFs on engine operating condition achieved from the discussions in **Chapter 3** and **Chapter 4.** In this regard, **Chapter 5.1** covers the derivation of the optimal ethanol content diagram, which can be used to find the optimal ethanol content for the arbitrary engine operating condition. Then, **Chapter 5.2** analyzes the overall sales volume of SI engines in South Korea,

and their corresponding thermodynamics state of the end gas. Finally, the discussion on the optimal ethanol content for knock suppression of light duty fleet in South Korea, and how the optimal ethanol content can be varied with the introduction of external-EGR was discussed in **Chapter 5.3**.

5.1 Optimal ethanol content diagram

Results from **Chapter 3** and **Chapter 4** give us the information on how the knocking characteristics depends on ethanol content at varying engine operating condition. Based on this, the optimal ethanol content maximizing E_{DTP}, thus maximizing knock suppression, was calculated as shown in **Figure 5.1**. It should be noted that **Figure 5.1** is for the condition without external-EGR, and the effect of external-EGR on the optimal ethanol content will be discussed on **Chapter 5.3**.

Figure 5.1 confirmed again that the higher ethanol content is optimal for the engine operating condition where the temperature–pressure profile satisfies $\frac{\Delta T}{T} < \frac{\gamma-1}{\gamma}\frac{\Delta P}{P}$, while the lower ethanol content is preferable for the condition with $\frac{\Delta T}{T} > \frac{\gamma-1}{\gamma}\frac{\Delta P}{P}$. In addition, at higher temperature and pressure than RON test condition, optimal ethanol content abruptly changes from ERF0 to ERF30 across the adiabatic compression line, $\frac{\Delta T}{T} = \frac{\gamma-1}{\gamma}\frac{\Delta P}{P}$, while it gradually varies at lower temperature and pressure condition. This diagram gives useful guideline for determining the optimal ethanol content at the given engine operating condition based on thermodynamic state of the end gas.

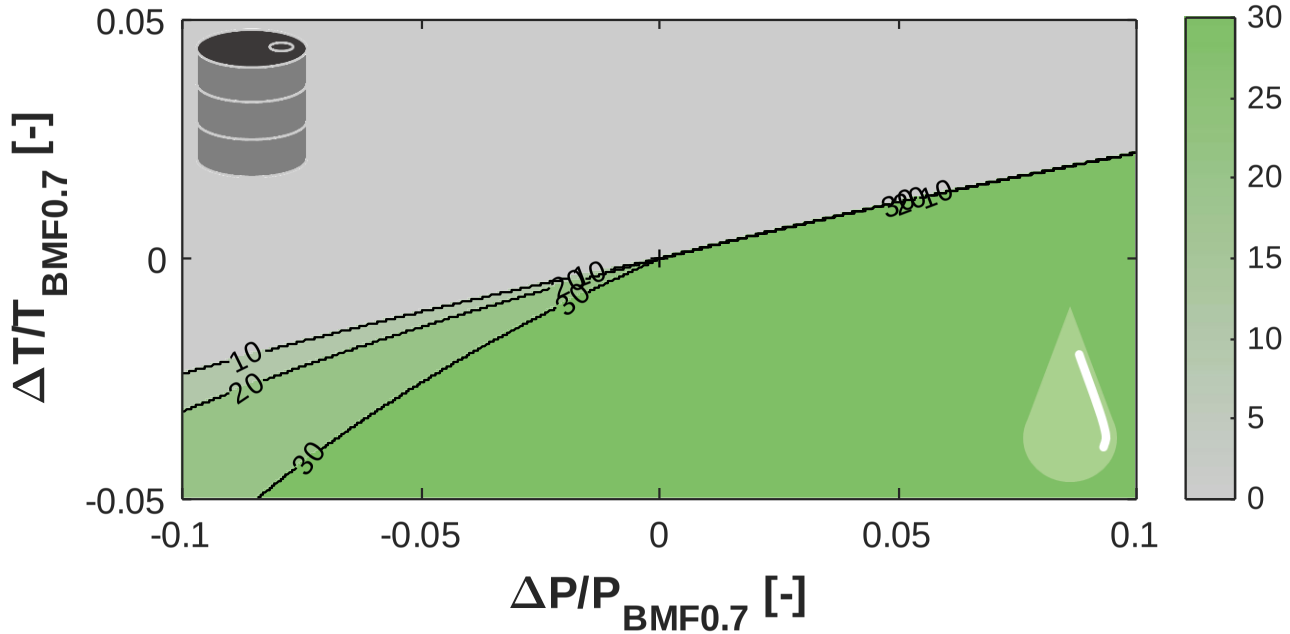

Figure 5.1 Optiaml ethanol content maximizing E_{DTP} for varying temperature and pressure

5.2 Thermodynamic state of SI engines in South Korea

In order to evaluate the optimal ethanol content for light duty fleet in South Korea, it was investigated which type of automobile occupies the major portion of light duty fleet in South Korea, based on the database from Korea Automobile Manufacturers Association (KAMA) [89]. **Figure 5.2** describes the gasoline fueled light duty vehicles sold in South Korea for model year (MY) 2018, which is sorted by the sales volume of each vehicles. As shown, the most popular vehicle has relatively small displacement volume of engine, and the natural aspired engine is more preferred in South Korea.

The above statistical data was manipulated to achieve the sales volume of each SI engine models. As shown in **Figure 5.3**, the most of gasoline-fueled automobile in South Korea is using the engine developed by Hyundai Motors Company (HMC), and HMC $\gamma 1.6$ engine, which is built in the Anvante and K3, is the most widely used model of SI engine. These statistical data will be considered for optimizing the ethanol content for light duty fleet in South Korea, by weighting the ethanol content which is optimal for the engine operating condition of more popular SI engine model.

The geometrical information of each engine are shown in **Table 5.1.** Because there are lack of information of valve timing of engines, the typical value of them was used [52]. Despite the intake temperature depends on the season of countries, which is around 298.55 K summer and 274.45 K for winter, it was represented as the average annual temperature in South Korea for 2018, 286.15 K. The engine speed was swept from 600 rpm of RON test condition to 1000 rpm since the modern SI engines operates at faster engine speed than RON test condition. Meanwhile, spark timing was kept to be MBT timing for all the engine operating conditions.

The thermodynamic state of end gas in the most popular SI engines was calculated with 0-D two-zone SI engine model, which was introduced in **Chapter 2.2**. It should be noted that the thermodynamics state of end gas depends on the intake pressure, thus the representative condition was chosen to be DBL condition, which is the condition of knock occurrence at given engine speed and spark timing. This is based on the idea that the optimal ethanol condition for knock suppression should be evaluated at the knock prone condition.

To determined DBL condition at the given engine speed, the knocking model was embedded into the 0-D two-zone SI engine model. The knock onset crank angle degree, θ_{KO}, was predicted with Livengood-Wu integration method described as **Eq. (5.1)**. The ignition delay of end gas was represented with that of ERF0, which is derived by Golsborough from extensive experimental database on the ignition delay of isooctane [68]. The DBL condition was determined as the condition where BMF at the knock onset crank angle degree to be critical BMF, 0.7 [57]. It should be noted that the calibration coefficient for ignition delay, C_τ, was introduced to calibrate the knock onset BMF of RON test condition to be 0.7; the range of C_τ was restricted to $\pm$34 % considering the standard error of the empirical correlation suggested by Golsborough [68].

$$\frac{1}{6\omega_{RPM}}\int_{\theta_0}^{\theta_{KO}}\frac{d\theta}{C_\tau\tau_{i,ERF0}} = 1 \qquad \textbf{Eq. (5.1)}$$

$$\tau_{i,ERF0} = f_{Goldsborough}(T_u, P, x_{O_2,u})$$

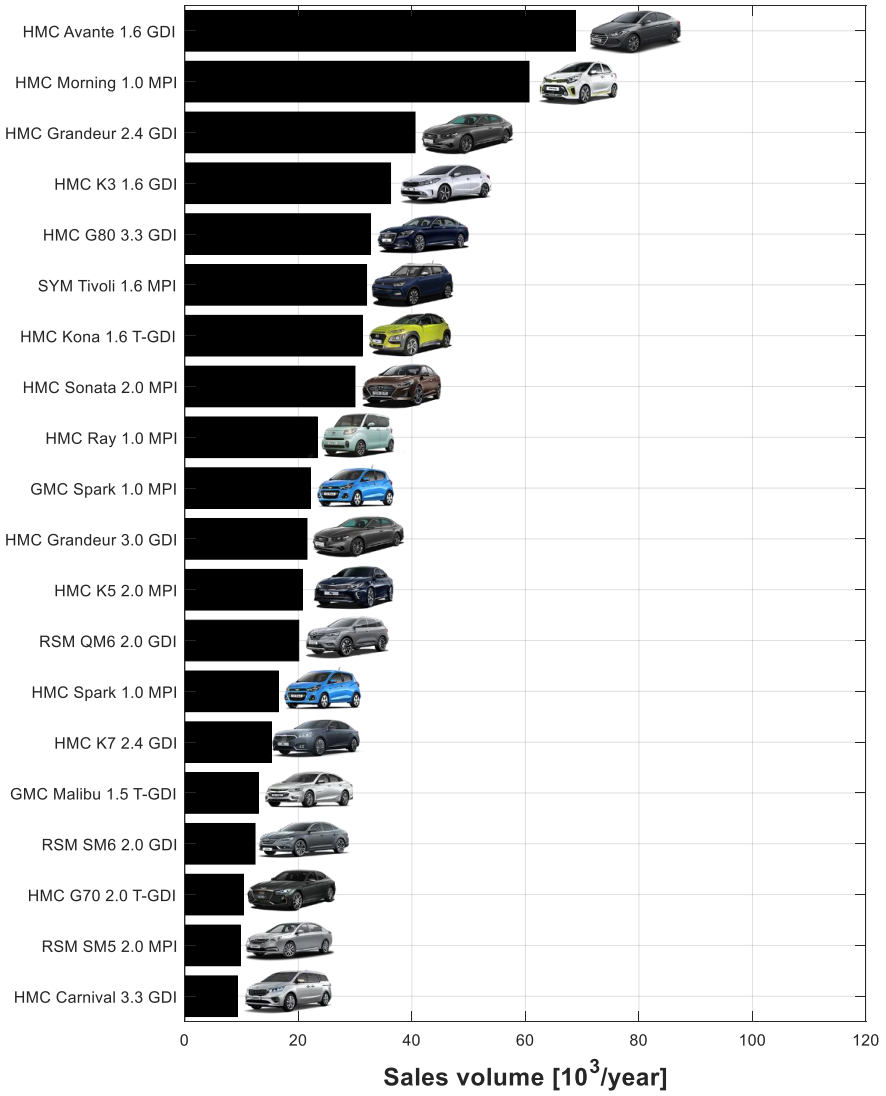

Figure 5.2 Sales volume of each automobile from South Korea in MY2018

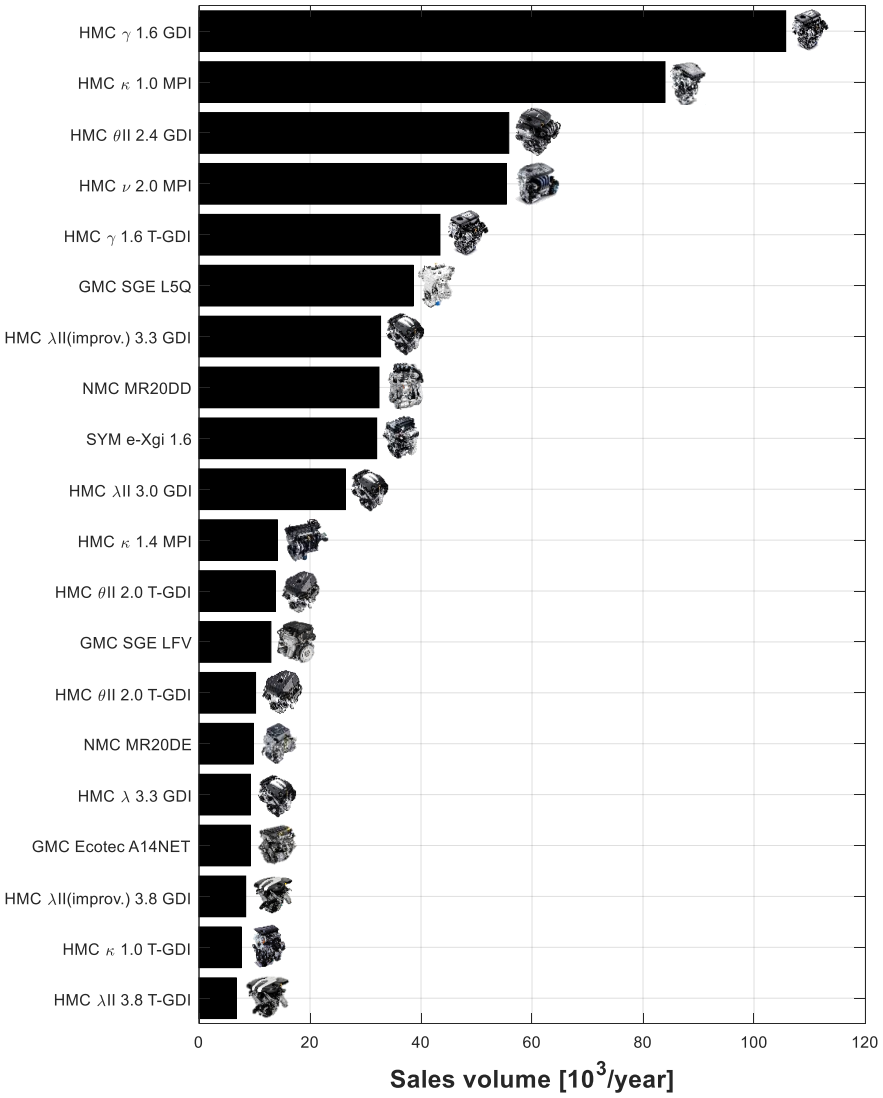

Figure 5.3 Sales volume of each SI engine from South Korea in MY2018

Table 5.1 Sale volume and geometry parameters for various SI engines sold in South Korea for MY2018

Model	Sale volume	Bore [mm]	Stroke [mm]	CR [-]
CFR engine	-	82.6	114.3	7.9
HMC γ 1.6 GDI	105709	77.0	85.4	11.0
HMC κ 1.0 MPI	83963	71.0	84.0	10.5
HMC θII 2.4 GDI	55816	88.0	97.0	11.3
HMC ν 2.0 MPI	55369	81.0	97.0	10.3
HMC γ 1.6 T-GDI	43409	77.0	85.4	9.5
GMC SGE L5Q	38573	74.0	77.7	10.5
HMC λII (improv.) 3.3 GDI	32713	92.0	83.8	12.0
NMC MR20DD	32427	84.0	90.1	11.2
SYM e-Xgi 1.6	32013	76.0	88.0	10.5
HMC λII 3.0 GDI	26361	92.0	75.2	12.0
HMC κ 1.4 MPI	14115	72.0	84.0	10.5
HMC θII 2.0 T-GDI	13701	86.0	86.0	10.0
GMC SGE LFV	12953	74.0	86.6	10.0
HMC θII 2.0 T-GDI	10189	88.0	86.0	9.5
NMC MR20DE	9777	84.0	90.1	10.2
HMC λ 3.3 GDI	9258	92.0	83.8	11.5
GMC Ecotec A14NET	9236	72.5	82.6	9.5
HMC λII (improv.) 3.8 GDI	8410	96.0	87.0	12.0
HMC κ 1.0 T-GDI	7578	71.0	84.0	10.0
HMC λII 3.8 T-GDI	6717	96.0	87.0	11.5
GMC SGE LE2	5584	74.0	81.3	10.0
GMC Ecotec LTG	5050	86.0	86.0	9.5
NMC HR16DE	4679	78.0	83.6	11.2
HMC λII 3.3 T-GDI	4441	92.0	83.8	10.0
HMC λII 3.3 GDI	3899	92.0	83.9	12.0
HMC λII (improv.) 3.3 T-GDI	2934	92.0	83.8	10.0

Table 5.1 Sale volume and geometry parameters for various SI engines sold in South Korea for MY2018 (continue)

Model	Sale volume	Bore [mm]	Stroke [mm]	CR [-]
HMC κ 1.4 T-GDI	2760	71.6	84.0	10.0
NMC MR16DDT	2119	79.7	81.1	9.5
GMC Ecotec LKW	1659	88.0	101.0	11.3
HMC τ (improv.) 5.0 GDI	962	96.0	87.0	12.0
NMC VQ25DE	497	85.0	73.3	9.8
HMC θII (improv.) 2.0 T-GDI	299	88.0	86.0	9.5
GMC HFV LFX	199	94.0	85.6	11.5
HMC τ 5.0 GDI	175	96.0	87.0	11.5
NMC VQ35DE	114	95.5	81.4	10.6

5.3 Optimal ethanol content maximizing knock suppression in South Korea

The temperature and pressure at BMF 0.7 for each SI engines were depicted on the optimal ethanol content diagram as **Figure 5.4 (a-1)**, especially for the condition with engine speed of 600 rpm as RON test condition without external-EGR. The sales volume of each engine was expressed with the size of circle around its operating condition, where the sales volume is proportional to the area of circles. As shown, 72 % of tested vehicles were being operated on region where ERF30 is optimal for knocking suppression; it implies that ERF30 is optimal ethanol content for light duty fleet in South Korea at the engine speed of 600 rpm.

Figure 5.4 (a-1), (a-2), and (a-3) describe the change of DBL condition according to engine speed, and the resultant deviation of temperature and pressure of end gas. As shown, as engine speed gets faster, the pressure at DBL condition

increases due to the expansion of knock limited load of engine, and the temperature decreases with reduced amount of residual gas. Consequently, the more engines get into the region where ERF30 is optimal for knocking suppression, which reinforces the conclusion that ERF30 is optimal ethanol content for light duty fleet in South Korea.

Chapter 4 inferred that the optimal ethanol content can be varied according to external-EGR rate. Despite of the most of SI engine models sold in South Korea do not be equipped with external-EGR system, it is assured that external-EGR system will be widely used in near future for reduction of NOx emission from SI engine. Thus, the following discussion is devoted to how the optimal ethanol content will be changed as the usage of external-EGR system is prominent in the future.

Figure 5.4 (a-1), (b-1), and (c-1) show the dependency of ethanol content on the external-EGR rate. As shown, only with 10 % of external-EGR rate, the optimal ethanol content becomes ERF10 due its high sensitivity to dilution effect of external-EGR. The region where ERF10 is optimal gets wider with more external-EGR rate.

However, the dilution effect of external-EGR gets weaker at higher engine speed as discussed on **Chapter 4.5**, thus the effect of external-EGR on the optimal ethanol content would be marginal. To verify this, the optimal ethanol content diagram for faster engine speed were drawn on **Figure 5.4 (b-2)**, **(b-3)**, **(c-2), and (c-3).** As shown, as engine speed get faster, the region where ERF10 is optimal becomes narrower, and the engine operating condition of light duty fleet closer to the region where ERF10. Consequently, there should be carefully inspection on the typical external-EGR rate and engine speed for optimizing ethanol content in light duty fleet with external-EGR system.

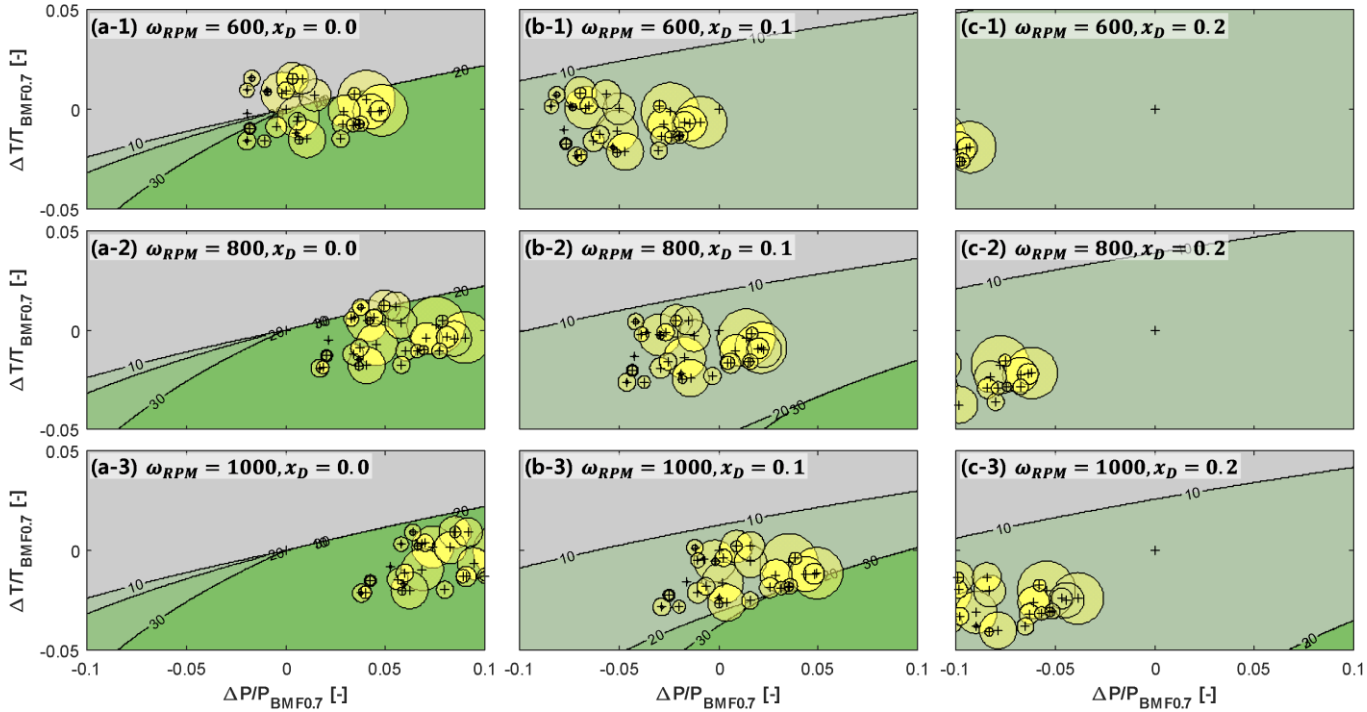

Figure 5.4 Distribution of various SI engine models in South Korea on optimal ethanol content diagram for varuing engine speed and external-EGR rate

5.4 Summary

In this research, the optimal ethanol content for the light duty fleet in South Korea. To this end, the optimal ethanol content diagram, which gives the optimal ethanol content at the given thermodynamic state of the end gas, was derived based on the understanding of the dependency of E_{DTP} on engine operating condition and ethanol content. Then, by calculating thermodynamic state inside each SI engine models sold in South Korea for MY 2018, the optimal ethanol content was achieved for various scenario. Here is the summary of the findings.

1. If the modern SI engine is operated on the engine speed of 600 rpm, which is the reference engine speed of RON test condition, the 72 % of SI engines in South Korea would operate in the region where ERF30 is optimal for knock suppression.

2. At faster engine speed than 600 rpm, the most engines becomes resistive to knocking, then operable range of in-cylinder pressure increases, which results in more SI engines in South Korea get into the region where ERF30 is optimal; at 1000 rpm, ERF30 is optimal for all of SI engines in South Korea.

3. The effect of external-EGR on the optimal ethanol content was investigated for the future scenario where external-EGR is widely accepted in South Korea. As a result, only with 10 % of external-EGR, the most of SI engines in South Korea would operate in the region where ERF10 is optimal, since ERF10 is sensitive to dilution effect of external-EGR. However, it was found that the effect of external-EGR is deemed at high engine speed due to decreased pre-heat release, thus the optimal ethanol content get closer to ERF30 again despite of external-EGR.

Chapter 6. Conclusion

In this study, the optimal ethanol content in gasoline-ethanol reference fuel with a fixed RON of 100 was derived for maximizing antiknock characteristics of fuel in light duty fleet in South Korea. To this end, the novel framework for analyzing knocking of fuel with varying ethanol content and engine operating conditions was developed with the ignition delay measurement from rapid compression machine. Based on the method, the optimal ethanol content for arbitrary engine operating condition was achieved and applied to find the optimal ethanol content for the entire light duty fleet in South Korea.

6.1 Knocking analysis based on the ignition delay

In order to analyze the knocking characteristics form the chemical kinetic point of view, the ignition delay for varying ERFs was measured using rapid compression machine, especially around the thermodynamic state of the end gas in RON test condition. Then, the measurement was regressed to derive the empirical correlation for ignition delay, and it was used to quantify how the ignition delay varies with five scenario of engine development: turbocharging, higher CR, lower heat loss, higher IT, and external-EGR. Conclusion is as follow:

1. Ignition delay measurement shows that all the tested fuel has different sensitivity on temperature and pressure despite of a fixed RON. The ignition delay of the fuel with higher ethanol content was found to be more sensitive to temperature and less sensitive to pressure.

2. Turbocharging raises the in-cylinder pressure while slightly reduces the temperature owing to decreased residual gas. This change of

thermodynamic state results in shorter ignition delay of the end gas, which implies more intensive knocking in turbocharged condition. Meanwhile, it was found that the effect of turbocharging on the ignition delay increases as ethanol content in the fuel decreases because the fuel with higher ethanol content is more sensitive to pressure deviation. Thus, it was concluded that the higher ethanol content is optimal for turbocharged condition.

3. Higher CR raises both in-cylinder pressure and temperature, thus reduces the ignition delay of end gas. Similarly with the cased of turbocharging, the fuel with higher ethanol content was found to be optimal in higher CR case, but the difference of the effect according to ethanol content was less that of turbocharging.

4. Lower heat loss also shorter the ignition delay by increasing pressure and temperature of the gas. However, the effect of lower heat loss on the ignition delay was found to be independent to the ethanol content, which gives a clue that there might be a condition for engine operating condition to have the identical knocking characteristics regardless of ethanol content, despite of different auto-ignition characteristics of the tested fuels.

5. Higher IT also reduces the ignition delay due to increased temperature of the end gas. However, the dependency of the effect of higher IT on the ethanol content was completely opposite to the above three operating conditions; the lower ethanol content is optimal. This is because the ethanol with lower ethanol content is less sensitive to temperature deviation.

6. External-EGR lowers both temperature and pressure because of reduced fuel supply rate and longer combustion duration, moreover it dilutes the end gas; thus the ignition delay of gas is significantly reduced. Because of dilution effect, the effect of external-EGR shows non-monotonic dependency on the ethanol content, where the 10 % of ethanol was found to be optimal.

Based on the result from the above five operating conditions, the optimal ethanol content was discussed for an arbitrary engine operating condition based on the thermodynamic state of the condition. Conclusion is as follow:

1. It was found that the optimal ethanol content at an arbitrary engine operating condition without dilution is determined by the amount of temperature deviation and pressure deviation, $\frac{\Delta T}{T}$ and $\frac{\Delta P}{P}$, from the RON test condition. Higher ethanol content is optimal for the condition where $\frac{\Delta T}{T}$ is less than $\frac{\gamma-1}{\gamma}\frac{\Delta P}{P}$, while lower ethanol content is preferable if $\frac{\Delta T}{T}$ is higher than $\frac{\gamma-1}{\gamma}\frac{\Delta P}{P}$. Especially, it was induced that the knocking characteristics becomes independent to ethanol content if and only if $\frac{\Delta T}{T}$ is equal to $\frac{\gamma-1}{\gamma}\frac{\Delta P}{P}$, which is the extension of adiabatic compression line from RON test condition.

2. Framework of this study was validated by comparing with Kalghatgi's K value principle. For this, OI for varying temperature and pressure profile was calculated based on the empirical correlation between K and T_{comp15}, which was suggested by Kalghatgi et al. [73, 76], then the

dependency of OI on engine operating condition and ethanol content is compared with that of ignition delay. Consequently, it was found Kalghatgi's K value principle gives the same conclusion: The optimal ethanol content depends on the magnitude of $\frac{\Delta T}{T}$ and $\frac{\gamma-1}{\gamma}\frac{\Delta P}{P}$, and the dependency of knock intensity on the ethanol content get deemed as the ethanol content increases.

3. For the prediction of optimal ethanol content in diluted condition, it was found that there are obvious correlation between the amount of pre-heat release and the amount of dilution effect, and the empirical correlation for them was achieved from regression analysis. Based on this correlation, the dilution effect at the higher engine speed, where the amount of pre-heat releases differs from RON test condition, was calculated. Consequently, it was predict that the optimal ethanol content varies from ERF0 to ERF10, depending on the engine speed.

6.2 Optimal ethanol content for South Korea

Analysis on the knocking characteristic based on the ignition delay was used to achieve the optimal ethanol content diagram, which depicts the optimal ethanol content according the thermodynamic state of the end gas. Then, it was investigated what kinds of SI engine models were sold for MY2018 in South Korea, and how the design parameters such as stroke, bore, or compression ratio are varied with the type of engine. Based on the statistics, it was discussed how the thermodynamic state of the end gas distributes for varying SI engine model, and how much ethanol content is optimal for light duty fleet in South Korea. Conclusion is as follow:

1. It was found that, at 600 rpm, about 72 % of SI engine vehicles operates in the thermodynamic state where ERF30 is optimal.

2. As the engine speed gets faster, the in-cylinder pressure at DBL condition increases, and eventually ERF30 becomes optimal to all of SI engine vehicles at 1000 rpm because of its low sensitivity of ignition delay on pressure.

3. For the scenario of using external-EGR, optimal ethanol content gets closer to ERF10 due to its high sensitivity of ignition delay to dilution effect. However, the dilution effect decreases as the engine speed increases, thus ERF30 is still optimal for almost all of SI engine vehicles at fast engine speed regardless of external-EGR.

6.3 Future work

This study assumed that the knocking intensity is solely dependent on BMF at the moment of knock occurrence. However, the recent studies on knocking suggests the knock intensity is determined not only by BMF but also by the structure of hot spot where the auto-ignition starts in the end gas [90-93]. Thus, careful analysis on the effect of inhomogeneity in the end gas should be considered and integrated to the result from this study. I tried some researches on the effect of fuel-air inhomogeneity on knocking characteristics of ERFs [49, 94], but it has a limitation that the effect of inhomogeneity is hard to be compared with the other effect such as the dilution effect or temperature-pressure profile effect; thus, more integrative framework including inhomogeneity is required.

Another point to be accounted for is the effect of using real gasoline, not surrogate fuel such as ERF. The real gasoline has different auto-ignition

characteristics with the surrogate; for example, OS of real gasoline is higher than PRF, or pre-heat release characteristics might be different from the surrogate. I tried to find optimal ethanol content for real gasoline based on Kalghatgi's K value principle, and it was found that 30% of ethanol content still be optimal in non-diluted condition. But there remains a question whether the effect of dilution differs from the case of PRF.

Regarding to the effect of external-EGR, even though this study clarified that the amount of pre-heat release determines the dilution effect, but there remains an issue of understanding and predicting the amount of pre-heat release of an arbitrary fuel. Although this study gives qualitative discussion based on Livengood-Wu integration and intensity of cool flame delay, but quantitative and thorough understanding on the pre-heat release must be achieved to predict the effect of external-EGR for arbitrary fuel.

Lastly, the last chapter of this study suggested how the optimal ethanol content for light duty fleet is varied with engine speed or the amount of external-EGR, but it is still questionable which engine speed or the amount of external-EGR rate the vehicles is operated most. In this regard, it would give more useful information if the optimal ethanol content is achieved with the assumption that all the vehicles run in specific type of driving cycle such as WLTP or NEDC.

Nomenclature

Physical variables

a_W	Efficiency parameter for Wiebe function, [-]
a_i	Coefficient of polynomial in exponential term of Arrehnius equation, [K^i]
A	Heat transfer area, [m^2]
b_i	Coefficient of polynomial in dilution exponent term of Arrehnius equation, [K^i]
C	Calibration variable, [-]
c_v	Constant volume specific heat, [$J\ K^{-1}\ kg^{-1}$]
c_p	Constant pressure specific heat, [$J\ K^{-1}\ kg^{-1}$]
D	Diameter, [-]
E_a	Activation energy, [$J\ kmol^{-1}$]
E	Effect of thermodynamic state deviation on the ignition delay, [-]
h_c	Convective heat transfer coefficient, [$W\ m^{-2}\ K^{-1}$]

$\boldsymbol{LW}$	The value of Livengood-Wu integration, [-]
$\boldsymbol{m}$	Mass, [kg]
$\boldsymbol{m_W}$	Form factor for Wiebe function, [kg]
$\boldsymbol{\dot{m}_b}$	Burning rate of fuel-air mixture, [kg s^{-1}]
$\boldsymbol{MW}$	Molecular weight, [kg $kmol^{-1}$]
$\boldsymbol{\overline{MW}}$	Mean molecular weight, [kg $kmol^{-1}$]
$\boldsymbol{n}$	Pressure exponent of ignition delay, [-]
$\boldsymbol{N_{species}}$	The number of species, [-]
$\boldsymbol{P}$	In-cylinder pressure, [Pa]
$\boldsymbol{Q_{PHR}}$	The amount of pre-heat release [J/kmol]
$\boldsymbol{\dot{Q}}$	Heat transfer rate, [J s^{-1}]
$\boldsymbol{R_u}$	Universal gas constant, [J K^{-1} kg^{-1}]
$\boldsymbol{S_L}$	Laminar flame speed, [m/s]
$\boldsymbol{\overline{S_P}}$	Mean piston speed, [m/s]
$\boldsymbol{t}$	Time, [s]
$\boldsymbol{T}$	Temperature, [K]

$\boldsymbol{u}$	Mass specific internal energy, [J kg^{-1}]
$\boldsymbol{V}$	Volume, [m^3]
$\boldsymbol{w}$	Characteristic flow speed, [-]
$\boldsymbol{x}$	Mole fraction, [-]
$\boldsymbol{y}$	Mass fraction, [-]
$\boldsymbol{z}$	Liquid volume fraction, [-]
$\boldsymbol{\gamma}$	Specific heat ratio, [-]
$\boldsymbol{\Delta h_v}$	Heat of vaporization, [J kg^{-1}]
$\boldsymbol{\Delta\theta}$	Combustion angle, [CAD]
$\boldsymbol{\rho}$	Gas density, [kg m^{-3}]
$\boldsymbol{\rho_L}$	Liquid density, [kg m^{-3}]
$\boldsymbol{\sigma}$	Stefan-Boltzmann constant, [W m^{-2} K^{-4}]
$\boldsymbol{\tau_i}$	Ignition delay, [s]
$\boldsymbol{\omega_{RPM}}$	Engine speed, [rpm]

Subscripts

a	Fresh air
amb.	Ambient
b	Burned zone in SI engine
B	Bore
c	Clearance
core	Adiabatic core
cyl.	Cylinder
D	Dilution
E	Ethanol
em	Exhaust manifold
f	Fresh fuel
G	Gasoline
i	The i^{th} zone in 0-D two-zone SI engine model
im,i(e)	Internal (or external) side of intake manifold
inert	Inert gas

j	The j^{th} speicies in 0-D two-zone SI engine model
KO	Knock onset timing
loss	Heat loss to the wall
m	Fresh fuel-air mixture at intake manifold
mod.	Modified engine operating condition
mtr	Motored cycle
original	Original ignition delay
r	Residual gas
react.	Reactive gas
s	Surface of intake manifold
u	Unburned zone in SI engine
wall	Cylinder wall

Abbreviation

BDC	Bottom dead center
BMF	Burned mass fraction
BON	Bench octane number
CA50	Crank angle at 50 % burned
CAD	Crank angle degree
CAFE	Corporate average fuel economy
CFR	Cooperative fuel research
CR	Compression ratio
DBL	Detonation borderline
EGR	Exhaust gas recirculation
EISA	Energy independence and security act
EOC	End of compression
ERF	Ethanol reference fuel
EVO	Exhaust valve opening
GDI	Gasoline direct injection

GMC	General motors company
HCCI	Homogeneous charge compression ignition
HMC	Hyundai motors company
IT	Intake temperature
IVC	Intake valve closure
KAMA	Korea automobile manufacturers association
KLSA	Knocking limited spark advance
LEZ	Low emission zone
MBT	Maximum brake toque
MON	Motor octane number
MTBE	Methyl tert-butyl ether
MY	Model year
NMC	Nissan motors company
NOx	Nitric oxide
NTC	Negative temperature coefficient
OI	Octane index
OS	Octane sensitivity

PFI	Port fuel injection
PRF	Primary reference fuel
RCM	Rapid compression machine
RFS	Renewable fuel standard
RMSE	Root mean square error
RON	Research octane number
SI	Spark-ignition
SNU	Seoul national university
SOC	Start of compression
SYM	Ssangyong motors
TDC	Top dead center

Reference

[1] U.S. Energy Information Administration, Monthly Energy Review (2019).

[2] The International Council on Clean Transportation, 2017 Global Update: Light-Duty Vehicle Greenhouse Gas and Fuel Economy Standards (2017).

[3] U.S. Environmental Protection Agency, 2017 and Later Model Year Light-Duty Vehicle Greenhouse Gas Emissions and Corporate Average Fuel Economy Standards; Final Rule, EPA-HQ-OAR-2010-0131 (2012).

[4] European Comission, Regulation (EC) No 443/2009 of the European Parliament and of the Council of 23 April 2009 Setting Emission Performance Standards for New Passenger Cars as Part of the Community's Integrated Approach to Reduce CO2 Emissions from Light-duty Vehicles (2018).

[5] J. Freeman, R. Stahman, Vehicle Performance and Exhaust Emission, Carburetion Versus Timed Fuel Injection, 1965 International Automotive Engineering Congress and Exposition (1965), paper 650863.

[6] R.A. Stein, D. Polovina, K. Roth, M. Foster, M. Lynskey, T. Whiting, J.E. Anderson, M.H. Shelby, T.G. Leone, S. Vandergriend, Effect of Heat of Vaporization, Chemical Octane, and Sensitivity on Knock Limit for Ethanol - Gasoline Blends, SAE International Journal of Fuels and Lubricants 5 (2012) 823-843.

[7] B. Lecointe, G. Monnier, Downsizing a Gasoline Engine Using Turbocharging with Direct Injection, SAE World Congress & Exhibition (2003), paper 2003-01-0542.

[8] D. Han, S.-K. Han, B.-H. Han, W.-T. Kim, Development of 2.0 L Turbocharged DISI Engine for Downsizing Application, SAE World Congress & Exhibition (2007), paper 2007-01-0259.

[9] U.S. Enviromental Protection Agency, Light-Duty Automotive Technology, Carbon Dioxide Emissions, and Fuel Economy Trends (2018).

[10] D. Splitter, A. Pawlowski, R. Wagner, A Historical Analysis of the Co-evolution of Gasoline Octane Number and Spark-ignition Engines, Frontiers in Mechanical Engineering 1 (2016) 16.

[11] P. Smith, J. Heywood, W. Cheng, Effects of Compression Ratio on Spark-ignited Engine Efficiency, SAE International Powertrain, Fuels & Lubricants Meeting (2014), paper 2014-01-2599.

[12] D.N. Assanis, T. Mathur, The Effect of Thin Ceramic Coatings on Spark-Ignition Engine Performance, SAE Transactions 99 (1990) 981-990.

[13] L.P. Wyszynski, C.R. Stone, G.T. Kalghatgi, The Volumetric Efficiency of Direct and Port Injection Gasoline Engines with Different Fuels, SAE World Congress & Exhibition (2002), paper 2002-01-0839.

[14] R. Nates, A. Yates, Knock Damage Mechanisms in Spark-ignition Engines, SAE Transactions (1994) 1970-1980.

[15] L. Ceschini, A. Morri, E. Balducci, N. Cavina, N. Rojo, L. Calogero, L. Poggio, Experimental Observations of Engine Piston Damage Induced by Knocking Combustion, Materials & Design 114 (2017) 312-325.

[16] F.A. Ayala, M.D. Gerty, J.B. Heywood, Effects of Combustion Phasing, Relative Air-Fuel Ratio, Compression Ratio, and Load on SI Engine

Efficiency, SAE 2006 World Congress & Exhibition (2006), paper 2006-01-0229.

[17] ASTM International, Standard Test Method for Research Octane Number of Spark-Ignition Engine Fuel, ASTM D2699-17 (2017).

[18] ASTM International, Standard Test Method for Motor Octane Number of Spark-Ignition Engine Fuel, ASTM D2700-17 (2017).

[19] G.T. Kalghatgi, Fuel Anti-Knock Quality-Part II. Vehicle Studies-How Relevant is Motor Octane Number (MON) in Modern Engines?, SAE International Fall Fuels and Lubricants Meeting and Exposition (2001), paper 2001-01-3585.

[20] N. Kawahara, E. Tomita, Y. Sakata, Auto-Ignited Kernels during Knocking Combustion in a Spark-Ignition Engine, Proceedings of the Combustion Institute 31 (2007) 2999-3006.

[21] T. Shinagawa, T. Okumura, S. Furuno, K.-O. Kim, Effects of Hydrogen Addition to SI Engine on Knock Behavior, SAE Fuels & Lubricants Meeting & Exhibition (2004), paper 2004-01-1851.

[22] H. Liu, Z. Wang, J. Wang, Methanol-Gasoline DFSI (Dual-Fuel Spark Ignition) Combustion with Dual-Injection for Engine Knock Suppression, Energy 73 (2014) 686-693.

[23] H. Wei, D. Feng, M. Pan, J. Pan, X. Rao, D. Gao, Experimental Investigation on the Knocking Combustion Characteristics of N-Butanol Gasoline Blends in a DISI Engine, Applied Energy 175 (2016) 346-355.

[24] D.A. Rothamer, J.H. Jennings, Study of the Knocking Propensity of 2, 5-Dimethylfuran–Gasoline and Ethanol–Gasoline Blends, Fuel 98 (2012) 203-212.

[25] V.F. Andersen, J. Anderson, T. Wallington, S. Mueller, O.J. Nielsen, Vapor Pressures of Alcohol−Gasoline Blends, Energy & Fuels 24 (2010) 3647-3654.

[26] H. Von Blottnitz, M.A. Curran, A Review of Assessments Conducted on Bio-Ethanol as a Transportation Fuel from a Net Energy, Greenhouse Gas, and Environmental Life Cycle Perspective, Journal of Cleaner Production 15 (2007) 607-619.

[27] M.L. Lopes, S.C. De Lima Paulillo, A. Godoy, R.A. Cherubin, M.S. Lorenzi, F.H.C. Giometti, C.D. Bernardino, H.B. De Amorim Neto, H.V. De Amorim, Ethanol Production in Brazil: a Bridge between Science and Industry, Brazilian Journal of Microbiology 47 (2016) 64-76.

[28] B.C. Klein, M.F. Chagas, M.D.B. Watanabe, A. Bonomi, R. Maciel Filho, Low Carbon Biofuels and the New Brazilian National Biofuel Policy (RenovaBio): A Case Study for Sugarcane Mills and Integrated Sugarcane-Microalgae Biorefineries, Renewable and Sustainable Energy Reviews 115 (2019) 109365.

[29] K-petro, Development of Optimization for Domestic Application Improvement of E3 Level Transport Biofuels (2016).

[30] S. Kim, J.-K. Kim, C.-K. Park, I.-H. Hwang, Study on Fuel Characteristics Depending on Mixing Ratio of Bio-Butanol and Bio-Ethanol, Transactions of the Korean Hydrogen and New Energy Society 28 (2017) 704-711.

[31] S. Kim, J.-K. Kim, M.-H. Lee, I.-H. Hwang, J.-M. Lee, Study on Emission Characteristics Depending on Mixing Fuels of Bio-Alcohol Transactions of the Korean Hydrogen and New Energy Society 29 (2018) 654-660.

[32] H. Jeon, K.-M. Go, S. Kim, J.-S. Jeong, A Study on the High-efficient Bioethanol Production Using Barley, Transactions of the Korean Hydrogen and New Energy Society 28 (2017) 697-703.

[33] S.M. Sarathy, P. Oßwald, N. Hansen, K. Kohse-Höinghaus, Alcohol Combustion Chemistry, Progress in Energy and Combustion Science 44 (2014) 40-102.

[34] J. Anderson, U. Kramer, S. Mueller, T. Wallington, Octane Numbers of Ethanol− and Methanol−Gasoline Blends Estimated from Molar Concentrations, Energy & Fuels 24 (2010) 6576-6585.

[35] T.M. Foong, K.J. Morganti, M.J. Brear, G. Da Silva, Y. Yang, F.L. Dryer, The Effect of Charge Cooling on the RON of Ethanol/Gasoline Blends, SAE International Journal of Fuels and Lubricants 6 (2013) 34-43.

[36] V. Mittal, J.B. Heywood, The Relevance of Fuel RON and MON to Knock Onset in Modern SI Engines, SAE Powertrains, Fuels and Lubricants Meeting (2008), paper 2008-01-2414.

[37] M. Mehl, T. Faravelli, E. Ranzi, T. Lucchini, A. Onorati, F. Giavazzi, P. Scorletti, D. Terna, Kinetic Modeling of Knock Properties in Internal Combustion Engines, SAE Powertrain & Fluid Systems Conference and Exhibition (2006), paper 2006-01-3239.

[38] G.T. Kalghatgi, Fuel Anti-Knock Quality-Part I. Engine Studies, SAE International Fall Fuels and Lubricants Meeting and Exposition (2001), paper 2001-01-3584.

[39] G. Kalghatgi, I. Algunaibet, K. Morganti, On Knock Intensity and Superknock in SI Engines, SAE International Journal of Engines 10 (2017) 1051-1063.

[40] G. Kalghatgi, K. Morganti, I. Algunaibet, Some Insights on the Stochastic Nature of Knock and the Evolution of Hot Spots in the End-Gas during the Engine Cycle from Experimental Measurements of Knock Onset and Knock Intensity, (2017), paper 2017-01-2233.

[41] C. Wang, A. Prakash, A. Aradi, R. Cracknell, H. Xu, Significance of RON and MON to a Modern DISI Engine, Fuel 209 (2017) 172-183.

[42] J.P. Szybist, D.A. Splitter, Understanding Chemistry-Specific Fuel Differences at a Constant RON in a Boosted SI Engine, Fuel 217 (2018) 370-381.

[43] S. Yitao, S. Shuai, W. Jianxin, X. Jianhua, Optimization of gasoline hydrocarbon compositions for reducing exhaust emissions, Journal of Environmental Sciences 21 (2009) 1208-1213.

[44] B. Masum, H.H. Masjuki, M. Kalam, S. Palash, M. Habibullah, Effect of Alcohol–Gasoline Blends Optimization on Fuel Properties, Performance and Emissions of a SI Engine, Journal of Cleaner Production 86 (2015) 230-237.

[45] A. Amer, H. Babiker, J. Chang, G. Kalghatgi, P. Adomeit, A. Brassat, M. Günther, Fuel Effects on Knock in a Highly Boosted Direct Injection Spark

Ignition Engine, SAE International Journal of Fuels and Lubricants 5 (2012) 1048-1065.

[46] National Renewable Energy Laboratory, Co-Optimization of Fuels & Engines: FY18 Year in Review (2019).

[47] C.S. Sluder, Estimation of the Fuel Efficiency Potential of Six Gasoline Blendstocks Identified by the US Department of Energy's Co-Optimization of Fuels and Engines Program, International Powertrains, Fuels & Lubricants Meeting (2019), paper 2019-01-0017.

[48] T.M. Foong, K.J. Morganti, M.J. Brear, G. Da Silva, Y. Yang, F.L. Dryer, The Octane Numbers of Ethanol Blended with Gasoline and Its Surrogates, Fuel 115 (2014) 727-739.

[49] J. Cho, H.H. Song, Understanding the Effect of Inhomogeneous Mixing on Knocking Characteristics of Iso-octane by Using Rapid Compression Machine, SAE World Congress Experience (2018), paper 2018-01-0212.

[50] J. Cho, H.H. Song, Development of a Predictive Model for Knock Intensity in a Spark-Ignition Engine with Gasoline-Ethanol-nButanol Blend Fuel by Using Rapid Compression Machine, 14th International Conference on Engines & VehiclesSociety of Automotive Engineers (SAE) (2019), paper 2019-24-0125.

[51] M. Mehl, W.J. Pitz, C.K. Westbrook, H.J. Curran, Kinetic Modeling of Gasoline Surrogate Components and Mixtures under Engine Conditions, Proceedings of the Combustion Institute 33 (2011) 193-200.

[52] J.B. Heywood, Internal Combustion Engine Fundamentals, McGraw-Hill Education, New York City, U.S., 2018.

[53] S. Hires, R. Tabaczynski, J. Novak, The Prediction of Ignition Delay and Combustion Intervals for a Homogeneous Charge, Spark Ignition Engine, SAE Transactions (1978) 1053-1067.

[54] K. Kar, W. Cheng, K. Ishii, Effects of Ethanol Content on Gasohol PFI Engine Wide-Open-Throttle Operation, SAE International Journal of Fuels and Lubricants 2 (2009) 895-901.

[55] C.P. Cooney, J.J. Worm, J.D. Naber, Combustion Characterization in an Internal Combustion Engine with Ethanol−Gasoline Blended Fuels Varying Compression Ratios and Ignition Timing, Energy & Fuels 23 (2009) 2319-2324.

[56] T.C.C. De Melo, G.B. Machado, L. De Oliveira Carvalho, C.R.P. Belchior, M.J. Colaco, J.E.M. Barros, C.E.F. Paiva, In Cylinder Pressure Curve and Combustion Parameters Variability with Ethanol Addition, (2012), paper 2012-36-0486.

[57] T.M. Foong, On the Autoignition of Ethanol-Gasoline Blends in Spark-Ignition Engines, The Department of Mechanical Engineering, The University of Melbourne, Doctor of Philosophy (2013).

[58] R.J. Middleton, J.B. Martz, G.A. Lavoie, A. Babajimopoulos, D.N. Assanis, A Computational Study and Correlation of Premixed Isooctane Air Laminar Reaction Fronts Diluted with EGR, Combustion and Flame 159 (2012) 3146-3157.

[59] G. Woschni, A Universally Applicable Equation for the Instantaneous Heat Transfer Coefficient in the Internal Combustion Engine, National Fuels and Lubricants, Powerplants, Transportation Meetings (1967), paper 670931.

[60] Y. Kim, A Study on the CAI Combustion Characteristics Using a Reduces Chemical Kinetics Mechanism, Department of Mechanical Engineering, Seoul National University, Doctor of Philosophy (2007).

[61] S.S. Goldsborough, S. Hochgreb, G. Vanhove, M.S. Wooldridge, H.J. Curran, C.-J. Sung, Advances in Rapid Compression Machine Studies of Low- and Intermediate Temperature Autoignition Phenomena, Progress in Energy and Combustion Science 63 (2017) 1-78.

[62] K.P. Grogan, S.S. Goldsborough, M. Ihme, Ignition Regimes in Rapid Compression Machines, Combustion and Flame 162 (2015) 3071-3080.

[63] M.F. Campbell, S. Wang, D.F. Davidson, R.K. Hanson, Shock Tube Study of Normal Heptane First-Stage Ignition near 3.5 atm, Combustion and Flame 198 (2018) 376-392.

[64] J.P. Szybist, D.A. Splitter, Pressure and Temperature Effects on Fuels with Varying Octane Sensitivity at High Load in SI Engines, Combustion and Flame 177 (2017) 49-66.

[65] Y. Yang, J.E. Dec, M. Sjöberg, C. Ji, Understanding Fuel Anti-Knock Performances in Modern SI Engines Using Fundamental HCCI Experiments, Combustion and Flame 162 (2015) 4008-4015.

[66] E. Kasseris, J.B. Heywood, Charge Cooling Effects on Knock Limits in SI DI Engines Using Gasoline/Ethanol Blends: Part 1-Quantifying Charge Cooling, SAE World Congress & Exhibition (2012), paper 2012-01-1275.

[67] M. Alabbad, T. Javed, F. Khaled, J. Badra, A. Farooq, Ignition Delay Time Measurements of Primary Reference Fuel Blends, Combustion and Flame 178 (2017) 205-216.

[68] S.S. Goldsborough, A Chemical Kinetically Based Ignition Delay Correlation For Iso-Octane Covering a Wide Range of Conditions Including the NTC Region, Combustion and Flame 156 (2009) 1248-1262.

[69] D. Delvescovo, S. Kokjohn, R. Reitz, The Development of an Ignition Delay Correlation for PRF Fuel Blends from PRF0 (N-Heptane) to PRF100 (Iso-Octane), SAE International Journal of Engines 9 (2016) 520-535.

[70] G. Kalghatgi, K. Morganti, I. Algunaibet, M. Sarathy, R. Dibble, Knock Prediction Using a Simple Model for Ignition Delay, SAE World Congress and Exhibition (2016), paper 2016-01-0702.

[71] L. Chen, T. Li, T. Yin, B. Zheng, A Predictive Model for Knock Onset in Spark-Ignition Engines with Cooled EGR, Energy Conversion and Management 87 (2014) 946-955.

[72] L. Chen, H. Wei, C. Chen, D. Feng, L. Zhou, J. Pan, Numerical Investigations on the Effects of Turbulence Intensity on Knocking Combustion in a Downsized Gasoline Engine, Energy 166 (2019) 318-325.

[73] P. Risberg, G. Kalghatgi, H.-E. Çngstrom, Auto-ignition Quality of Gasoline-Like Fuels in HCCI Engines, SAE Powertrain & Fluid Systems Conference & Exhibition (2003), paper 2003-01-3215.

[74] G.T. Kalghatgi, R. Head, The Available and Required Autoignition Quality of Gasoline-Like Fuels in HCCI Engines at High Temperatures, 2004 SAE Fuels & Lubricants Meeting & Exhibition (2004), paper 2004-01-1969.

[75] P. Risberg, G. Kalghatgi, H.-E. Angstrom, The Influence of EGR on Auto-Ignition Quality of Gasoline-Like fuels in HCCI Engines, SAE Transactions (2004) 1477-1486.

[76] G.T. Kalghatgi, Auto-Ignition Quality of Practical Fuels and Implications for Fuel Requirements of Future SI and HCCI Engines, SAE World Congress & Exhibition (2005), paper 2005-01-0239.

[77] T. Boningari, P.G. Smirniotis, Impact of Nitrogen Oxides on the Environment and Human Health: Mn-Based Materials for the NOx Abatement, Current Opinion in Chemical Engineering 13 (2016) 133-141.

[78] European Commission, Type Approval of Motor Vehicles with Respect to Emissions from Light Passenger and Commercial Vehicles (Euro 5 and Euro 6) and on Access to Vehicle Repair and Maintenance Information, 52019PC0208 (2007).

[79] J. Cho, H.H. Song, Dimensionless parameters determining the effect of dilution on ignition delay of syngas and hydrocarbon fuels, Combustion and Flame 213 (2020) 279-290.

[80] K. Skalska, J.S. Miller, S. Ledakowicz, Trends in NOx Abatement: A Review, Science of the Total Environment 408 (2010) 3976-3989.

[81] B. Grandin, H.-E. Çngström, P. Stålhammar, E. Olofsson, Knock Suppression in a Turbocharged SI Engine by Using Cooled EGR, International Fall Fuels and Lubricants Meeting and Exposition (1998), paper 982476.

[82] S. Diana, V. Giglio, B. Iorio, G. Police, Evaluation of the Effect of EGR on Engine Knock, International Fall Fuels and Lubricants Meeting and Exposition (1998), paper 982479.

[83] D.A. Splitter, J.P. Szybist, Experimental Investigation of Spark-Ignited Combustion with High-Octane Biofuels and EGR. 2. Fuel and EGR Effects on Knock-Limited Load and Speed, Energy & Fuels 28 (2014) 1432-1445.

[84] J. Cho, H.H. Song, Understanding the effect of external-EGR on anti-knock characteristics of various ethanol reference fuel with RON 100 by using rapid compression machine, Proceedings of the Combustion Institute 36 (2017) 3507-3514.

[85] J. Su, M. Xu, T. Li, Y. Gao, J. Wang, Combined Effects of Cooled EGR and a Higher Geometric Compression Ratio on Thermal Efficiency Improvement of a Downsized Boosted Spark-Ignition Direct-Injection Engine, Energy Conversion and Management 78 (2014) 65-73.

[86] B. Hoepke, S. Jannsen, E. Kasseris, W.K. Cheng, EGR Effects on Boosted SI Engine Operation and Knock Integral Correlation, SAE International Journal of Engines 5 (2012) 547-559.

[87] P.E. Bengtsson, C. Brackmann, J. Bood, I. Denbratt, B. Grandin, A Study of the Influence of Exhaust Gas Recirculation and Stoichiometry on the Heat Release in the End-Gas Prior to Knock Using Rotational Coherent Anti-Stokes-Raman Spectroscopy Thermometry, International Journal of Engine Research 3 (2002) 209-221.

[88] V. Hosseini, W.S. Neill, W.L. Chippior, Influence of Engine Speed on HCCI Combustion Characteristics Using Dual-Stage Autoignition Fuels, SAE World Congress & Exhibition (2009), paper 2009-01-1107.

[89] Korea Automobile Manufacturers Association, Automobile Statistics (2018).

[90] D. Bradley, C. Morley, X. Gu, D. Emerson, Amplified Pressure Waves During Autoignition: Relevance to CAI Engines, SAE Powertrain & Fluid Systems Conference & Exhibition (2002), paper 2002-01-2868.

[91] D. Bradley, G. Kalghatgi, Influence of Autoignition Delay Time Characteristics of Different Fuels on Pressure Waves and Knock in Reciprocating Engines, Combustion and Flame 156 (2009) 2307-2318.

[92] P. Dai, C. Qi, Z. Chen, Effects of Initial Temperature on Autoignition and Detonation Development in Dimethyl Ether/Air Mixtures with Temperature Gradient, Proceedings of the Combustion Institute 36 (2017) 3643-3650.

[93] T. Zhang, W. Sun, Y. Ju, Multi-Scale Modeling of Detonation Formation with Concentration and Temperature Gradients in N-Heptane/Air Mixtures, Proceedings of the Combustion Institute 36 (2017) 1539-1547.

[94] J. Cho, H.H. Song, Understanding the Effect of Inhomogeneous Fuel–Air Mixing on Knocking Characteristics of Various Ethanol Reference Fuels with RON 100 Using Rapid Compression Machine, Proceedings of the Combustion Institute 37 (2019) 4911-4919.

국문초록

본 논문에서는 리서치옥탄가(Research octane number; RON)가 100 으로 고정된 상황에서 가솔린−에탄올 혼합 연료 내 에탄올 함량을 최적화하여 불꽃점화(Spark ignition; SI)엔진에서의 노킹을 억제하는 방법에 관해 논하였다. 이를 위해 에탄올표준연료(Ethanol reference fuel; ERF) 내 에탄올 함량 혼합을 바꾸어가며 총 4 가지 테스트연료를 선정한 다음, 급속압축장치를 이용하여 해당연료의 점화지연을 측정하였다. 측정결과를 바탕으로 각 ERF 의 노킹특성이 엔진운전조건에 따라 어떻게 변화하는지를 분석하였으며, 이를 통해 임의의 엔진운전조건에서 최적의 에탄올 함량을 도출하는 방법을 제시하였다.

본 연구의 첫 번째 목표는 엔진운전조건에 따라 실린더 내 온도−압력 프로파일이 변화할 시, 서로 다른 ERF 연료들의 노킹 특성이 각각 어떻게 변화하는지를 분석하는 것이다. 이를 위해 온도, 압력 및 에탄올 함량 변화에 따른 점화지연을 측정하고, 회귀분석을 통해 이에 대한 경험식을 도출하였다. 그 후, 0−D 2 구역 SI 엔진 시뮬레이션을 사용하여 다양한 엔진운전조건 변화에 따른 온도−압력 프로파일의 편차를 계산한 뒤, 온도−압력 프로파일의 편차가 점화지연을 어떻게 변화시키는지 정량적으로 분석하였다. 그 결과, 테스트연료의 점화지연은 RON 이 동일함에도 불구하고 온도 및 압력에 대해 상이한 의존성을 나타내는 것으로 밝혀졌다. 특히, 에탄올 함량이 높을 수록 점화지연의 활성화 에너지가 높기 때문에 온도 편차 $\frac{\Delta T}{T}$에 더 민감하며, 압력 편차 $\frac{\Delta P}{P}$에 덜 민감한 것을 발견하였다. 또한, 점화지연에 대한 온도−압력 편차의 영향은 $\frac{\Delta T}{T}$ 가 $\frac{\gamma-1}{\gamma}\frac{\Delta P}{P}$ 와 동일한 경우에만 에탄올

함량과 무관하다는 것이 밝혀졌다. 본 결과는 Kalghatgi 의 K 값 원리에서 예측 한 것과 일치하는 것으로 확인되었으며. 결과적으로 본 연구에서 사용한 방법론을 통해 엔진운전조건에 따른 연료 별 노킹 특성에 대한 새로운 관점을 제시할 수 있었다.

상기 결과는 외부 배기 가스 재순환(External exhaust gas recirculation; external-EGR)을 사용하는 조건에서도 적용할 수 있도록 확장되었다. 앞선 방법론과 유사하게, External-EGR 이 엔진 내 점화지연에 미치는 영향을 희석 효과 및 온도-압력 프로파일 효과로 나누어 개별적으로 평가하였다. 그 결과, External-EGR 의 희석효과는 연료 내 에탄올 함량이 10 %일 때(ERF10) 극대화된다는 사실을 발견하였다. 이 원인을 분석하기 위해 회귀 분석을 진행한 결과, 화염전파 동안 미연소가스에서 방출된 열량과 희석 효과의 크기 사이에 강한 상관관계가 있음을 발견 하였다. 따라서, ERF10 가 희석효과에 가장 민감한 이유는 화염전파 동안의 열 방출량이 크기 때문인 것으로 이해된다. 한편, External-EGR 에 의한 온도-압력 프로파일 효과는 연료 내 함량이 많을수록 더 크게 나타나는 것을 확인하였으며, 이는 External-EGR 에 의한 온도-압력 프로파일의 편차가 항상 $\frac{\Delta T}{T} > \frac{\gamma-1}{\gamma}\frac{\Delta P}{P}$ 의 조건을 만족시키기 때문인 것을 알 수 있었다. 결과적으로, RON 측정조건에서 Externa-EGR 이 사용될 시 최적의 에탄올 함량은 10 %로 확인되었다. 이에 더하여, 엔진속도가 변화함에 따라 화염전파 동안의 열 방출량이 줄어드는 상황을 모사하여, 최적의 에탄올 함량이 엔진속도에 따라 0 %에서 10 %까지 변할 수 있다는 점도 알 수 있었다.

엔진운전조건에 따른 최적 에탄올함량에 대한 이해를 바탕으로, 대한민국 내 SI 엔진차량군의 노킹억제를 최대화할 수 있는 최적 에탄올 함량을 제시하였다. 이와 관련하여, 2018 년 대한민국

자동차판매통계를 이용하여, 각 SI 엔진모델 별 판매량을 도출하였다. 그 후, 0-D 2 구역 SI 엔진 모델을 사용하여 노킹경계선(Detonation borderline; DBL) 조건에서의 각 SI 엔진모델 내 열역학적 상태를 계산하였다. 그 결과, 2018 년 대한민국에서 판매된 SI 엔진차량군의 72 %가 ERF30 이 최적인 영역에서 운행되는 것을 알 수 있었다. 또한 엔진속도가 빨라질수록 DBL 조건에서의 실린더 내 압력이 증가하여 ERF30 이 최적인 영역에서 운행되는 SI 엔진차량이군이 더 많아지는 것을 확인하였다. 본 연구결과를 확장하여, 미래에 External-EGR 이 활발히 사용되는 상황에서 최적의 에탄올함량이 어떻게 변화할 것인지를 분석하였다. 결과적으로, Extern-EGR 이 도입됨에 따라 최적의 에탄올 함량은 ERF10 에 가까워 질 것이며, 이는 ERF10 에서 External-EGR 의 희석 효과가 극대화되기 때문인 것으로 밝혀졌다. 그러나 엔진속도가 빨라짐에 따라 희석 효과가 줄어들기 때문에, 고 RPM 영역에서는 External-EGR 에 관계없이 ERF30 가 여전히 최적인 것으로 확인되었다.

본 연구는 다양한 엔진운행조건에 따라 연료 별 점화지연 특성을 분석하고 본 결과와 노킹 현상 사이의 상관 관계를 제시한 최초의 실험연구이다. 또한, 본 연구는 임의의 엔진운행조건에서 최적의 에탄올함량을 결정하는 다이어그램을 제안하여, 향후 대한민국에 가솔린-에탄올 혼합연료가 도입될 시 최적에탄올 함량을 결정할 수 있도록 하였다는 점에서도 의의를 지닌다.

주요어: 에탄올, 노킹, 옥탄가, 급속압축장치, 점화지연, 불꽃점화엔진

학번: 2014-21867